University of Calgary

PRISM Repository **https://prism.ucalgary.ca**

The Vault Open Theses and Dissertations

2019-09-10

Comparative Evaluation of Electrical Heating Methods for Oil Sand Reservoirs

Ji, Dongqi

Li, D. (2019). Comparative Evaluation of Electrical Heating Methods for Oil Sand Reservoirs (Doctoral thesis, University of Calgary, Calgary, Canada). Retrieved from https://prism.ucalgary.ca.
http://hdl.handle.net/1880/110916
Downloaded from PRISM Repository, University of Calgary

UNIVERSITY OF CALGARY

Comparative Evaluation of Electrical Heating Methods for Oil Sand Reservoirs

by

Dongqi Ji

A THESIS

SUBMITTED TO THE FACULTY OF GRADUATE STUDIES

IN PARTIAL FULFILMENT OF THE REQUIREMENTS FOR THE

DEGREE OF DOCTOR OF PHILOSOPHY

GRADUATE PROGRAM IN CHEMICAL AND PETROLEUM ENGINEERING

CALGARY, ALBERTA

SEPTEMBER, 2019

© Dongqi Ji 2019

Abstract

For thermal heavy oil recovery, conventional steam injection processes are generally limited to reservoirs of relatively shallow depth, high permeability, thick pay zones and homogeneity. An alternative approach of applying electrical energy, including methods of electric heater, electrical resistance heating and electromagnetic heating, can be used to generate heat in reservoirs that are not suitable for steam injection or to improve the economics of the heavy oil recovery compared with steam injection processes. However, in the current, the most widely used simulation method of electrical heating is the data coupling of two simulators, one is used for calculation of electrical heating and the other is used for calculation of a oil reservoir. The work in this thesis provides a single simulator that is capable of modelling all electrical heating processes for heavy oil and oil sands thermal recovery and the computational overhead and complexity of swapping data back and forth between two simulators has been omitted.

In this work, a new numerical simulator is developed that handles the three electrical heating processes, such as electric heater, electrical resistance heating and electromagnetic heating. New models regarding the physical processes of the electrical heating methods have been derived and used for numerical simulation. The electric current balance was used for the modelling of electrical current flow in oil sands reservoirs with an appropriate treatment of electrical conductivity between neighbouring grids. A Helmholtz equation for the magnetic field by deformation of Maxwell's equations is presented that makes it feasible to find electromagnetic field solutions for an inhomogeneous medium, such as a oil reservoir.

Also, it has not been possible until now to model all three electrical heating processes in a single model and the work in this thesis enables a direct comparison of the different methods to be made. The feasibility of electrical heating in oil sands reservoirs is examined in two case

categories: a) a horizontal well containing a heating source and b) a horizontal well-pair with heating sources located in both wells. Simulation results are compared in temperature, water saturation and electrical energy dissipation in the three electrical heating processes.

Acknowledgements

I would like to show my utmost gratitude and thankfulness to my supervisor Dr. Zhangxing Chen and co-supervisor Dr. Mingzhe Dong for their helpful guidance and great support at each stage of my studies at the University of Calgary.

I am also grateful to Dr. Thomas Grant Harding for his valuable guidance and suggestions regarding my thesis research and work experience.

Last but not least, thanks to all my friends for making my time at the University of Calgary enjoyable.

Dedication

To my family,

I wish to express my deep appreciation for their unconditional support and eternal love throughout my life.

Table of Contents

Abstract ii
Dedication iii
Table of Contents iv
List of Tables vii
List of Figures and Illustrations viii
List of Symbols, Abbreviations and Nomenclature xi

CHAPTER 1 INTRODUCTION 1
1.1 Background 1
1.2 Overview of electrical heating processes for oil sand reservoir recovery 3
1.2.1 Categories of electrical heating methods for oil sand reservoir 3
Electric heater 3
Resistive Heating 5
Inductive Heating 7
Electromagnetic Heating 8
1.2.2 Lab Experiments 11
1.2.3 Field Applications 18
1.3 Developments of mathematical modelling in electrical heating processes 23
1.3.1 Analytic Modelling 23
Electric Heater 23
Resistive Heating 23
Electromagnetic Heating 24
1.3.2 Numerical modelling 28
1.4 Comparison of electrical heating to steam injection processes 35
1.5 New Technologies in Electrical Heating Processes 37
1.5.1 Electro-Thermal Dynamic Stripping Process (ET-DSP) 37
1.5.2 Solvent/Gas additive in resistive heating 38
1.5.3 Thermal solvent reflux 40
1.5.4 Electromagnetic Steam-Assisted Gravity Drainage (EM-SAGD) 40
1.5.5 Tight-Shell Design 41
1.5.6 Nano-particle Addition 41
1.5.8 Electromagnetic-Flood process 43
1.5.9 Ceramic Material Addition 44
1.5.10 Cylindrical Conductor Array Equivalent Heating 44
1.5.11 In-situ Reflux 44
1.6 Motivations and Objectives 45

CHAPTER 2 RESERVOIR SIMULATION UNDER ELECTRICAL HEATING 48
2.1 Reservoir model 48
2.1.1 Mass and Energy Conservations 49
2.1.2 Constraint equations 51
2.1.3 Variable Section 53
2.2 Reservoir Characterization 54
2.2.1 Rock Properties 54

2.2.2 Fluid Properties 54
2.2.3 Rock/Fluid Properties 59
2.2.4 Dielectric Properties of Oil Sands 60
2.3 Electrical heating model 68
2.3.1 Electric heater 68
2.3.2 Electrical resistance heating 69
2.3.3 Electromagnetic heating 72
2.4 Boundary conditions 76
2.4.1 Well Modelling 76
2.4.2 Heat loss 79
2.4.3 Heating Source and outer boundary conditions in electric heater process 81
2.4.4 Current voltage source and outer boundary conditions in resistive heating process 82
2.4.5 Electromagnetic Wave Source and outer boundary conditions in Electromagnetic Heating process 85

CHAPTER 3 NUMERICAL METHODS 94
3.1 Discretization 94
3.2 Treatment of connections 99
3.3 Newton-Raphson method 101
3.4 Grid and Jacobian Assembling 102
3.5 Time Step Control 103

CHAPTER 4 MODEL VALIDATION 104
4.1 Reservoir Model 104
4.2 Initial Conditions 105
4.2 Validation of Electric Heater process 108
4.3 Validation of resistive heating process 113
4.4 Validation of electromagnetic heating process 114

CHAPTER 5 SIMULATION RESULTS AND DISCUSSIONS 122
5.1 Cases of electric heater process 122
5.1.1 Effect of input power 125
5.1.2 Application of a single horizontal well with continuous production 127
5.1.3 Application of a single horizontal well under cyclic heating and production129
5.2 Cases of resistive heating process 131
5.2.1 Effect of Salinie Water Electrical Conductivity and Applied Voltage at Electrodes 134
5.2.2 Application of a single horizontal well under continuous production 137
5.3 Cases of electromagnetic heating process 140
5.3.1 Evaluation of Power and Frequency at Source 145
5.3.2 Application of a single horizontal well under continuous production 147
5.3.3 Application of a single horizontal well under cyclic Heating and production150
5.3.4 Application of a horizontal well-pair 151

CHAPTER 6 COMPARISON OF ELECTRICAL HEATING PROCESSES 156
6.1 Heat generation mechanism 156

6.2 Effect of vaporization on energy dissipation 158
6.3 Oil Production performance.....161

CHAPTER 7 CONCLUSIONS AND RECOMMENDATIONS 163

REFERENCES 169

List of Tables

Table 1.1 Summary of electrical heating methods 10

Table 1.2 Table of literature on laboratory experiments of electric heater 15

Table 1.3 Table of literatures on laboratory experiments of electrical resistance heating 15

Table 1.4 Table of literature on laboratory experiments of inductive heating 16

Table 1.5 Table of literature on laboratory experiments of electromagnetic heating 16

Table 1.6 Table of literature on field applications of electrical heating 22

Table 1.7 Table of literature on numerical simulation methods of electrical heating 34

Table 2.1 Parameters of the fit (Eq. 3-17 to Eq. 3-32): 67

Table 4.1 Characterization of Rock and Fluids 105

Table 4.2 Relative permeability of water-oil system 106

Table 4.3 Relative permeability of gas-oil system 107

Table 5.1 Application of electric heater by a single horizonal well under continuous heating .. 124

Table 5.2 Application of electric heater by a single horizonal well under cyclic heating and production 124

Table 5.3 Application of electrical resistive heating by a single horizonal well under continuous heating 133

Table 5.4 Application of electromagnetic heating by a single horizonal well without production 143

Table 5.5 Application of electromagnetic heating by a single horizonal well with continuous production 143

Table 5.6 Application of electromagnetic heating by a single horizonal well cyclic heating and production 143

Table 5.7 Application of electromagnetic heating by a well-pair 144

List of Figures and Illustrations

Figure 1.1 Illustration of electric heater application in oil sand reservoir (Rehman and Meribout, 2012). 5

Figure 1.2 Illustration of resistive heating application in oil sand reservoir 7

(Chhetri and Islam, 2008). 7

Figure 1.3 Illustration of inductive heating application in oil sands reservoir (Mustafina et al., 2013). 8

Figure 1.4 Illustration of RF/MW heating application in oil sand reservoir (Chhetri and Islam, 2008). 10

Figure 1.5 Illustration of data exchange of a reservoir simulator (CMG STARS) and an electromagnetic field simulator (COMSOL). 47

Figure 2.1 Mean values of conductivity, σ, and relative dielectric constant, εR, as a function of frequency for oil sands A, B, and C at 24°C (Chute et al., 2009). 63

Figure 2.2 The single layer PML technique: Maxwell's equations and the PML formulations are solved by FDFD technique inside a computational domain and a PML layer, respectively. The computational domain is surrounded by a single PML layer whose properties have been predicted. 90

Figure 2.3 Calculation results of electric field magnitude by using PML, background is pure water (DW). Truncation locations are selected at a short one (TS) and a long one (TL) and the source power is selected at a high one (HP) and a low one (LP), respectively. Results are compared to analytic solutions. 92

Figure 2.4 Calculation results of electric field magnitude by using PML, background is saline water (SW). Truncation locations are selected at a short one (TS) and a long one (TL) and the source power is selected at a high one (HP) and a low one (LP), respectively. Results are compared to analytic solutions. 93

Figure 2.5 Jacobian structure of a single equation system with single variable and discretized in a 5-grid system 102

Figure 2.6 Illustration of half reservoir model with initial pressure distribution 104

Figure 4.1 Oil viscosity versus temperature 107

Figure 4.2 Comparison of temperature profiles by CMG STARS and the simulator in this thesis by maximum heating source temperature at 200 ℃. Time is selected at 90, 360 and 720 days. 109

Figure 4.3 Comparison of water saturation profiles by CMG STARS and the simulator in this thesis by maximum heating source temperature at 200 ℃. Time is selected at 90, 360 and 720 days. 110

Figure 4.4 Comparison of temperature profiles by CMG STARS and the simulator in this thesis by maximum heating source temperature at 350 ℃. Time is selected at 90, 360 and 720 days. 111

Figure 4.5 Comparison of water saturation profiles by CMG STARS and the simulator in this thesis by maximum heating source temperature at 350 ℃. Time is selected at 90, 360 and 720 days. 112

Figure 4.6 The results of electrical field potential of analytic solution and simulator in this thesis. 114

Figure 4.7 Comparison of electric field intensity distribution by analytic solution and numerical model in homogeneous media..... 116

Figure 4.8 Profiles of electric field distribution versus distance under various water saturations by Yee's method, Helmholtz's equation for electric field (Eq. 1-1) and Helmholtz's equation for magnetic field (Eq. 2-79) in this work for an inhomogeneous medium. (a) is electric field distribution under EM source frequency of 1.0 MHz..... 118

Figure 4.9 Profiles of electric field distribution versus distance under various water saturations by Yee's method, Helmholtz's equation for electric field (Eq. 1-1) and Helmholtz's equation for magnetic field (Eq. 2-79) in this work for an inhomogeneous medium. (a) is electric field distribution under EM source frequency of 10.0 MHz..... 119

Figure 4.10 Profiles of electric field distribution versus distance under various water saturations by Yee's method, Helmholtz's equation for electric field (Eq. 1-1) and Helmholtz's equation for magnetic field (Eq. 2-79) in this work for an inhomogeneous medium. (a) is electric field distribution under EM source frequency of 100.0 MHz..... 120

Figure 4.11 Profiles of electric field distribution versus distance under various water saturations by Yee's method, Helmholtz's equation for electric field (Eq. 1-1) and Helmholtz's equation for magnetic field (Eq. 2-79) in this work for an inhomogeneous medium. (a) is electric field distribution under EM source frequency of 1000.0 MHz..... 121

Figure 5.1 Temperature (℃) and water saturation profiles under heating by electric heater of Case 1-1 and Case 1-2..... 126

Figure 5.2 Temperature (℃) and water saturation profiles under heating by electric heater of Case 1-3 and Case 1-4..... 128

Figure 5.3 Cumulative oil produced of Case 1-3 and Case 1-4. 129

Figure 5.4 Cumulative oil produced of Case 1-5 and Case 1-6. 130

Figure 5.5 Temperature (℃), water saturation and electrical potential (voltage) profiles under resistive heating of Case 2-1, Case 2-2 and Case 2-3, at 90 days. 136

Figure 5.6 Temperature (℃), water saturation and electrical potential (voltage) profiles under resistive heating of Case 2-4 and Case 2-5, at 2880 days (8 years). 139

Figure 5.7 Cumulative oil produced of Case 2-4 and Case 2-5. 140

Figure 5.8 Temperature (℃), water saturation and magnitude of electric field (V/m) profiles under heating by electromagnetic waves of Case 3-1 to Case 3-4..... 146

Figure 5.9 Temperature (℃), water saturation and magnitude of electric field (V/m) profiles under heating by electromagnetic waves of Case 3-5 to Case 3-6..... 149

Figure 5.10 Cumulative oil produced by electromagnetic heating of Case 3-5 and Case 3-6.... 150

Figure 5.11 Cumulative oil produced by electromagnetic heating of Case 3-7 and Case 3-8.... 151

Figure 5.12 Temperature (℃), water saturation and magnitude of electric field (V/m) profiles under heating by electromagnetic waves of Case 3-9 at 90 days, 1800 days and 2880 days. 154

Figure 5.13 Cumulative oil produced by electromagnetic heating of Case 3-8 and Case 3-9.... 155

Figure 6.1 Illustration of the location from left heating source to right reservoir boundary in view of cross-section..... 160

Figure 6.2 Distributions of water saturation and electrical potential in the lateral direction from electrode to right reservoir boundary at day 1 and day 2880, Case 2-4. 160

Figure 6.3 Distributions of water saturation and magnitude of electric field in the lateral direction from electrode to right reservoir boundary at day 1 and day 2880, Case 3-9..... 161

Figure 6.4 Comparison of cumulative oil produced of the three electrical heating processes. Case 1-6 applies electric heater, Case 2-5 applies electrical resistance heating and Case 3-9 uses electromagnetic heating. 162

List of Symbols, Abbreviations and Nomenclature

Symbol	Definition	Unit
a	Constant	
B	Magnetic induction	Tesla
D	Electric displacement field	C/m^2
E	Electric field intensity	V/m
H	Magnetic field strength	A/m
J	Free current density	A/m^2
Nc	Number of components in a phase	
Np	Number of phase	
m	Constant	
n	Constant	
t	Time	s
ε	Dielectric permittivity	F/m
ε_R	Real part of dielectric permittivity	
ε_I	Imaginary part of dielectric permittivity	
ε_r	Dielectric constant	
μ	Magnetic permeability of free space	H/m
σ	Electrical conductivity	S/m
ω	Angular frequency	Hz
σ_w	Water electrical conductivity	S/m
σ_{w0}	Reference water electrical conductivity	S/m
T_r	Reference Temperature	℃
T_c	Critical temperature	K
T_{ci}	Critical temperature of component i	K
ϕ	Porosity	
ϕ_0	Reference porosity	
P	Pressure	kPa
P_0	Reference pressure	kPa
P_c	Critical pressure	kPa
P_{ci}	Critical pressure of component i	kPa
C_{rP}	Compressibility of rock	1/kPa
C_{rT}	Thermal expansion coefficient of rock	1/℃
ε_r	Real part of permittivity	
ε_i	Imaginary part of permittivity	
ρ_p	Molar density of phase p	
$\rho_{p,i}$	Component i in liquid mole density	$mole/m^3$
ρ_{p,i,P_0,T_0}	Component i in liquid mole density at reference pressure and reference temperature	$mole/m^3$
$C_{LP,i}$	Liquid compressibility of the component i	1/kPa
$C_{LT,i}$	Liquid thermal expansion coefficient of the component i	1/℃
ρ_g	Molar density of gas	$mole/m^3$

ρ_w	Molar density of water	mole/m^3
ρ_s	Density of rock	kg/m^3
u_p	Flow velocity of phase p	m/s
u_g	Flow velocity of gas	m/s
u_o	Flow velocity of oil	m/s
u_w	Flow velocity of water	m/s
R	Universal gas constant	m^3·Pa/(K·mol)
S_p	Saturation of phase p	
S_l	Liquid saturation	
S_l^*	A small value in pseudo k-value calculation	
S_o	Oil saturation	
S_w	Water saturation	
μ_p	Viscosity of phase p	cP
μ_w	Viscosity of water	cP
μ_g	Viscosity of gas	cP
$\mu_{o,i}$	Component i viscosity, oil phase	cP
Φ_p	Flow potential of phase p	Pa
T	Temperature	℃
$q_{p,i}$	Sink/source term of component i in phase p	mole/s
q_{oi}	Sink/source term of oil phase	mole/s
$\hat{k}_{g,l,i}$	K-value for component i in liquid phase and gas phase	
k_value	K-value provided by CMG STARS	
$kv1$	Constant coefficient in K-value calculation provided by CMG STARS	
$kv2$	Constant coefficient in K-value calculation provided by CMG STARS	
$kv3$	Constant coefficient in K-value calculation provided by CMG STARS	
$k_{g,l,i}$	Pseudo k-value	
$x_{g,i}$	Molar fraction of component i in gas phase	
$x_{l,i}$	Molar fraction of component i in liquid phase	
K_w	K-value of water	
K	Thermal conductivity of reservoir	W/(m·℃)
k	Absolute permeability	darcy
k_{rp}	Relative permeability of phase p	
k_{ro}	Relative permeability of phase oil	
k_{rocw}	The relative permeability to oil at connate water and zero gas saturation	
k_{row}	Oil relative permeability in oil-water system	
k_{rw}	Water relative permeability in oil-water system	
k_{rog}	Oil relative permeability in oil-gas system	

k_{rg}	Gas relative permeability in oil-gas system	
H_p	Enthalpy of phase p	J/mole
H_g	Enthalpy of gas phase	J/mole
H_o	Enthalpy of oil phase	J/mole
H_w	Enthalpy of water phase	J/mole
U_p	Specific internal energy of phase p	J/mole
U_g	Specific internal energy of gas	J/mole
U_o	Specific internal energy of oil	J/mole
U_w	Specific internal energy of water	J/mole
U_r	Specific internal energy of rock	
C_r	Specific heat capacity of the solid	J/(mole·℃)
$CPL(T)$	Liquid heat capacity	J/(mole·℃)
$HVAP(T)$	Vaporization enthalpy	J/mole
q_{ssg}	Production/injection rate of heat by gas	J/(m^2·s)
q_{sso}	Production/injection rate of heat by oil	J/(m^2·s)
q_{ssw}	Production/injection rate of heat by water	J/(m^2·s)
q_{LOSS}	Heat loss to overburden and underburden	J/(m^2·s)
E_0	Electric field intensity at EM source	V/m
x	Distance from EM source	m
γ_p		
Z	z-factor of gas	

Chapter 1 Introduction

1.1 Background

Over 50% of global oil reserves are found in the form of heavy oil and oil sands bitumen, and as a result, heavy oil and bitumen are considered to be some of the most crucial resources to meet energy demand in the future. Of these heavy oil and oil sand reserves, by far the largest amounts are found in (Alberta) Canada and (Eastern Venezuelan) Venezuela (Meyer et al., 2007). The high viscosity and low API gravity of heavy oil and bitumen result in low oil recovery, 10% or less by primary production (Butler and Yee, 2002).

In recent decades, thermal oil recovery has been used as a method to recover heavy oil and bitumen by raising oil temperature and dramatically reducing its viscosity. Conventional thermal recovery processes based on steam or hot water injection, like Steam-Assisted Gravity Drainage (SAGD), Cyclic Steam Stimulation (CSS), and Steam Flood, are well known in this regard. Unfortunately, due to the extensive need of steam generation, which comes from natural gas combustion, these methods may not achieve economic criteria and possess environmental constraints. In addition, they may not be applicable to certain types of reservoirs, like those with high clay contents, low injectivity, great depth or high levels of heterogeneity (Bera and Babadagli, 2015).

Recently, there has been interest in using electrical heating to overcome these challenges, which have plagued the steam-based recovery processes (Vermeulen and McGee, 2000). The basic function of electrical heating is to raise reservoir temperature and thus increase oil mobility by reducing its viscosity, because reservoirs can be heated up by applying transformation of electrical energy to heat energy (Ritchey, 1956). The electrical heating methods can be classified under three main categories depending on a heating source used for heating: (1) the application

of electrical downhole heaters, where the resistive heaters generate heat in accordance with Joule's effect, increasing the temperature near a wellbore (Rodríguez et al., 2008). In this instance, the heat is primarily transferred by conduction and a relatively long time is required to heat up a reservoir; (2) the use of low frequency electric current, ohmic heating or resistive heating takes place in an oil reservoir. Electric current flow in a formation is primarily via ionic conduction through the water-saturated portion of the interconnected pore spaces in an oil reservoir (Hasanvand and Golparvar, 2015); and, (3) the application of high frequency (Radiofrequency (RF) and microwave) radiation to the formation. In this case, dipoles are formed by molecules (mainly water) that tend to align with the electric field. As a result, the molecular movement produces heat in an oil reservoir through frictions (Bera and Babadagli, 2015).

Electrical heating has some advantages over conventional thermal oil recovery methods to overcome their existing challenges. In the results of experiments, simulations and field applications, such as those in Brazil, the Netherlands, Russia, Canada, Venezuela and the USA, most field trials demonstrate the feasibility of electrical heating for heavy oil and oil sands recovery, and its promise as an alternative to steam injection. The advantages of using electricity can be summarized as follows: elimination of the equipment and operating costs associated with fluid injection, improvement of oil rates due to a reduction in water flowing in an oil reservoir because of elimination of water injection, reduced sensitivity to fluid injection in reservoirs containing swelling and other clays, reduced energy requirements due to lower operating temperatures, improved volumetric sweep efficiency by effective electrical heating occurring in low permeability areas, and applicability in deep reservoirs by overcoming the limitation caused by high reservoir pressure in steam injection processes. However, the limitations of electrical

heating are also observed. The tight well spacing required in the process of an electric heater may make this method uneconomic due to the high drilling and completion costs associated with this process. Water dependent electrical conductivity limits electric current flow in an oil reservoir due to the vaporization under resistive heating. The short penetration depth of electromagnetic heating, which is dependent on wavelength, impairs an application of this method in heating up a large reservoir.

1.2 Overview of electrical heating processes for oil sand reservoirs recovery

In this section of thesis, the processes of electrical heating for oil sand reservoirs recovery have been introduced, including the categories of the electrical heating methods, lab experiments as well as related field applications.

1.2.1 Categories of electrical heating methods for oil sand reservoirs

Electric heater

One method of electrical heating is the utilization of electric conductors, also named Electric Downhole Heating (EDH), as a heating source to increase the temperature of a wellbore (McGee and Donaldson, 2009). The electric current flows through a conductor implemented at a certain depth of a reservoir and increases temperature by ohmic heating. Thermal conduction is the major method of heat transfer from a conductor to its surrounding formations as shown in Figure 1.1. One advantage is the possible application of direct power transformation with the power range of hundreds of kilowatts. However, the tight drilling spacing requirement due to the limited heat transfer by conduction raises the cost of operation (Wacker et al., 2011).

EDH systems were used to lower the viscosity of oil in reservoirs to increase the flow rates of crude oil and improve oil recovery. EDH systems are very efficient and reliable, and are an

easily controlled method to allow production of heavy, high viscosity oils. The total system is very space-efficient in both downhole and on the surface (Samuel and Parman, 2013). The primary purpose of a heating system is to strategically place supplemental heat to sections of a wellbore, so the pressure drop can be reduced in production tubulars. The goal is to add varying amounts of heat along a horizontal well, so the oil temperature increases strategically, thus lowering the viscosity of the oil. This will result in lower pressure drops in tubulars. A heating system used consists of a unique mineral insulated (MI) heating cable with zones of differing resistances. The different resistances produce varying watt densities and allow for strategic placement of heat in the lateral direction. This system was designed to strategically place more heat at the toe of a well with decreasing amounts of heat as a fluid moves to the heel of a horizontal well (or to a location near the downhole pump). This reduces the viscosity of the oil along the lateral and thus allows for a relatively consistent pressure drop in a horizontal well which, in turn, leads to an increase in production. A heater was attached to a “stinger” pipe placed below a Progressive Cavity Pump (PCP). The power output of heaters in the “hot zones” ranged from 558 W/m (170 W/ft) to over 850 W/m (280 W/ft). The total heater system power load ranged from 25 kW to 50 kW. These wells were installed with a thermocouple located in the top of a hot zone, which was used for temperature monitoring and control of the heater.

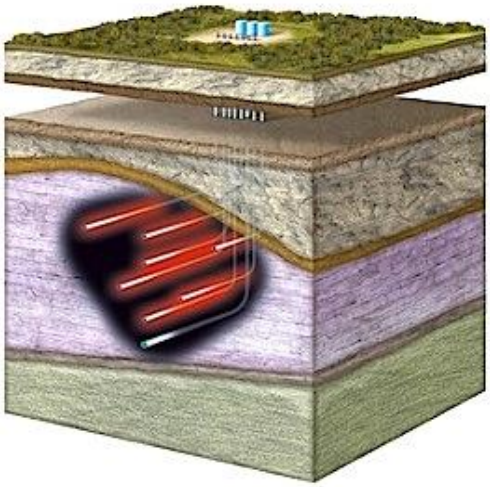

Figure 1.1 Illustration of electric heater application in oil sand reservoir (Rehman and Meribout, 2012).

Electrical Resistance Heating

Electrical Resistance heating applied with low frequency is also an application of ohmic heating. In this approach, electric current passes through a formation and heat is produced in conductive materials which, in turn, heats up a reservoir. This approach can be employed by using two wells in a reservoir containing brine (conductive materials): one well is the anode and the other is the cathode as shown in Figure 1.2 (Chhetri and Islam, 2008). By an application of a potential difference between these two wells, the flow of electric current through a formation acts as a source of heating due to power dissipation. When the electric resistivity of the formation is low, in the range of around 100 ohm-m, for example, 60 Hz commercially available alternative current (AC) power can be utilized to dissipate heat at field scale rates (Glandt and Hsu, 1992). This process can be employed in different types of reservoirs with varying formation porosity, permeability, temperature and pressure (Oliveira et al., 2009). Heating with the frequency less than 300 kHz can be described as resistive heating (Maggard and Wattenbarger, 1991).

A disadvantage of the electrical resistance heating is that electrodes must be used. The electric current flows along the path of least resistance, leading to huge current densities on these paths where conductivity is high. Hot spots at the points of an electrode with high electric current densities may be generated leading to coking and, therefore, loss of electrode-to-reservoir contact, which may not be reversible. Furthermore, the temperature should be maintained below the boiling point of water to maintain continuity. Corrosion may occur on electrodes in a high salt concentration reservoir (Rehman and Meribout, 2012).

In electrical resistance heating, the electric circuit is completed through in-situ water in a formation. Joule's heating can be reduced where there is only a small water content due to vaporization because of temperature over its boiling point. Another consideration in electrical resistance heating is wellbore power transmission and associated power loss. For many common wellbore casings, current levels as low as 100 A rms cause nonlinear magnetization of wellbore steel. This, in turn, causes hysteresis power loss in a casing and leads to impedances that are much greater than those observed at low current levels (Stroemich et al., 1990). To improve the efficiency of electrical resistance heating, it is necessary to keep the power dissipated in a wellbore delivery system to a small fraction of the power dissipated in the formation (Sahni et al., 2000). Thus, a good understanding of the electrical properties of insulating materials and their degradation under changes of temperature, pressure and fluids needs to be known.

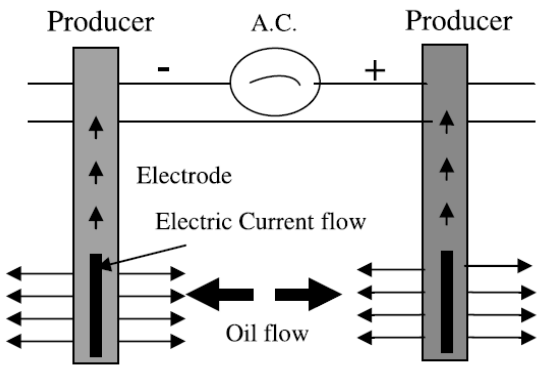

Figure 1.2 Illustration of resistive heating application in oil sand reservoir (Chhetri and Islam, 2008).

Inductive Heating

In this process, Alternating Current (AC) flows through a conductor (exciting winding) to induce a magnetic field in its surrounding formations. Thus, a varying magnetic field is used to generate secondary electric current (eddy current), which circulates in a formation. Eddy currents flow through the conductive materials producing heat and raising temperature, while the temperature of rocks and other inorganic materials present in an oil reservoir are raised by heat transfer. The governing factors of the heating process include the specific heat of materials, frequency of the induced current, magnetic permeability of reservoir materials and resistance of the materials to current flow (Vermeulen and McGee, 2000). In the application of inductive heating (Figure 1.3), an inductor (AC loops) is installed above horizontal wells. The inductor acts as an inductively heated source to radiate heat in an oil reservoir (Mustafina et al., 2013). A study of inductive heating conducted by Fisher (1980) shows that the maximum temperature rise of oil sand reservoirs is 300℃ and the maximum input power requirement is 123 kWh/ton. In addition, because there is no need for direct contact with a reservoir to generate the currents, neither brine nor well stimulation is necessary (Wacker et al., 2011). However, due to the relatively small

amount of conductive (metallic) materials normally found in an oil reservoir, which are the dominant components for transforming electrical energy to heat, inductive heating is not applicable for most oil reservoirs. In this thesis, the process of inductive heating is not considered.

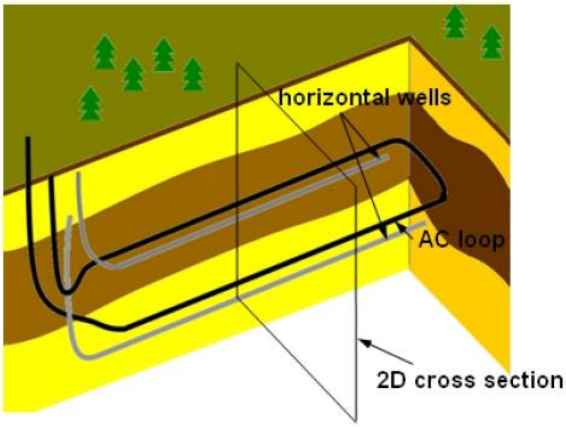

Figure 1.3 Illustration of inductive heating application in oil sands reservoir (Mustafina et al., 2013).

Electromagnetic Heating

Frequency is defined as the number of oscillations of Electromagnetic (EM) energy per second. In general, frequencies ranging from 3 kHz to 300 GHz are referred to as radio frequencies (RF) (Islam, 1999). Microwaves (MW) are a subset with high frequency ranging between 300 MHz and 300 GHz. In general, the ability of RF/MW to transfer energy to a medium depends on preferential absorption of RF/MW energy, which is determined by its molecular composition and dielectric properties of the materials. The existence in reservoirs of mobile molecules with molecular dipole moments (like water) enables reservoir heating with oscillating electric fields generated by passing of waves. The oscillating polar molecule (mainly water) generates frictional heat and this heat may then be transferred to its neighbours (mainly rock and oil) which

elevates the temperature of the entire medium (the reservoir). The level of temperature elevation is determined by the amount of RF/MW energy absorbed by irradiated materials (Okassa et al., 2010). Because crude oil is a poor absorber due to its low dielectric constant, RF/MW receptors (activated carbon, iron oxide and methanol) have been used to stimulate a heating process by enhancing absorption power. Studies by mathematical simulation show that RF/MW heating is more promising than other thermal methods because heat loss can be reduced through applications under control (Ovalles et al., 2002). As shown in Figure 1.4, an oil reservoir is heated-up under radiation by microwaves emitted from an antenna located in a wellbore and the oil is being produced to the surface through a production well (Chhetri and Islam, 2008). There is also a limitation of this process that the penetration depth of RF/MW wave is relatively small and depends mainly on the frequency of operation and composition of a reservoir. Different from the electrical resistance heating methods that rely on the presence of the water phase to establish ionic conduction paths of heating, the RF heating can be adjusted to accommodate any water saturation, especially for low water content (Sresty et al., 1986). It has been suggested to heat a reservoir by applying microwaves at 2.45 GHz, because this frequency can produce the resonance effect of water (Kovaleva et al., 2010b). However, such strict control of source frequency may not be necessary in field applications.

In Table 1.1, the electrical heating processes, including an electric heater, electrical resistance heating, inductive heating and electromagnetic heating have been summarized with respect to their applied frequency range, heat generation method and heat dissipation location, as mentioned above.

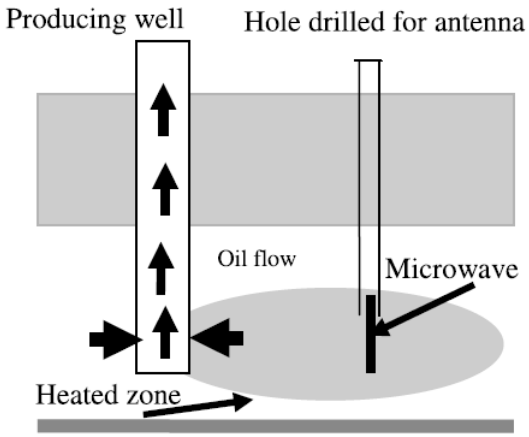

Figure 1.4 Illustration of RF/MW heating application in oil sand reservoir (Chhetri and Islam, 2008).

Table 1.1 Summary of electrical heating methods

Electrical heating method		Heat generation	Heat dissipation location		References
Method	Frequency applied		Formation	Electrode	
Electric heater	60 Hz typically	Ohmic heating by applied current at electrode within wellbore		X	Wacker et al., 2011
Electrical Resistance heating	60 kHz ~300 kHz	Ohmic heating by applied current through formation	X		Maggard and Wattenbarger, 1991
Inductive heating	1 kHz~1 MHz	Ohmic heating by induced eddy current and molecular friction under radiation by displacement currents	X		Mustafina et al., 2013
Electromagnetic heating	3 kHz ~300 GHz	Molecular friction under radiation	X		Islam, 1999

1.2.2 Lab Experiments

Experiments based on heavy oil from Bohai oilfield, China showed the effectiveness of an electric heater on oil recovery, as summarized in Table 1.2 in detail (Zhong et al., 2015). The first lab experiment of using brine to improve bulk electrical conductivity was conducted by El-Feky (1977) and later by Harvey et al. (1979). Direct Current (DC) was applied and transmitted to the core through platinum electrodes placed in a separate electrode (Amba et al., 1964). A technique was used to achieve selective heating of portions of an oil reservoir by injection of fresh water or saline water prior to the electric heater process. A set of laboratory experiments were conducted to determine oil recovery from a five-spot pattern combining electric current flow and saline water injection. With NaCl aqueous solution of 200,000 ppm, the final recovery was 13% greater with electrical heating than that with waterflood alone. Experiments of electrical resistance heating have been conducted with electrodes installed at a SAGD-like well pair (Zhong et al., 2011). Offshore heavy oil with viscosity of 1,573 mPa.s under initial reservoir conditions was used in the experiments. An average oil production rate was 1.6 to 1.85 times greater than the cold production rate with power supply at 1kW and 2 kW, respectively. A summary of lab experiments on electrical resistance heating is shown in Table 1.3 according to available information in publications.

An experiment was conducted by using a solenoidal coil placed horizontally within a pay zone representing a possible electrode configuration to establish uniform heating within a well-defined region of a formation (Vermeulen and Chute, 1983). The pay zone was modelled using oil sands that was 5 times as conductive as the actual formation and the presence of overburden or underburden was neglected. To provide proper scaling, frequency of 1.62 MHz was selected. From the temperature distribution achieved in the horizontal plane, it was found that heating at

higher power for a shorter period can produce the same temperature distribution. A sandbox test was conducted with an inductive heating circuit provided within a box filled with sands and salt-water-solution in the scale of 1:1000 (Koolman et al., 2008), and the details are summarized in Table 1.4. The temperature profiles read from fibre optical temperature sensors showed a temperature rise along the sensor with power of 7.2 kW within a 10 min period. The dry sands within the conduit remained relatively cold compared to the wet sands where the inductive heating started around the conduit.

Some experiments were conducted to exam the effectiveness of the RF/MW heating methods. A moderate frequency current in the range of 5 to 20 MHz was used to heat up thin heavy oil reservoirs with a well configuration similar to SAGD, in which electromagnetic waves were introduced from an upper well and oil was collected from the lower one. Effective heating with minimal heat loss was demonstrated. A high frequency provided a fast heat-up rate, existence of water was essential for continuous wave propagation and a high salinity enhanced the conduction of electromagnetic waves (Chakma and Jha, 1992). Room condition experiments showed that RF heating can increase the temperature up to 150 ℃ of diatomaceous earth and an oil sample from Bakersfield was heated up to 150 ℃ after 49 min under 400 W of heating source (Kasevich et al., 1994). Based on the experiments with the help of microwave heating and gas injection, the results showed that the high frequency can provide faster heating rates and overcome problems associated with discontinuity of media, such as an oil reservoir (Jha and Chakma, 2010).

A comparison of microwave heating and electrical resistance heating was conducted with better results shown for microwave heating. It was noted that a much earlier start was possible with microwave heating compared to electrical resistance heating because of heavy components desorption in microwave heating (Kovaleva et al., 2010a). The obtained visualization of the

asphaltenes structure before and after a microwave treatment showed the orientation of asphaltenes in the direction of the field action and higher interaction with each other. This was attributed to the fact that microwave irradiation influences polar components of oil and desorbs these components from a rock surface to add production. Less asphaltene precipitation and pore plugging were found compared to electrical resistance heating under the effect of microwave irradiation.

Lab experiments by the using of electromagnetic heating are summarized in Table 1.5 with information of physical models, applied power/frequency and oil production performance. An experiment of microwave assisted gravity drainage has been conducted by heating up a core sample in the Mehsana field (Jha et al., 2011). Magnetron tubes were used to generate the microwave power. After heating of 1 minute, an obvious oil viscosity reduction was found. The efficiency measurements of different heating methods were also compared by experiments, such as thermal heating, electrical resistance heating, inductive heating and microwave heating methods. A heating process was tested in a sand pack using a crude oil of 17.3 API and 540.52 cP. It was reported that the average power consumptions were 2570, 39 and 3.775 W.hr/cc for electrical resistance heating, inductive heating and microwave heating methods, respectively (Alomair et al., 2012). A laboratory experiment was conducted with an application of 2.45 GHz frequency, which is the water molecule resonance frequency, to irradiate oil sands with variable power from 1 to 2 kW. When temperature is above 100 ℃, a heating rate decrease was observed due to initial water vaporization (Bientinesi et al., 2013). A Teflon core holder packed with glass beads was designed to study the recovery of a heavy oil sample from an Iranian reservoir under microwave heating (Eskandari at al., 2015). Experimental results found an increase in temperature around a heating source under high water saturation or high salinity, respectively.

In addition, the impacts of microwave irradiation on crude oil properties were tested. It was possible to upgrade crude oil by microwave irradiation, in which a permanent oil rheology change was observed due to presence of asphaltenes exposed to the microwave irradiation (Gunal and Islam, 2000). The upgrading of heavy oil by using variable frequency microwave was conducted at a facility in North Carolina. In this measurement, 6,700 MHz was chosen with the most efficient energy translation to a sample (Jackson, 2002). As found in laboratory measurements of thermal decomposition of Canadian oil sands using short-time microwave pluses (3-5s) under the atmosphere pressure, several light hydrocarbons were detected, and their molar distribution did not change (Depew et al., 1991).

Table 1.2 Table of the literature on laboratory experiments of electric heater

Experimental model	Power and source temperature applied	Production performance	Oil type	Rock matrix	Reference
A sand-pack (Ø550×750mm) installed with 16 thermocouples and a pair of screen pipes as horizontal wells powered by electrical power.	Heating source was powered by 2 and 5 KW.	Electric is favorable applied at conventional heavy oil reservoirs. CO_2 can be sequestrated and utilized to accelerate oil rate.	Dead oil viscosity at 50℃ is 12500 cp, CO_2 was used as injected gas.	Bohai oil field, China	Zhong et al., 2015

Table 1.3 Table of the literature on laboratory experiments of electrical resistance heating

Experimental model	Power applied	Production performance	Oil type	Rock matrix	Reference
10-inch internal diameter polyethylene sleeve having a one-inch alundum disc and a rubber stopper was placed in a $1^{3/4}$-inch copper conductor.	Direct current was applied and transmitted to the core through platinum electrodes placed in separate electrode.	The flow rate of oil and water were increased during primary and secondary recovery. With potential gradient increase from 0 to 6.94 V/cm, flow rate was improved from 6.64 to 9.46 cc/sec.	Kerosene was used as oil phase	Silica	Amba et al., 1964
Sand-pack model(Ø325×1000mm) with 16 thermocouples and 4 pressure sensors installed was surrounded by insulation materials, and two slotted pipes were used as the well-pair of injection and production wells.	-	Average oil rate was 1.6 times and 1.85 times of cold production for 1KW and 2KW power supply, respectively. Average oil rate was 5.81 to 6.37 times of cold production with N_2 injection under 2 KW heating source. Average oil rate was 5.47 to 6.24 times of cold production with CO_2 injection under 2 KW heating source.	Dead oil viscosity at 56℃ is 1681 cp. N_2 or CO_2 was used as injected gas.	-	Zhong et al., 2011

Table 1.4 Table of the literature on laboratory experiments of inductive heating

Experimental model	Source power	Production performance	Oil type	Rock matrix	Reference
A sandbox was provided with an inductive heat circuit with a box filled with sand and brine. The fiber optical temperature sensors were used.	The power is 7.2 kW under 142 kHz.	Temperature increase of 4.5 °F was observed after 10 min heating.	-	-	Koolman et al., 2008.

Table 1.5 Table of the literature on laboratory experiments of electromagnetic heating

Experimental model	RF/MW frequency and source power	Results	Oil type	Rock matrix	Reference
20×20×10cm Plexiglass filled with sand	5, 10, 20 MHz	29, 32 and 37% of OOIP produced for 5, 10, 20 MHz, respectively. The recovery is 45% under combination of EM heating and N_2 injection.	Oil viscosity is 1000 cp at room temperature.	Reservoir sands	Chakma and Jha, 1992; Jha and Chakma, 2010;
55 gallon drum with diatomaceous earth and soil	1kW with 50.55 MHz and 200W with 144 MHz	Diatomaceous earth could be efficiently heated to the temperature of 150 ℃.	Texaco oil in Bakersfield, California.	Diatomite reservoir	Kasevich et al., 1994
Crushed rock packed with crude and water in core holder	Fixed frequency of 2450 MHz with 10 levels of power. The maximum power is 700 W.	Carbonate formation was heated up with irradiation without the presence of water. Asphaltenes cause permanent changes in crude oil rheology under irradiation.	United Arab Emirates(UAE) crude with viscosity of 5.27cp under room temperature. The initial asphlaltene concentration is 3% by weight.	Carbonate rock from Jabel Hafeet region of Al-Ain, UAE.	Gunal and Islam, 2000
Samples were placed in the oven in 125 ml Erlenmeyer flasks.	6700+-507.5 Mhz	Upgrading using microwave energy produced oil with pipeline specification viscosity and density.	Crude oil from Polver Lake reservoir in the Lloydminster of Saskatchewan. The viscosity is 11300 cp at room temperature.	-	Jackson, 2002
300 ml cylindrical stainless-steel reactor in which EM energy penetrates from the top.	2.45 GHz	Determination of microwave heating on heavy oil reservoir and validation with mathematical model.	Lake Maracaibo heavy oil and Orinoco Basin extra-heavy crude	Silica	Ovalles et al., 2002

Experimental model	RF/MW frequency and source power	Results	Oil type	Rock matrix	Reference
Graphite core holder (Ø5.2×8.5cm) packed with crushed limestone premixed with crude oil and water.	Microwave oven with 1450 MHz and 1400 W.	High water saturations lead to higher oil production and high salinity promotes microwave heating.	Oil samples from conceptual reservoirs (Bati Raman 9.5°API, Garzan 12°API, Camurlu 18°API) in southeast Turkey.	Limestone	Hascakir et al., 2009
Polyvinyl chloride pipes of 0.5 m in length and 22.5 mm in inner diameter was filled with silica sand.	81.36 MHz with 6 kW used to heat up sample.	Microwave heating is more effective on small size sand particles.		Dry silica sand	Kovaleva et al., 2010a
A cubical stainless case with open top and edge length of 7 cm was filled with 16 °API heavy oil in crushed sandstone.	3.0 GHz with 1000W microwave oven.	Sample temperature was raised up to 100℃. Effect of initial water saturation, wettability, porosity and permeability on dielectric heating was discussed.	16 °API heavy oil	Sandstone	Jha et al., 2011
Core holder (Ø2×12inch)	1100W microwave oven.	10.34 to 20.79% of oil was produced.	Heavy oil with viscosity of 540.52 cp at room temperature.	Berna sandstone, glass beads, sand-pack	Alomair et al., 2012
Sandbox of 1.25×1.25×0.75m.	2.45 GHz with variable power from 1 to 2 kW.	Heating temperature is up to 200 ℃.	Oil sands	Oil sands	Bientinesi et al., 2013
Buchner filter tunnel	2.45 GHz microwave with variable power from 100 to 1000 W.	Nano-nickel catalysts increase the efficiency of microwave heating. Up to 90% oil recovery depending on operation conditions.	Heavy oil from northern Alberta, Canada. The viscosity is 120cp at 60 ℃.	Glass beads	Greff and Babadagli, 2013

1.2.3 Field Applications

Between the late 1890s and the early 1960s, several wells in California used electric heaters to stimulate oil well production from heavy oil reservoirs. Although it was reported there was an early success, resistance heaters exhibited a high failure rate (Sierra et al., 2001).

DC heating has been applied in heavy oil fields in the Santa Maria Basin, California, USA and in eastern Alberta, Canada (Hill et al., 2008) by Electro-Petroleum Inc. The Santa Maria basin contains a reservoir with 100-foot thick of unconsolidated sand buried at a depth of approximately 2,088 ft. With DC flow through the reservoir, a heavy oil production rate was increased by ten-fold with a water cut decrease from 45% to 12%. For the eastern Alberta plains, an oil production rate was increased from 0.21 to 0.91 m^3/day by the comparison of primary production and utilization of DC. The low frequency electrical resistance heating conducted in Rio Panan field, Brazil showed an oil production increase from 1.2 bbl/day (primary production) to 10 bbl/day after 70 days of heating (Pizarro and Trevisan, 1990). Uentech implemented many pilot projects between the mid-1980s to the early 1990s at a reservoir with 15 °API oil and deposit depth of 270 ft. In 1984, substantial electrical resistance heating applications have been demonstrated successfully by near-wellbore heating in Ardmore, Oklahoma (Pizarro and Trevisan, 1990). A several-fold production rate increase was noted. EOR International conducted a single well electrical resistance heating from November 1989 to August 1990 in SCH-280 well at Bentheim reservoir of Schoonebeek field in Netherlands (Pizarro and Trevisan, 1990). For the pay zone thickness of 31m and in-situ viscosity of 160 cp, the oil production rate was increased by two folds.

In 1995, two deviated vertical wells (15D-25-56-2W4 and 13C-30-56-1W4) were used to heat a horizontal well (16D-25-56-2W4) through the application of electrical resistance heating. This project tested the Lloydminster heavy oil operated by Texaco Canada Petroleum Inc. and partnership with the Alberta Department of Energy (McGee et al., 1999). Wells were drilled into the Lower Waseca formation within the Mannville Group with 3-5 m in thickness. The production response in vertical wells as a result of electrical resistance heating showed an increase of two to four times over primary production. Prior to connecting horizontal wells into the electrical circuit, the two horizontal wells were heated from May 1-3. On May 3, 1995, a horizontal well was electrically connected to the vertical wells via power supply. However, no production and a small temperature response were observed at the horizontal wells because of the flow restriction in casing annulus by electrical resistance heating equipment in the wellbores.

There are limited amount of RF/MW heating applications in field scales. Only a few trials have been conducted in California and Utah (USA), Alberta and Saskatchewan (Canada), and Bashkortostan and Tatarstan (Russia). A RF heating system has been applied in well 100D at Texaco Denver Producing Division's Midway area, N. Midway field, California, in 1992. To monitor temperature profiles, three observation wells T10, T20 and T30 located 10, 20 and 30 feet from well 100D were drilled. A high frequency electromagnetic wave of 25 kW and 13.56 MHz was used and the temperature of the observation well, which was 10 feet from the heating source well, was increased from 293 to 393 K over 20 hours. Production performance demonstrated the ability of the RF applicator to focus its radiation pattern into the desired region which was centered at the 620-foot applicator (Kasevich et al., 1994). Two small-scale field experiments were

conducted in the Asphalt Ridge tar sand deposit near Vernal, UT with the result of heating about 25 m^3 of the deposit by RF energy and 35% oil recovery during the first 3-week period (Sresty et al., 1986). The operating frequency of 20 MHz raised temperature to about 150 ℃. In a field test in Oklahoma in the early 1990s, three waveguides were inserted into a formation to heat up a limited amount of the oil-bearing formation. In this test, 300 MHz of radiation was used to raise the temperature near the wellbore region from 18℃ and up to 100℃. At 15 feet from the well, a temperature of 33℃ was reached. The results included an increase in the oil production without any details provided (Sresty et al., 1984).

The first MW heating introduced to Canada was operated at Wildmere, Alberta in 1986. Before MW heating, oil was produced at 0.95 ton/day and the rate was increased soon and settled at 3.18 tons/day under MW heating. The oil rate of second well was also enhanced from 1.59 tons/day to an average of 4.77 tons/day with the peak rate of 9.54 tons/day (Mukhametshina and Marttnova, 2013). Two MW heating stimulation projects were conducted in the Lloydminster heavy oil area at two wells (A1-11-48-25 W3M Lashburn and A8-6-51-27 W3M Northminster) to produce heavy oil from the Sparky formations (Davison, 1995). A majority of the heavy oil reservoirs around Lloydminster were well suited to the application of MW heating since the formations were relatively thin and not well suited for other secondary, tertiary or thermal recovery methods. Both projects indicated a quick response to heating even at low power input levels. However, neither project had been heated for a substantial period of time (Lashburn-two months and Northminster-three weeks) due to casing insulation failure.

Two MW heating field tests were conducted in Yultimirovskoye, Russia in 1980. Three stages were conducted at a well: first, about 20 kW power was applied and the bottomhole temperature was increased from 282 to 389 K in 36.5 hours; in the second stage, higher power of 30 kW was applied, and the temperature changed to 423 K within 4 hours, and in the last stage, the maximum power of 60 kW was set, and the temperature increased fast in 5.5 hours from 417 to 463 K. In this pilot, deep heat penetration was found (up to 5 m in the reservoir). During the next 32 hours, a short circuit was found between casing and tubing (Mukhametshina and Marttnova, 2013). In 2012, a joint venture for pilot scale implementation of RF heating, known as the Effective Solvent Extraction Incorporating Electromagnetic Heating (ESEIEH), successfully demonstrated heat generation and distribution in a field by an RF source (Saeedfar et al., 2016). In its second phase of field testing combined RF heating with injection of solvent at a low temperature was planned. For an oil field with the production rate of 10,000 bbl/day, ESEIEH was estimated to cost $50/bbl while under similar economic assumptions SAGD would cost $70/bbl (Wise and Patterson, 2016; Sadeghi at al., 2017a).

In Table 1.6, the field applications of electrical heating have been summarized with information of an applied field name, a heating method, production results and relevant references. All these applications show that electrical heating is feasible to heat oil reservoirs and increase an oil production rate, compared to cold production.

Table 1.6 Table of the literature on field applications of electrical heating

Field name	Heating method	Results	Reservoir properties	References
Ishimbayskoye oil field in Bashkortostan and Yultimirovskoye bitumen field, Russia	High frequency heating of electro-magnetic radiation at setting temperature of 110 ℃.	Oil rate is increased by 2.5 times and water cut is reduce to 1/3.	-	Sayakhov, 1970
Avintaquin Canyon and Asphalt Ridge, Utah, USA	13.56 MHz at power from 5 to 20 kW was applied at Avintaquin Canyon, 13.56 MHz at 200 kW was applied at Asphalt Ridge	Avintaquin Canyon was heated up to 637 K and Asphalt Ridge was heated up to 473 K.	-	Bridges et al., 1979
Asphalt Ridge tar sand near Vernal, Utah, USA	RF power carried from 40 to 75 kW and the frequency was changed from 2.2875 to 13.56 MHz.	About 25 m^3 of the tar sand colume was heated. Average deposit temperature was about 200 ℃. Bitumen recovery was expected in the range from 50 to 80%.	-	Sresty et al., 1986
Rio Panan oil field, Brazil	Low frequency at 30 kW is applied between neighboring wells, 328 feet apart.	Oil rate increases from 1.2 to 10 bbl/day after 70 days of heating.	$h = 27\ ft$; $\phi = 0.27$; $k = 4\ darcies$; $\mu_o = 2452cp\ at\ 100$ °F; $\mu_o = 100cp\ at\ 220$ °F $P_i = 284\ psi$	Pizarro and Trevisan, 1990
Lashburn and Northminster, Lloydminster heavy oil area, Canada	Heating with 30 kW power. Single well heating, current flows into formation from electrically isolated casing and up through the overburden to surface ground wells to complete the circuit.	Quick response heating but failed due to electricity delivery system and sand production. Oil rate is 1.27 and 3.75 times of primary production under heating of Northminster and Lashburn, respectively.	-	Davison 1992; Davison 1995
North Midway field, California, USA	13.56 MHz at 25 kW is applied between neighboring wells, 328 feet apart.	Oil rate increases from 1.2 to 10 bbl/day after 70 days of heating.	$h = 27\ ft$; $\phi = 0.27$; $k = 4\ darcies$; $\mu_o = 2452cp\ at\ 100$ °F; $\mu_o = 100cp\ at\ 220$ °F $P_i = 284\ psi$	Kasevich et al., 1994
Wildmere field, Alberta, Canada.	EM heating	Oil rate was increased to 3.18 tonnes/day under EM heating from 0.95 tonnes/day of primary production.	-	Mukhametshina and Martynova, 2013; Bera and Babadagli, 2015
Dover site, Alberta, Canada.	EM heating with solvent (ESEIEH)	For an oil production rate of 10,000 bbl/day, ESEIEH was estimated to cost $50/bbl while under similar economic assumptions SAGD would cost $70/bbl	-	Wise and Patterson, 2016; Sadeghi at al., 2017a

h is reservoir thickness, ϕ is porosity, k is permeability, μ_o is oil viscosity.

1.3 Developments of mathematical modelling in electrical heating processes

1.3.1 Analytic Modelling

Mathematically, all electrical heating methods including electric heaters, resistive heating and electromagnetic heating, can be derived from the system of Maxwell equations with a generalized description of heating power field, based on effective electric conductivity of a medium for the entire the range of applied frequency (Bogdanov et al., 2011b).

Electric Heater

In the analytic modelling of an electric heater in an oil sand reservoir, heat output from this type of heating source typically is included in the term for power, which is added to the equation of heat balance. Then, the temperature profiles can be obtained according to time and spatial distributions.

Electrical Resistance Heating

From a mathematical modeling viewpoint, the solution of electrical resistance heating provides a right-hand side term to the energy conservation equation. Baylor et al. (1990) used a simple method to predict power dissipation in a radial model in which power was described by a cumulative fraction of the total power ($\frac{P(r)}{P_0}$) dissipated in a reservoir zone within a specific radius:

$$\frac{P(r)}{P_0} = \frac{ln(r/r_w)}{ln(r_e/r_w)}$$

Eq. 1-1

where r_e is the reservoir outer boundary and r_w is the wellbore radius.

Later, due to faster electric field propagation than any other physical field in an oil reservoir, the heating-power distribution can be taken as a stationary field. In other words, the time derivatives in the electric equation can be dropped

The heating power density is defined as (Bogdanov et al., 2011a)::

$$P = \sigma|\nabla_r \upsilon|^2$$

Eq. 1-2

Electromagnetic Heating

The amount of dissipated power per unit volume can be approximated in several ways. A time-varying electric current in a linear antenna generates a circulating and time-varying magnetic field, which produces a circulating electric field according to Faraday's law. In return, the generated time-varying electric field produces a magnetic field described by Ampere's law. The cross-linked electric and magnetic fields propagate away from the current source. In the analytic modelling of MW heating, most of the work is done to predict a temperature profile in the range outside a heating source.

For a linear homogeneous medium, plane radiation propagating in the x direction will be absorbed according to the following relationship (Abernethy, 1976):

$$\frac{d\Phi(x)}{dx} = -\alpha\Phi(x)$$

Eq. 1-3

where $\Phi(x)$ is the power density and α is the absorption coefficient.

By the assumption of a cylindrical element due to the presentation of microwave at the center, the absorbed power by water can be estimated. An equation of power adsorption has been developed to describe the power density (power/area) in radial coordinates (Abernethy, 1976; Fanchi, 1990; Soliman, 1997):

$$\frac{d\Phi(r)}{dr} = -\left(\alpha + \frac{1}{r}\right)\Phi(r)$$

Eq. 1-4

The power $\mathrm{P}(r)$ is defined by the total radiated power in a cylinder of height h:

$$\mathrm{P}(r) = 2\pi r h \Phi(r)$$

Eq. 1-5

By combination with Eq. 1-5 and differentiating and integrating Eq. 1-4 in distance, the radiated power can be achieved:

$$\mathrm{P}(r) = P_0 e^{-\alpha(r-r_0)}$$

Eq. 1-6

In Abernethy's models with heat loss neglected, by the sum of radiation, convection of fluid flow and conduction, the energy balance can be established with the unit volume energy change to calculate temperature profiles. More studies have been carried out by using the simplified Maxwell's equations under the conditions of an electromagnetically linear and isotropic porous medium. Power attenuation has been calculated by the approximation of radiation field (Fanchi, 1990). Temperature is calculated by noting that it falls exponentially with radial distance from a source and its rate is proportional to the

power attenuation coefficient. In the region away from the electromagnetic source, Maxwell's equation can be reduced to (Eskandari et al., 2015):

$$\nabla \times E = -\frac{\partial B}{\partial t}$$

Eq. 1-7

$$\nabla \times H = -\frac{\partial D}{\partial t}$$

Eq. 1-8

$$\nabla \cdot D = 0$$

Eq. 1-9

$$\nabla \cdot B = 0$$

Eq. 1-10

where E and H represent electric and magnetic field intensities, and D and B are electric and magnetic flux densities, respectively.

With the simplifications of Maxwell's equations, the average dissipated power in volume unit was calculated as:

$$P_{ave} = \omega \varepsilon_0 \varepsilon'' E_{rms}^2$$

Eq. 1-11

where ω is the angular frequency ($2\pi f$), ε_0 is the permittivity, and ε'' is the loss factor.

By the assumption of cylindrical space with heat transfer in the form of convection and irradiation (conduction was neglected), a temperature distribution around a linear source was:

$$\frac{\partial T}{\partial t} = \frac{1}{2\pi r h\left[C_{p,r}\rho_r(1-\phi) + C_{p,o}\rho_o\phi(1-S_w) + C_{p,w}\rho_w\phi S_w\right]}\left[\frac{\alpha P_0 e^{-\alpha(r-r_0)}}{4.18} + \rho_o q_o C_{p,o}\left(\frac{\partial T}{\partial r}\right)\right]$$

Eq. 1-12

where r is the radius distance from the source, α is the attenuation coefficient per unit length, $C_{p,r}$ and ρ_r denote the rock specific heat and density, ϕ is the porosity, S_w is the water saturation, $C_{p,o}$ and ρ_o are the oil specific heat and density, and $C_{p,w}$ and ρ_w are the water specific heat and density, respectively.

The oil production rate may be estimated by taking into account the temperature effect on oil viscosity and developing a 1D expression for the density of heat sources (Abernethy, 1976; Davletbaev et al., 2011):

$$q = 2\alpha_d J_b \frac{r_d}{r} exp\left(-2\alpha_d(r - r_d)\right)$$

Eq. 1-13

where α_d is the damping factor of microwave, J_b is the intensity of radiation at a well bottom, and r_d is the radius of a microwave radiator.

Another approach of Lambert's equation was used to calculate energy absorption, in which reflections or interferences were neglected. Unfortunately, it was only applicable in semi-infinite cases (Ayappa, 1997).

1.3.2 Numerical modelling

In the simulation of a electrical resistance heating process, which is electrical heating under low frequency, four kinds of equations govern the phenomena: continuity, momentum, energy and electric charge conservation (Pizarro and Trevisan, 1990). The electrically enhanced oil recovery is a process of multicomponent and multiphase fluid flow in which temperature, saturation, mole fraction, pressure, and electrical potential in an oil reservoir need to be obtained (Killough and Gonzalez, 1986). In the electrical resistance heating process under low frequency, most of the approaches are reduced to an electrical dissipation problem that involves solving Ohm's law and the equation of electric current conservation (Lashgari et al., 2014).

A fully implicit 3D reservoir simulator has been developed to model the electrically-enhanced oil recovery process, in which an electrical current passes through a conductive oil-bearing formation and the electrical resistance heating increases temperature as well as reduces oil viscosity (Killough and Gonzalez, 1986). In this simulator, the rigorous modeling of physical phenomena includes: a treatment of resistivity as a function of temperature, water resistivity, and salinity; ability to simulate DC or multiphase AC electrical power; capability of handling vaporization of connate water with resulting effects on resistance and power levels; curvilinear, radial, or Cartesian grid systems and capability for horizontal electrodes and conductive fractures. The electrical heating of two phases (oil and water) flowing in an oil reservoir model has been developed in radial

coordinates (Pizarro and Trevisan, 1990). Baylor et al. (1990) compared the two modeling approaches: 1D single-phase flow radial power model and a 2D two-phase flow *r-z* power model. A modification of the commercial numerical reservoir simulator, TETRAD, has been achieved to simulate the process of electrical resistance heating in the frequency range from 2 to 60 Hz (Vinsome et al., 1994). The rate of energy generation per unit volume was calculated according to Joule's heating and electrical conductivity of an oil reservoir was approximated with the weights of the water phase and rock properties. Lashgari et al. (2014) implemented electrical Joule's heating in a four-phase (water, oil, emulsion and steam) reservoir simulator (UTCHEM) to model vaporization and condensation phenomena around a wellbore. In addition, two simplified models for a spatial electrical power distribution in a reservoir were proposed in the process of electrical resistance heating. In the radial power model, the power dissipation was a straight semi-log line given by Baylor et al. (1990). The *r-z* power model assumed 2D, single phase, low frequency AC electrical current.

Since electric current follows the path of least resistance, it is important to know the dynamic electrical properties and geology of an oil reservoir during the heating process (McGee and Vermeulen, 2007). Once the data is known, it is possible to control an electric field distribution to preferentially heat the entire oil sands using a voltage control strategy. This allows the heating process to be optimized throughout the entire life of a project, not just during initial conditions. Thus, the solution of an electric field distribution is critical to determine design issues such as injection rates into an electrode, the duration of heating and spacing between an electrode and a production well.

Another main aspect that receives much attention is the utilization of preheating of a reservoir by electrical heating, which is focused on the coupling of a well (an electrode) and its vicinity reservoir. A radial electrothermic model has been developed to calculate the currents resulting from the near-wellbore effects of high current densities (Todd and Howell, 1978). An electrical heating reservoir simulator has been developed with a full set of Maxwell equations accounting for all frequency ranges (Glandt and Hsu, 1992). Due to the deep deposition and high initial pressure of the reservoirs in Faja, conventional steam-based methods cannot be efficiently applied. A simulation model described by Eclipse Thermal was used to simulate the process of electrical resistance heating based on Orinoco Belt (Faja) in Venezuela (Rodriguez et al., 2008) to stimulate wells.

In an induction heating process, several inductors are attached to the bottom of a production tubing and positioned opposite to a pay zone. This system utilizes production casing as an inductively heated element to conduct heat into the zone surrounding a wellbore (Sierra et al., 2001). The induction heating takes place at frequencies of 10^{-3} to 1 MHz and the principle is based on eddy current generation in the mineralized connate water and its Joule's heating (Wacker et al., 2011). As a source of electric circuit, a medium frequency converter, depending on reservoir properties, feeds a capacitive compensated inductor, which is installed in the reservoir as a loop (Mustafina et al., 2013). As no contact is needed to generate the currents, neither brine injection nor well stimulation is necessary (Wacker et al., 2011).

A mathematical analysis of inductive heating can be quite complex. Electrical energy in the eddy currents is converted into heat along these pathways because of the electrical

resistivity of connate water, which contains a large number of ions resulting from dissolved salts (Ghannadi et al., 2014). Inductive heating is based on the Joule's effect of the eddy currents and eddy loss is based on displacement currents. AC flowing through a coil generates an alternating magnetic field that passes through an oil reservoir, and the eddy currents dissipate energy and cause heat in a phenomenon called 'eddy current loss'. This loss only propagates in a conductive medium. There is another loss which is called 'displacement loss', which propagates in both conducting and non-conducting media. Eddy current loss is caused by conductive current and displacement loss is caused by displacement current.

Most of the studies on RF/MW heating for heavy oil recovery were conducted based on simulation and modeling (Bera and Babadagli, 2015). Several attempts were made on the propagation of microwaves through a porous media for the purpose of reservoir delineation. To explain the behavior of microwaves, one may use Maxwell's equations that contain Faraday's law, Ampere's law and Gauss' law. Typical multilayered oil sands where the electrical properties may vary from layer to layer by orders of magnitude have been modelled by a developed 2D simulator, MEGAERA (Hiebert et al., 1986).

An algorithm was proposed to achieve reasonable accuracy through the integration of a Finite Difference Time Domain (FDTD) based solver with CMG's STARS reservoir simulator (Pasalic et al., 2014). In this approach, the microwave field distribution was obtained by solving Maxwell's equations in the discretized domain used by the FDTD-based solver:

$$\nabla \times \vec{H} = \varepsilon_0 \varepsilon_r \frac{\partial \vec{E}}{\partial t} + \sigma \vec{E}$$

Eq. 1-14

$$\nabla \times \vec{E} = \mu_0 \mu_r \frac{\partial \vec{H}}{\partial t} + \sigma^* \vec{H}$$

Eq. 1-15

where $\vec{H}$ and $\vec{E}$ are the magnetic and electric field vectors, ε_0 and μ_0 are the permittivity and permeability of a medium, ε_r and μ_r are the relative permittivity and permeability of the medium, and σ and σ^* are the electrical and magnetic conductivities, respectively.

Because of expensive calculations involved in solving Maxwell's equations and the energy equation simultaneously, a simplified solution has been achieved by the recognition of vastly different propagation time of a microwave field and fluid/thermal transfer. In a field case, only nanoseconds are required to establish a microwave energy distribution, while hours, days or years are required by fluid/thermal flow. Thus, in the simulation process, the total time was divided into user-defined time steps, in which CMG SATRS calculates the flow of fluids in an oil reservoir, temperature distribution and changes of reservoir conditions and the temperature and brine distributions were used by the FDTD-based solver to calculate microwave heat generation. Next, the heat generation was fed to CMG STARS to continue the next time step.

Harris Corporation offers a proven solution, Coupled Electromagnetic Reservoir Simulator (CEMRS), to evaluate the use of a RF/MW heating technology for heavy oil and oil sand reservoirs. Typical areas of collaboration are: core sample characterization, system architecture assessment, reservoir analysis and process development, reservoir characterization, reservoir model development, process development and economic assessment (Linkewich, 2014).

As a summary, Table 1.7 collects the methods of numerical simulation on electrical heating processes. According to these methods, it is found that the most popular method used by people is coupling of an electromagnetic simulator, such as COMSOL, and a reservoir simulator, such as CMG STARS. Besides, there are some simulators developed which can only be applied for a simple calculation of fluid flow in an oil reservoir, such as a single-phase flow. Thus, the motivation of this work was to develop a single simulator that is capable of modelling all electrical heating processes for heavy oil and oil sands thermal recovery. This is mainly to avoid the necessity of using two simulators, one for the electrical heating (especially in the case of EM, such as COMSOL) and one for the phase behaviour and multiphase fluid flow (such as CMG STARS). The computational overhead and complexity of swapping data back and forth was to be avoided if a single, comprehensive simulator is developed. Also, it has not been possible until now to model all three electrical heating processes in a single model and this enables a direct comparison of the different methods to be made.

Table 1.7 Table of the literature on numerical simulation methods of electrical heating

Heating method	Reservoir simulator	Electro-magnetic simulator	Coupling method	References
Electric heater	CMG, STARS		-	Hascakir et al., 2010
Electric heater	Eclipse Thermal		-	Rodriguez et al., 2008; Zhong et al., 2015
Electric heater	CMG, STARS		-	Gasbarri et al., 2011
Resistive heating	MEGAERA		-	Hiebert et al., 1986
Resistive heating	Developed 2-D, two-phase numerical model		Superposition in space was obtained to predict potential distribution.	Pizarro and Trevisan, 1990
Resistive heating	MEGAERA 4.0		MEGAERA solves the heat generation by current flow through reservoir, heat transfer by conduction and convection under single, impressible oil phase flow.	Sumbar et al., 1992
Resistive heating	Developed model		Developed compositional, three-phase model, in which oil is only in liquid phase.	Wadadar and Islam, 1994
Resistive heating/ Inductive heating	TETRAD		Treatment of electrical conductivity as a function of temperature, salinity and saturation.	Vinsome et al., 1994; Vermeulen and McGee, 2000
Resistive heating and inductive heating	CMG, STARS		-	Sierra et al., 2001
Resistive heating	CMG, STARS		-	Rangel-German, 2004
Resistive heating	CMG, STARS		-	Das, 2008
Resistive heating	CMG, STARS		-	Koolman et al., 2008
Resistive heating	CMG, STARS		-	Wang et al., 2008
Resistive heating	CMG, STARS	COMSOL	STARS solves the energy and component transports and COMSOL computes instantons heating power distribution.	Bogdanov et al., 2011a; Bogdanov et al., 2012; Bogdanov et al., 2014;
Resistive heating	CMG, STARS		Microwave heating is modeled using the SATRS by assigning a constant heating value to each block.	Bogdanov et al., 2011b
Resistive heating	CMG, STARS		-	Zhu et al., 2013
Inductive heating	CMG, STARS	ANSYS	SATRS contains detailed geophysical information, ANSYS computes heat sources based on electrical configuration and geology. ANSYS was capable to simulate steady-state, time transient, time-harmonic low frequency electric and magnetic field studies.	Koolman et al., 2008; Mustafina et al., 2013
Inductive heating	CMG, STARS	ANSYS	ANSYS is used to giver the behavior of inductor and of temperature distribution in reservoir.	Wacker et al., 2011
Radio-Frequency heating	FDTD electromagnetic numerical modeling technique		FDTD electromagnetic numerical modeling technique is used to present specific power absorption pattern data	Kasevich and Price, 1997
Microwave heating	TERASIM		TERASIM is a 3-D, 3-phase (oil, water and gas) finite difference simulator.	Sahni et al., 2000
Microwave/Radio-Frequency heating	CMG, STARS		-	Ovalles et al., 2002
Microwave/Radio-Frequency heating	COMSOL		COMSOL is used to simulate single-phase flow in a reservoir when EM source is applied.	Carrizales and Lake, 2009
Radio-Frequency heating	COMSOL		Electrical parameters were calculated on a computer with MATLAB and COMSOL simulated reservoir behavior.	Godard and Rey-Bethbeder, 2011

Radio-Frequency heating	CEMRS (coupling of electromagnetic simulator and reservoir simulator)		-	Linkewich, 2014
Radio-Frequency heating	CMG, STARS	Solving Maxwell's equation and heat generation by FDTD	STARS calculates the flow of the fluids in the reservoir, temperature distribution and change of the reservoir conditions. Obtained temperature and salinity concentration distributions are used to calculate wave field distribution.	Pasalic et al., 2014
Microwave/Radio-Frequency heating	Eclipse	Solving Maxwell's equation by FDTD	Electro-magnetic wave propagation is solved numerical.	Katterbauer et al., 2015

1.4 Comparison of electrical heating to steam injection processes

Thermal methods for heavy oil and bitumen recovery include the injection of steam in the form of SAGD, CSS and steam flood, whereby thermal energy is transferred to oil, reduces its viscosity and allows it to flow towards a production well. These methods have not been yet investigated for the large fraction of oil sands for thinner, less permeable, heterogeneous reservoirs or connected by water. Electrothermal methods have attracted more attention as an alternative to conventional thermal methods for the difficult reservoirs where conventional thermal methods are not expected to work well (Wang et al., 2008).

The comparative studies of electrical resistance heating and SAGD have been conducted by using CMG's STARS on the types of marginal bitumen reservoirs, such as a thin pay zone and a thin pay zone with thick bottom water and low permeability. Simulation results showed the potential of electrical resistance heating to recover bitumen from a pay zone of 5 m thickness, where SAGD is not applicable. Furthermore, a pay zone with a thick bottom water layer cannot be recovered by SAGD, and electrical resistance heating can produce 14% bitumen from a reservoir with an equivalent Steam-to-Oil Ratio (SOR) of 4.6. Due to the limitation of a low

permeability reservoir on SAGD application, oil production is significantly decreased with low permeability. Fortunately, low permeability has a small effect on the electrical resistance heating process. By the simulation of a reservoir with 300 md, electrical resistance heating can recover 12% of bitumen, while only 2% of bitumen is produced by SAGD (Wang et al., 2008). In the application of Microwave-Assisted Gravity Drainage (MWAGD), due to the speedy heat transfer by MW heating, MWAGD is less time consuming than SAGD or any other conventional thermal methods. Also, MWAGD does not cause any consequential damage and provides greater oil displacement efficiency (Jha et al., 2011). By the comparison of a ratio of incremental oil recovered with respect to energy input, a homogeneous reservoir model has an averaged ratio of 62 kWh/bbl, while a heterogeneous model has an averaged ratio of 80 kWh/bbl. For an average SOR of 3 and for 225°C steam (in-situ), the electricity demand per barrel of bitumen produced for an In-situ Reflux (ISR) process is about 268 Wh/m (Harding et al., 2016). Thus, with electrical heating in a reservoir, the heterogeneity does not significantly affect the overall energy efficiency compared to a steam injection process (Rangel-German et al., 2004).

Most of the MW heating cases were designed like a SAGD well pair. A comparative study was carried out by using CMG STARS based on Athabasca McMurray oil sands. In this reservoir model, electrodes were placed in a triangular form and each electrode was connected to a three-phase power delivery system. Three types of reservoirs were simulated. For a 5m pay zone, results showed a higher oil production rate in the case of MW heating than the steam injection process. For a 15m pay zone with bottom water, MW heating recovered 14% of bitumen after 14 years whereas SAGD only recovered 1%. Under favourable conditions, MW heating has

potential to recover heavy oil/bitumen from thin and low permeability reservoirs (Wang et al., 2008).

Despite there being a wide application of steam based heavy oil/oil sands reservoirs recovery methods, they still have challenges which can be solved by electrical heating processes. Steam needs to be introduced into a reservoir under pressure and temperature following its saturation curve to prevent condensation at a well toe. The typical range is between 200 to 250 ℃, which is far above the required temperature to move oil. This overheating leads to much heat loss through overburden and underburden. In some cases, top/bottom water or top gas exists in oil sand reservoirs and in such reservoirs the steam injection process is negatively affected when a steam chamber is in touch with these regions resulting in significant heat loss (Wacker et al., 2011).

1.5 New Technologies in Electrical Heating Processes

1.5.1 Electro-Thermal Dynamic Stripping Process (ET-DSP)

Due to the preference of electric current flow from the ends of an electrode placed in oil sand reservoirs, there will be great heating at the ends. Consequently, as the temperature of a medium increases, the electrical conductivity also increases with the results of more current leaving the ends. Since the power density is proportional to the square of the current, the water vaporization of rapid overheating at the ends reduces input power. Commercially available mineral-insulated (MI) cables are used as self-contained electric resistive heaters (Afkhampur, 1985). In this method, electric current flows through the conductors packed with graphite and polymers. As heater temperature increases, electrical resistance of the mineral insulation increases, and thus a self-regulating mechanism is achieved to prevent the overheating.

The Electro-Thermal Dynamic Stripping Process (ET-DSP) was proposed to solve the problem of non-uniform heating (McGee and Vermeulen, 2007). In ET-DSP, water is injected at a relatively low rate (about 1m^3/d per electrode) into the ends of electrodes where the power density is the greatest to prevent vaporization. Instantaneous control of power to each electrode enables maximum power to be delivered to oil sands without electric current stealing. Three periods were included in ET-DSP: a preheat phase, a production period and production with turning off heating. From simulation results, ET-DSP offers several advantages over steam injection processes in heating an oil reservoir: rapid and uniform heating without the need of fluid injection, and increased pressure and energy of a reservoir prior forces mobilizing oil flow to a production well. However, a large number of wells drilled to implement the ET-DSP due to a limited heating distance may impair the economics of the process. From September 2006 to August 2007, a proof of the concept test of ET-DSP was completed by E-T Energy Ltd. in the Athabasca oil sands (Mcgee, 2008; Mcgee et al., 2008). Production performance achieved includes additional in-situ thermal recovery, high thermal efficiency, and more than 75% in final oil recovery. Lessons learned may allow further advancement of the ET-ESP process, such as utilization of PCP for artificial lift and redesigned electrode well completion.

1.5.2 Solvent/Gas additive in resistive heating

A combination of electrical resistance heating and Vapor Extraction (VAPEX) has been proposed to enhance horizontal well efficiency and an overall oil production rate. A well pattern similar to that in SAGD was used, and an electrode was placed along with a producer or injector and solvent was injected from an injector (Zhu et al., 2012). Three features were involved in this process: (1) good heat communication established between the injector and producer; (2) the

horizontal well conformity can be improved by the electrical resistance heating and (3) solvent can reduce the viscosity of heavy oil in the unheated zone where electrical resistance heating cannot reach. CMG's STARS was used to evaluate the performance of the hybrid electrical resistance heating and solvent injection. Through a sensitivity analysis, an electrode was placed along with the upper injector to prevent much heat loss to underburden, a better oil recovery process than VAPEX was achieved and the new method had a better result with heterogeneous reservoirs than VAPEX.

The effect of gas injection on a MW heating process was investigated by introducing gases, such as N_2, CO_2, flue gas and hydrocarbon gas, at the same time with electrical resistance heating to recover heavy oil. Parallel horizontal wells or combination of upper vertical and lower horizontal wells were used as electric dipoles in this process (Chakma and Jha, 1992). Gas was injected through the upper well and heated oil was collected at the lower well. Experiments based on Bohai oilfield, China showed a larger heating chamber of gas additive than that of only electrical resistance heating. The oil rate of a gas additive process was similar to that of the process of conventional SAGD. With an oil viscosity reduction with gas dissolution, heat loss decreased by gas accumulation at the top of an oil reservoir, maintenance of high reservoir pressure, and an enlarged heating chamber, the gas additive process seemed better than the electrical heating process alone (Zhong et al., 2011; Zhong et al., 2015). Simulation with propane injection was performed with the results that gas injection has little effect on oil production, when the reservoir pressure is higher than the bubble-point pressure (Rangel-German et al., 2004).

A method including three stages was proposed to combine RF heating and solvent injection for viscous oil recovery (Davletbaev et al., 2007). The first stage is injection of a miscible solvent

into a production well with the simultaneous treatment of a bottomhole zone by an RF field. The second is the oil production and the third stage is the continuous production without RF heating. Simulation results show that the greater the ratio of the oil and solvent viscosities, the more intense the process of oil and solvent mixing in the bottomhole zone. The necessary dynamics of temperature variation in a wellbore can be achieved by choosing the optimal combination of EM radiator power and bottomhole pressure.

1.5.3 Thermal solvent reflux

To improve the production performance of SAGD, electric heaters are installed inside two wellbores and used to develop a solvent-assisted process for recovery of heavy oil from thick, cold reservoirs (Ivory et al., 2010). Solvent is injected through the upper well and the oil is produced from the lower well together with heating inside the two wellbores. Under the heating, the in-situ recycle of solvent can be achieved through the reboil of solvent to accelerate solvent dissolution in the oil phase. Two experiments using Hillmond oil show the similar oil rate and recovery of the thermal solvent reflux (electric heater) and steam-solvent hybrid (steam injection) processes. In thermal solvent reflux, without steam injection, some benefits can be achieved by an in-situ solvent recycle: less heat requirement, lower emissions, a smaller solvent recycle plant on the surface, no need of water injection, no need of boiler feed water treatment and minimal oil/water separation facilities.

1.5.4 Electromagnetic Steam-Assisted Gravity Drainage (EM-SAGD)

EM-SAGD used a medium-frequency electric field in the range of 1 to 200 kHz by running an EM loop along the SAGD well-pairs to heat up bitumen (Wacker et al., 2011). The electrically inductive process was simulated by the coupling of the finite element software ANSYS and

CMG STARS. An improved technology was proposed by the combination of EM heating and SAGD, EM-SAGD. The EM-SAGD showed better oil production and lower energy consumption when compared to SAGD. With the varying frequency from 60 Hz to 300 MHz for a thick reservoir, the simulation results showed 10% more oil was recovered after 20 years operation than SAGD. The increase is more significant for a thin reservoir at around 38% in recovery improvement (Koolman et al., 2008). However, the promising EM-SAGD was limited due to the lack of a technology for drilling horizontal wells that can be drilled upward and end at the surface (inductors must be drilled horizontally and end at the surface for creating a closed loop for feeding a subsurface coil from a converter located at the surface) and the need of expensive fiberglass casings (Ghannadi et al., 2014).

1.5.5 Tight-Shell Design

Due to the microwave problems of extremely high temperatures at the well containing a radiating element and the strong dependence of temperature profiles on local variation of reservoir material properties, solutions have been proposed involving insertion of a tight shell made of a low dielectric material around a radiating well and by selecting the proper irradiation frequency (Bientinesi et al., 2013). Numerical and experimental studies confirmed the capability of a low loss material shell in efficiently lowering the temperature near the well and reaching uniform heating of a large volume of an oil reservoir.

1.5.6 Nano-particle Addition

The investigation of extent of thermal alterations of crude oil properties due to MW irradiation has been done through experiments. In a region near a wellbore, MW irradiation can be used to remedy wellbore problems that are temperature dependent (Gunal and Islam, 2000). In the

process of heavy oil recovery, high efficiency is needed to be achieved by producing all components present within the oil, such as asphaltenic components. The nano-size metal particles have been utilized to enhance a MW heating process with the catalyst breaking of carbon-sulfur bonds within asphaltenic components (Greff and Babadagli, 2013). With this method, oil viscosity was dramatically reduced by a decrease in the average molecular weight. Nickel has been demonstrated to yield a better recovery than iron and iron oxides, especially in high energy cases.

Nano-metal oxides were well-known to have the potential to absorb microwaves and increase system temperature. Experiments have been conducted to investigate the effect of nano-metal oxides on a MW heating process in glass beads saturated with crude oil in presence of iron oxides, copper and nickel (Greff and Babadagli, 2013). Nickel showed the best performance of these three materials with a significant recovery increase at a lower microwave power. On one hand, oil viscosity was reduced with metal oxide nano-powder by the addition of metal nano-particles to a certain limit due to attraction of maximum asphaltene molecules on the metal surface, making the bulk oil less viscous. On the other hand, with an increase in metal ion concentration, the structural complexity of asphaltene molecules was increased through coordination reactions and the oil viscosity was increased (Shokrlu and Babadagli, 2011). Under MW heating, the nano-metal oxides absorbed microwave and generated heat to increase temperature.

1.5.7 Enhanced/Effective Solvent Extraction Incorporating EM Heating (ESEIEH)

Recently, a technology was developed by a consortium consisting of several oil companies: The Harris Corporation of Melbourne Florida, CNOOC limited/Nexen Inc., Devon Canada and

Suncor Energy Inc. In ESEIEH, a familiar horizontal well pair commonly used in Canadian oil sands is used and the process couples an RF antenna with solvent injection, such as butane and propane. Due to a combination of solvent injection and RF heating, there is no need to have a steam plant and no water treatment, gas emission is reduced and fuel costs are decreased. In Phase 1, conducted in January 2012, there was a successful completion of a 12.5m horizontal heating experiment at Suncor mine. In Phase 2 commencing in early 2015, the ESEIEH consortium continued to test a 100m lateral horizontal RF heater and solvent injector start-up in a 150 m deep Athabasca oil sand reservoir.

1.5.8 Electromagnetic-Flood process

The concept of Electromagnetic-Flood (EMF) process was proposed by McPherson et al. (1985), in which horizontal wells are used as waveguides to generate a heat front penetrating into a formation, thereby generating a hot zone of low-viscosity bitumen which is suitable for in-situ recovery. In this method, horizontal wells are drilled at the bottom and near the top of a pay zone to serve as injectors and producers, as well as high-frequency electrodes. Attaching a high-frequency power source between the upper/lower electrode pairs will result in the generation of an EM wave travelling from the source horizontally into the pay zone, and the generation of a heat front which also moves horizontally into the pay zone area. This moving heat front induced by the EM wave is referred to as EMF. To accelerate oil production, an additional displacement factor, such as gas injection at the top of a reservoir, is used to supplement steam generation inside the reservoir from the connate water. Numerical simulation results showed that it is possible to obtain a heated-up region to 200m length with an average temperature of 100 ℃ and a total production rate by gravity drainage of 0.15 m^3/day.

1.5.9 Ceramic Material Addition

An artificially created medium converting the emitted EM power into heat was proposed by addition of materials, such as ceramics, that could positively interact with RF/MW emission (Okassa et al., 2010). In this method, the absorbed RF/MW energy is converted into heat within the material, resulting in an increase in temperature. By removing water from the material, RF/MW radiation could heat the ceramic up to very high temperature, over 1400 ℃ (Sutton and Johnson, 1980). Simulation studies showed that the ceramic materials placed in an oil reservoir via hydraulic fractures and under an EM field could considerably increase oil temperature. The system is expected to have low energy consumption and has a minimal impact on the environment.

1.5.10 Cylindrical Conductor Array Equivalent Heating

In the process of RF/MW heating, a substantially uniform electric field can be achieved by the application of voltage between two buried parallel plates with dimensions greater than the distance separating the plates. Leakage fields or radiation can be suppressed with a triplate line configuration – three parallel plates are buried in a deposit and the middle plate is excited. In practice, a cylindrical conductor array, rows of buried tubular conductors, is a practical application of the triplate configuration obtainable with conventional drilling techniques. With adherence to specific design requirements, this arrangement can retain the desired energy confinement and uniformity in properties of the flat plate configuration (Sresty et al., 1986).

1.5.11 In-situ Reflux

The In-situ (steam) Reflux (ISR) process is a novel, efficient and effective way to deliver electricity energy as a heat source to a bitumen or heavy oil reservoir (Harding et al., 2016). In

the concept of ISR, it is included that vaporization of formation connate water into steam and that rises od steam in a formation forms a steam chamber above the heater well similar to the steam chamber formed in SAGD. Latent heat loses to the surrounding formation matrix, connate water and bitumen, as the steam rises it. As a consequence, steam condensate and heated bitumen of low viscosity travel downward by gravity where, as these fluids approach the ISR heater well. These fluids encounter the formation in vicinity of the well, in which temperatures above the saturated steam temperature under certain pressure and the water is re-vaporized and 'refluxed' back into the steam chamber by density difference. Heated bitumen continues its downward path towards the lower production well (Harding et al., 2016).

1.6 Motivations and Objectives

Great efforts have been given to the studies of methods in modelling electrical heating processes for oil sand reservoirs recovery over the recent decades. However, there is a limited number of publications that have focussed on effective modelling of the electrical heating processes and determination of the effectiveness of electrical heating methods.

In particular, numerical studies of EM heating in oil reservoirs have been reported for coupling of EM waves and thermal reservoir models. Beer-Lambert's power formulation was reported and widely used as a tool to model power distribution at a distance from an EM source into a far field cold oil reservoir. An absorption coefficient, which was inaccurately assumed as a constant, was reported as a critical parameter for controlling efficiency of the heating process (Kislitsyn and Nigmatulin, 1991; Carrizales et al., 2010). Simple coupling of EM wave propagation and reservoir fluid flow simulation of the ESEIEH process predicted the temperature response in the vicinity of an antenna (Sadeghi at al., 2017a). In most numerical simulation methods, exchange

of EM reservoir heating estimates is made with a thermal reservoir flow simulator, such as CMG STARS, which is used to model the multi-phase flow and phase behaviour in a reservoir (Figure 1.1). An EM field solver, such as COMSOL or ANSYS HFSS, is applied to solve for EM wave distributions; these models are run independently to simulate the process of EM heating and then coupled to the fluid flow simulation model through an interface program. Helmholtz's equations for the electric field based on a homogeneous reservoir (Eq. 1-1) with respect to dielectric properties were frequently used in the literature for modelling of EM wave distribution in oil reservoirs (Sadeghi et al., 2017b). The derivation of Eq. 1-1 shows that it is not capable of solving EM waves in a medium with inhomogeneous dielectric properties, such as oil sands with dynamic saturations with time under heating (Ovalles at al., 2002). These simplifying assumptions for wave propagation through a medium can result in inaccurate prediction of heating and oil production performance (Fanchi, 1990; Sadeghi et al., 2017b).

$$\nabla \times \nabla \times \vec{E} = -j\omega\mu\left(\sigma\vec{E} + j\omega\varepsilon\vec{E}\right).$$

Eq. 1-16

In this study, a fully implicit 3D numerical modelling approach is used to simulate, in a single model, the fluid flow, fluid phase behavior, heat transfer and EM heating of inhomogeneous media comprised of space dependent dielectric properties. This single simulator avoids the computational overhead and complexity of swapping data back and forth between two simulators, as mentioned in Section 1.3.2.

This novel approach is based on deformation of Maxwell's equations for EM wave propagation in media with varying dielectric properties. By discretization of the Helmholtz equation for a

magnetic field, the capability of EM wave propagation between neighbouring grids is determined by properly averaging the dielectric permittivity and electric conductivity. The Helmholtz equation is solved by a Finite-Difference Frequency-Domain (FDFD) method for efficient simulation performance. A brief discussion on heating and production performance of EM heating in oil sands reservoirs is provided in this study. The simulation results demonstrate the feasibility of heating oil sands by application of EM waves because a desiccated zone is observed above the implemented antenna. This new simulation capability allows evaluation and optimization of EM heating combined for oil sands in-situ recovery.

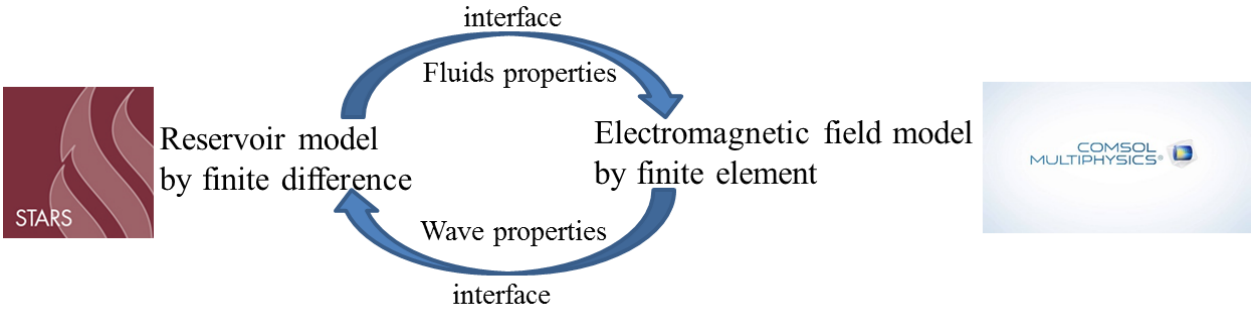

Figure 1.5 Illustration of data exchange of a reservoir simulator (CMG STARS) and an electromagnetic field simulator (COMSOL).

In this study, a single simulator will be provided to improve the ability of industry to model electrical heating processes more accurately and reliably to allow effective comparison amongst the process options that are available. The development and application of a new and comprehensive simulator for all electrical heating processes will be of great benefit. Based on the simulation results, a comparative evaluation of three electrical heating methods has been conducted including the following: heat generation mechanisms; a heat transfer process; oil production performance.

Chapter 2 Reservoir Simulation Under Electrical Heating

This chapter presents a discussion of the general reservoir model as well as equations used to model the new thermal processes of electrical heating. It includes the information of a general thermal reservoir model and describes its implementations. The first section of this chapter gives the governing equations of the electrical heating models. Then, the selection of the primary and secondary variables, the numerical solution methods, the technique to decouple the equations, and the procedure to eliminate the secondary variables are presented. The type of a linear solver used is presented in the following sections. This chapter also discusses handling of the phase change, heat transfer, time step control, numerical convergence, heat loss model, well model and the treatment of the electrically generated heat terms, which are all important in the thermal model.

2.1 Reservoir model

The numerical model used for the thermal reservoir simulation in this research is based on the following assumptions (Huang 2009; Dong 2012):

1. Phase equilibrium is reached immediately in control volumes.
2. Kinetic and potential energy are neglected in this model.
3. Convection and conduction heat transfer are considered during the simulation process.
4. Components are not absorbed by a rock surface and do not react with the rock.
5. The reservoir behaves as a closed boundary: fluids are restricted at outer reservoir model.
6. The multiphase Darcy’s flow equation is used to compute fluid flow in a porous media.

Based on these assumptions, the governing equations are constructed.

2.1.1 Mass and Energy Conservations

For an oil reservoir consisting of Nc components and Np phases, the mass conservation equation of component i can be described mathematically as (Chen et al., 2007; Huang 2009; Dong 2012):

$$\frac{\partial \sum_{p=1}^{Np}\left(\phi S_p \rho_p x_{p,i}\right)}{\partial t} = -\nabla\left(\sum_{p=1}^{Np} x_{p,i}\rho_p u_p\right) + q_{p,i}$$

Eq. 2-1

At reservoir conditions, the velocity of Eq. 2-1 is expressed by Darcy's law:

$$u_p = -\left(k\frac{k_{rp}}{\mu_p}\nabla\Phi_p\right)_{p=o,w,g}$$

Eq. 2-2

Combining Eq. 2-1 and Eq. 1-2 yields:

$$\frac{\partial \sum_{p=1}^{Np}\left(\phi S_p \rho_p x_{p,i}\right)}{\partial t} = \nabla\left(\sum_{p=1}^{Np} x_{p,i}\rho_p K\frac{k_{rp}}{\mu_p}\nabla\Phi_p\right) + q_i$$

Eq. 3-3

The energy balance includes heat conduction, heat convection and heat generation by electrical heating, and the energy conservation equation is integrated into the system as:

$$\frac{\partial}{\partial t}\left[\phi\sum_{p=1}^{Np}\left(S_p\rho_p U_p\right)+(1-\phi)U_r\right]=\nabla(K\nabla T)-\nabla\left(\sum_{p=1}^{Np}\rho_p H_p u_p\right)+\sum_{p=1}^{Np}q_{ssp}+q_{ELE}-q_{LOSS}$$

Eq. 2-4

Combining Eq. 2-4 and Eq. 2-2 yields:

$$\frac{\partial}{\partial t}\left[\phi\sum_{p=1}^{Np}\left(S_p\rho_p U_p\right)+(1-\phi)U_r\right]$$
$$=\nabla(K\nabla T)+\nabla\left(\sum_{p=1}^{Np}\rho_p H_p K\frac{k_{rp}}{\mu_p}\nabla\Phi_p\right)+\sum_{p=1}^{Np}q_{ssp}+q_{ELE}-q_{LOSS}$$

Eq. 2-5

where

$$\nabla\Phi_p=\nabla P_p+\gamma_p\nabla \mathrm{z}$$

Eq. 2-6

In terms of fluid flow in an oil reservoir, Darcy's law is used to express the three-phase flow velocities. The mole fractions of hydrocarbons in the gas and oil phases as well as the water mole fraction in the gas phase are governed by vapor-liquid equilibrium using temperature and pressure dependent K-values (Chen et al., 2006).

2.1.2 Constraint equations

In addition to the mass and energy conservation mentioned in the previous section, constraint equations as auxiliary ones are also implemented to have a closed system. These constrains include an overall saturation constraint equation in each considered domain and the mole fraction constraint equations for each phase by definitions as shown below:

(1) Volume constraint

$$\sum_{p=o,w,g}^{Np} (S_p) = 1$$

Eq. 2-7

(2) Mole fraction constraint

$$\sum_{i=1}^{Ni} (x_{p,i}) = 1$$

Eq. 2-8

(3) Phase Equilibrium Equations

Phase equilibrium equations are specified to describe the phase equilibrium behaviour under reservoir conditions. In this study, K-values are used to describe distribution of particular components in different liquid-gas phases. The definition of K-values is expressed as the equilibrium phase (gas to liquid) mole fraction ratio (STARS manual).

$$\hat{k}_{g,l,i} = \frac{x_{g,i}}{x_{l,i}}$$

Eq. 2-9

In Eq. 2-8, the K-value of component i in the phase gas (g) and phase liquid (l) is the ratio of the mole fractions of component i in these two phases.

K-values can be obtained by Equations-of-State (EOSs) or correlations. In this model, the following correlation (STARS manual) are used:

$$k_value = \left(\frac{kv1}{P} + kv2P + kv3\right)^{e^{\frac{kv4}{T-kv5}}}$$

Eq. 2-10

where P and T stand for pressure and temperature and kv1 – kv3 are the constant coefficients obtained from input files. As stated in CMG STARTS manual, constant coefficients in the model indicate that the K-values are independent on any other component mole fractions that exist in the system. They are only the functions of pressure and temperature.

Data on each K-value can be entered by interpolation of values from tables or by equations. The heavy hydrocarbon component and water K-values are pseudo K values defined as (Crookston et al., 1979):

$$k_{g,l,i} = \hat{k}_{g,l,i}\left(\frac{S_l}{S_l + S_l^*}\right)$$

Eq. 2-11

The terms in the brackets in Eq. 2-11, are nearly 1.0, except when So or Sw approaches zero (phase disappearance).

The rationale involved in the pseudo K-values has been discussed regarding $k_{g,l,i}$. When a liquid water is present, y5, which is the mole fraction of steam in gas phase, is determined by the local temperature and pressure due to phase equilibrium. However, once there is no liquid water phase by vaporization, phase equilibrium is no longer available to give y5 in terms of other dependent variables, and the mass conservation equation of water have to be rewritten into using steam composition in the gas phase, as one dependent variable, instead of water saturation. The pseudo K-value expressed in Eq. 2-11 avoids dealing with two-problem formulations and switching from one to the other as the liquid water phase vaporized and condensed.

This approximation incurs a slight inaccuracy when the liquid water phase exists, and water saturation is lower than a certain value. This method allows the three-phase formulation to extend into the water disappearance region. Based on results from several tests, negligible numerical difficulties have been found in the use of this pseudo-K value and thus far has worked well (Crookston et al., 1979).

2.1.3 Variable Section

To easily construct a Jacobian matrix , "natural variables" $\left(P, T, S_p, x_{p,i}\right)$ are selected as independent variables in the development of the simulation model in this research(Huang 2009; Dong 2012).

The total independent number of variables for a control volume is Nc + Np + 2. The other variables included in the simulation processes are the arbitrary combinations of these independent variables (Huang 2009; Dong 2012).

2.2 Reservoir Characterization

2.2.1 Rock Properties

The effect of compressibility and thermal expansion of the rock on porosity have been considered in this model. Those properties are given by the correlation:

$$\phi = \phi_0 e^{(P-P_0)C_{rP}-(T-T_0)C_{rT}}$$

Eq. 2-12

where ϕ_0 is the porosity of the control volume at the reference pressure P_0 and reference temperature T_0.

Rock thermal capacity is estimated as a constant value. Therefore, the internal energy of rock matrix is expressed as:

$$U_r = C_r(T - T_0)$$

Eq. 2-13

where, C_r is the heat capacity of rock.

2.2.2 Fluid Properties

to establish a process if efficient simulation, thousands of various components of bitumen are lumped into several pseudo-components. The properties of gas, aqueous and oleic dependent on the pseudo-component fluid properties in the gas and liquid phases.

The component I in a liquid phase and its liquid mole density is dependent on the reference mole density, compressibility, thermal expansion coefficient, and local pressure and temperature:

$$\rho_{p,i} = \rho_{p,i,P_0,T_0} e^{(P-P_0)C_{LP,i}+(T-T_0)C_{LT,i}}$$

Eq. 2-14

where, $C_{LP,i}$ is the liquid compressibility of the component i and $C_{LT,i}$ stands for the liquid thermal expansion coefficient of the component i.

The mixing rule of molar density of the liquid mixture is considered as:

$$\rho_p = \frac{1}{\sum_{c=1,2,3\ldots} x_{p,i}\rho_{p,i}}$$

Eq. 2-15

For the molar density of a gas phase, an equation of state (EOS) is applied to estimate the Z factor. Then the gas phase molar density is calculated by:

$$\rho_g = \frac{P}{ZRT}$$

Eq. 2-16

where, R is the universal gas constant.

The Redlich-Kwong EOS is used to estimate Z factor, the cubic equation in the polynomial format shown as below and Z is the largest root of:

$$Z^3 - Z^2 + (A - B^2 - B)Z - AB = 0$$

Eq. 2-17

where,

$$A = 0.42748\left(\frac{P}{P_c}\right)\left(\frac{T}{T_c}\right)^{2.5}$$

Eq. 2-18

$$B = 0.08664\left(\frac{P}{P_c}\right)\left(\frac{T}{T_c}\right)$$

Eq. 2-19

Critical P and T (in absolute units) are estimated by composition of gas phase and Redlich-Kwong mixing rules, assuming zero in interaction coefficients:

$$T_c = \left(\frac{a^2}{b}\right)^{2/3}$$

Eq. 2-20

$$P_c = \frac{T_c}{b}$$

Eq. 2-21

$$a = \sum_{i=1}^{N_c} y_i\, T_{ci}\sqrt{T_{ci}^{1/2}/P_{ci}}$$

Eq. 2-22

$$b = \sum_{i=1}^{N_c} y_i\, T_{ci}/P_{ci}$$

Eq. 2-23

The water phase viscosity is estimated according the flowing equations:

$$\mu_w = 0.0047352e^{\frac{1515.7}{T}}$$

Eq. 2-24

The gas viscosity is calculated by the following equation:

$$\mu_g = 0.0136 + 3.8 \times 10^{-5}T$$

Eq. 2-25

This method is very quick in calculation and is very often quite sufficient, for the reason that the compositional effects on μ_g are small (CMG STARS, 2017).

The composition dependent oil viscosity may be specified using the following option:

$$\mu_{oi} = a_i e^{\frac{b_i}{T}}$$

Eq. 2-26

The oil phase viscosity is then obtained by a logarithmic mixing rule:

$$ln(\mu_o) = \sum_{i=1}^{N_c} x_{oi} ln(\mu_{oi})$$

Eq. 2-27

The correlations used to describe the enthalpy of the liquid and gas phase are based on liquid heat capacities:

$$CPL(T) = cpl1 + cpl2 \cdot T + cpl3 \cdot T^2 + cpl4 \cdot T^3$$

Eq. 2-28

$$HL(T) = \int_{TEMR}^{T} CPL(T)dT$$

Eq. 2-29

where, $TEMR$ is the temperature of liquid phase and $HL(TEMR) = 0$.

If $(T_c > T)$,

$$HVAP(T) = hvr \cdot (T_c - T)^{ev}$$

Eq. 2-30

$$HG(T) = HL(T) + HVAP(T)$$

Eq. 2-31

Otherwise,

$$HG(T) = HL(T)$$

Eq. 2-32

The internal energy is estimated by enthalpy minus work by pressure:

$$U_p = H_p - \frac{P}{\rho_p}$$

Eq. 2-33

2.2.3 Rock/Fluid Properties

According to the Stone II (Stone, 1973) model, three phase relative permeability provided by Aziz and Settari modification (1979) is used in this thesis for the modelling of water, oil and gas flow in an oil sand reservoir. The following assumptions have been made in this model (Dong, 2012):

(1) The relative permeability of water in the oil-gas-water system is equal to the water relative permeability in the oil-water system. The water permeability only depends on the water saturation Sw.

(2) The relative permeability of gas in the oil-gas-water system is equal to the gas relative permeability in the oil-gas system. The gas permeability only depends on the gas saturation Sg.

(3) The relative permeability of oil depends on the water and gas saturations.

Three-phase oil relative permeability is calculated by using the following equations:

$$k_{ro} = k_{rocw}\left(\left(\frac{k_{row}}{k_{rocw}} + k_{rw}\right)\left(\frac{k_{rog}}{k_{rocw}} + k_{rg}\right) - k_{rw} - k_{rg}\right)$$

Eq. 2-34

where, $k_{rg} = k_{rg}(S_g)$ and $k_{rw} = k_{rw}(S_w)$. k_{rocw} is the relative permeability to oil at connate water and zero gas saturation.

2.2.4 Dielectric Properties of Oil Sands

The response of an oil reservoir to electrical excitation can be characterized in terms of its electrical properties (Chute and Vermeulen, 1979). Dielectric properties of the material vary with the fluid content of the reservoir, applied frequency and temperature, and can be measured in the laboratory or in the field with special equipment (Kim, 1987; Kasevich et al. 1994).

Archie's law specifies the variation of reservoir electric conductivity with water saturation and temperature. The electrical conductivity of water depends on the water phase composition and temperature, which can be estimated.

The Archie's law is used in current work which reads as (Godard and Rey-Bethbeder, 2011; Swiech et al., 2013; Lashgari et al., 2016):

$$\sigma = \sigma_w(T)\frac{\phi^m s_w^n}{a}$$

Eq. 2-35

$$\sigma_w(T) = \sigma_{w0}\frac{T - 251.65}{T_0 - 251.65}$$

Eq. 2-36

where σ_w is the water conductivity and ϕ is the porosity. The exponent m is represents the effect of the porous geometric structure and the value of n shows the effect of connectivity of the water phase, and thereby to the wettability of the oil reservoir on electrical conductivity. The following values have been assumed: m is 1.37, n is 2.0 and a is 0.88 (Lashgari et al., 2014).

Oil sands do not exhibit magnetic behaviour; therefore, it is accepted that the magnetic permeability of the medium is the same as that of a vacuum ($\mu = \mu_0$) (Kim, 1987; Chute and Vermeulen, 1979).

Microwave engineering requires precise knowledge of electromagnetic properties, particularly dielectric properties of materials at microwave frequencies (Chen et al., 2004) since the dielectric properties of the materials determine the success of application of microwaves. These properties are defined in terms of dielectric constant (ε') and loss factor (ε") (Meissner and Wentz, 2004). A dielectric is a non-conducting substance, i.e. an insulator whose permittivity is given by:

$$\varepsilon = \varepsilon_r - j\varepsilon_i$$

Eq. 2-37

Permittivity is defined as a complex number. In the application in engineering, it is very common to use permittivity in terms of its relation to permittivity of free space:

$$\varepsilon = \varepsilon_0 \varepsilon_r$$

Eq. 2-38

where, ε_0 is the permittivity of free space, $8.8541887817 \times 10^{-12}$.

In some simulation work, the relative permittivity of oil sands is assumed at a constant value without variation under changing in temperature, saturations or applied frequencies (Fanchi, 1990; Godard and Rey-Bethbeder, 2010).

Chute and Vermeulen (1979, 1990) conducted several laboratory measurements of the electrical properties of the Athabasca oil sand in Alberta. Samples with different densities and moisture content were analyzed within a frequency range from 60 to 10^9 Hz as well as temperatures over the range from 75 to 482 °F. The average mean values for ε_r from measurements in three samples (Athabasca oil sands) with different water content at various frequencies are plotted in Figure 2.1. However, Chute and his colleagues in 2009 only provided the real part of dielectric permittivity (ε_r) of oil sands without estimations of the imaginary part (ε_i,), which is the critical parameter for calculation of electrogenic waves attenuation and heat generation in oil sands reservoir.

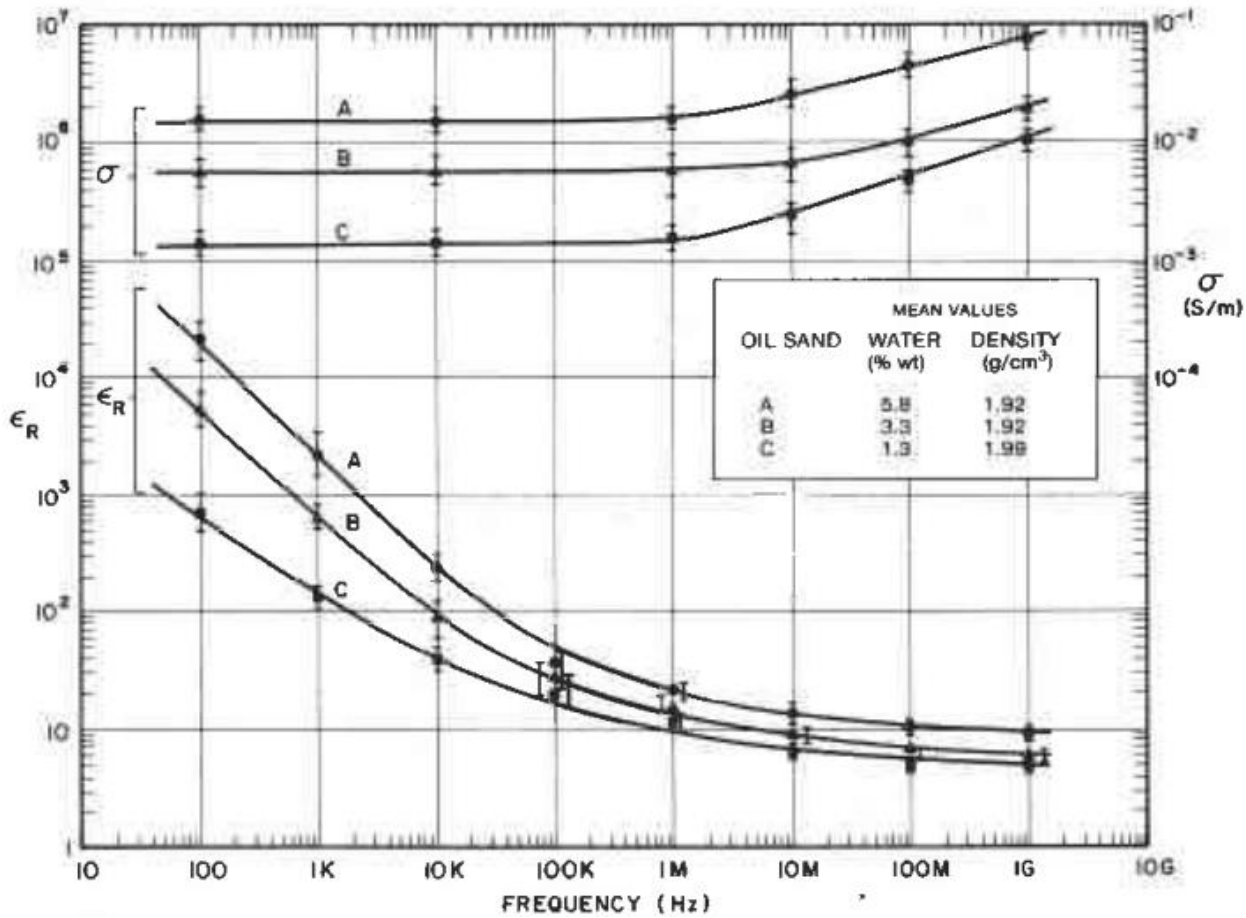

Figure 2.1 Mean values of conductivity, σ, and relative dielectric constant, ε_R, as a function of frequency for oil sands A, B, and C at 24°C (Chute et al., 2009).

In this thesis, a single Debye relaxation law can be used to estimate the complex dielectric permittivity (including both real parts, ε_r, and imaginary part, ε_i) of saline water (Debye, 1929):

$$\varepsilon_w(T,S) = \varepsilon_\infty + \frac{\varepsilon_S(T,S) - \varepsilon_\infty}{1 + \left(j\frac{v}{v_R(T,S)}\right)^{1-\eta}} - j\frac{\sigma_w(T,S)}{(2\pi\varepsilon_0)v}$$

Eq. 2-39

Later, the dielectric constant is fit with the double Debye relaxation law with two Debye Relaxation Fits for water. The general form reads, as well as the electrical conductivity of water (Meissner and Wentz, 2004):

$$\varepsilon_w(T,S) = \frac{\varepsilon_S(T,S) - \varepsilon_1(T,S)}{1 + j\frac{v}{v_1(T,S)}} + \frac{\varepsilon_1(T,S) - \varepsilon_\infty(T,S)}{1 + j\frac{v}{v_2(T,S)}} + \varepsilon_\infty(T,S) - j\frac{\sigma_w(T,S)}{(2\pi\varepsilon_0)v}$$

Eq. 2-40

$$\sigma_w(T,S) = \sigma_w(T,S=35) \cdot R_{15}(S) \cdot \frac{R_T(S)}{R_{15}(S)}$$

Eq. 2-41

$$\sigma_w(T,S=35) = 2.903602 + 8.607 \times 10^{-2}T + 4.738817 \times 10^{-4}T^2 - 2.991 \times 10^{-6}T^3 + 4.3047 \times 10^{-9}T^4$$

Eq. 2-42

$$R_{15}(S) = S\frac{(37.5109 + 5.45216S + 1.4409 \times 10^{-2}S^2)}{(1004.75 + 182.283S + S^2)}$$

Eq. 2-43

$$\frac{R_T(S)}{R_{15}(S)} = 1 + \frac{\alpha_0(T-15)}{(\alpha_1 + T)}$$

Eq. 2-44

$$\alpha_0 = \frac{(6.9431 + 3.2841S - 9.9486 \times 10^{-2}S^2)}{(84.850 + 69.024S + S^2)}$$

Eq. 2-45

$$\alpha_1 = 49.843 - 0.2276S + 0.198 \times 10^{-2}S^2$$

Eq. 2-46

For the remaining five constants, the ansatz is used:

$$\varepsilon_S(T,S) = \varepsilon_S(T,S=0)e^{[b_0S+b_1S^2+b_2TS]}$$

Eq. 2-47

$$v_1(T,S) = v_1(T,S=0)[1 + S(b_3 + b_4T + b_5T^2)]$$

Eq. 2-48

$$\varepsilon_1(T,S) = \varepsilon_1(T,S=0)e^{[b_6S+b_7S^2+b_8TS]}$$

Eq. 2-49

$$v_2(T,S) = v_2(T,S=0)[1 + S(b_9 + b_{10}T)]$$

Eq. 2-50

$$\varepsilon_\infty(T,S) = \varepsilon_\infty(T,S=0)[1 + S(b_{11} + b_{12}T)]$$

Eq. 2-51

For the properties of pure water:

$$\varepsilon_S(T,S=0) = \frac{3.70886 \times 10^4 - 8.2168 \times 10^1 T}{4.21854 \times 10^2 + T}$$

Eq. 2-52

$$\varepsilon_1(T, S = 0) = a_0 + a_1 T + a_2 T^2$$

Eq. 2-53

$$v_1(T, S = 0) = \frac{45 + T}{a_3 + a_4 T + a_5 T^2}$$

Eq. 2-54

$$\varepsilon_\infty(T, S = 0) = a_6 + a_7 T$$

Eq. 2-55

$$v_2(T, S = 0) = \frac{45 + T}{a_8 + a_9 T + a_{10} T^2}$$

Eq. 2-56

Table 2.1 Parameters of the fit (Eq. 3-17 to Eq. 3-32):

i	a_i	b_i
0	5.723	-3.56417×10^{-3}
1	2.2379×10^{-2}	4.74868×10^{-6}
2	-7.1237×10^{-4}	1.15574×10^{-5}
3	5.0478	2.39357×10^{-3}
4	-7.0315×10^{-2}	-3.1353×10^{-5}
5	6.0059×10^{-4}	2.52477×10^{-7}
6	3.6143	-6.28908×10^{-3}
7	2.8841×10^{-2}	1.76032×10^{-4}
8	1.3652×10^{-1}	-9.22144×10^{-5}
9	1.4825×10^{-3}	-1.99723×10^{-2}
10	2.4166×10^{-4}	1.81176×10^{-4}
11	/	-2.04265×10^{-3}
12	/	1.57886×10^{-4}

The units are T (degrees centigrade), S (parts per thousand), and σ_w (siemens per meter).

2.3 Electrical heating model

Mathematical models are provided for the physics involved in the processes of electrical heating, such as power input by down-hole electric heater, electric current flow in a reservoir and electromagnetic waves propagation through a reservoir. In order to simulate the processes accurately and efficiently, new formulations are derived for both governing equations and boundary conditions.

2.3.1 Electric heater

Electric heaters usually are electrodes, are placed within the wellbore and are operated at very high temperature. Heat transfers from the surface of the electrode into the reservoir are by thermal conduction (McGee and Donaldson, 2009). Electrical heating for oil sand reservoirs recovery can be classified into four disciplines according to electric current frequency applied and locations of heat generation (Table 2.1), such as electric heater, electrical resistance heating, inductive heating and RF/MW heating (Wacker et al., 2011). At this point, the parameter of interest is the heat flux required to maintain constant temperature at the cylinder's surface (Moini and Edmunds, 2013). For the case where a heat source of constant power (e.g., an electrical rod) is present inside the cylinder, the heat-source value is q_{ELE}, energy per unit length per unit time. As mentioned before, this case models a wellbore with a constant heat source (e.g., an electrical rod installed inside of the wellbore). The electrical power of the rod is the known parameter, and the unknown is the temperature on the wellbore wall. For example, for a 500 m long horizontal well with electric heater installed inside, the heating source can be expressed as a total output power of 500 kW or 1 kW/m.

2.3.2 Electrical resistance heating

Electric current balance (Killough and Gonzalez, 1986; Hiebert et al., 1986; Baylor et al., 1990; Vinsome et al., 1994) is:

$$0 = \Delta(\gamma_e \Delta E) + q_e$$

Eq. 2-57

In the DC case, the electric current balance equation is a result of the application of Kirkhoff's rule and Ohm's law to each of the grid blocks in a model (El-Feky, 1977). This simply implies that the sum of the currents entering and leaving a cell is zero and that the voltage drop is proportional to the current at any point in the model. The electrical capacitance of the reservoir is assumed to be zero so that the left-hand-side of Eq. -2-57 is zero (i.e., elliptic partial differential equations) regardless of whether DC or AC is being applied to the oil reservoir.

The electrical conductance term γ_e is a function of temperature, water saturation, and mole fraction of salt (NaCl):

$$\gamma_e = \gamma_e(T, S_w, x_{NaCl})$$

Eq. 2-58

For the energy balance equation, the electrical dissipation q_{ELE} is approximated as:

$$q_{ELE} = \Delta E \cdot (\gamma_e \Delta E)$$

Eq. 2-59

The solution for the equations when the electric current sources are multiphase AC is based on the use of complex voltages and electric currents. That is, the currents and voltages have both real and imaginary portions (Killough and Gonzalez, 1986). A multiphase power source can be expressed as having an amplitude and phase angle or equivalently as being a complex voltage with real and imaginary portions:

$$E = E_{Real} + E_{Imaginary}$$

Eq. 2-60

$$|E| = \left(E_{Real}^2 + E_{Imaginary}^2\right)^{1/2}$$

Eq. 2-61

$$\psi = arctan\left(\frac{E_{Imaginary}}{E_{Real}}\right)$$

Eq. 2-62

where $|E|$ and ψ are the amplitude and phase angle of the multiphase voltage, respectively. Since the differential operator for the electric current balance equation is linear and real, Eq. 2-57 can be split into two separate equations for the real and imaginary portions of the complex voltage:

$$0 = \Delta(\gamma_e \Delta E_{Real}) + q_{eR}$$

Eq. 2-63

$$0 = \Delta\left(\gamma_e \Delta E_{Imaginary}\right) + q_{eI}$$

Eq. 2-64

The energy dissipation associated with the complex voltage can be evaluated using the amplitude of the complex voltage as follows:

$$q_{ELE} = 0.5\gamma_e \cdot |\Delta E|^2 = 0.5\gamma_e \cdot \left[(\Delta E_{Real})^2 + \left(\Delta E_{Imaginary}\right)^2\right]$$

Eq. 2-65

where the factor 0.5 is the result of averaging (integrating) the dissipation over a period of $\frac{2\pi}{\omega}$ where ω is the frequency of the AC.

In this manner, the solution of any multiphase AC problem is reduced to the solution of two equations for the real and imaginary voltages regardless of the number of phases for the current sources. The solution in this reservoir simulator for multiphase power is performed in a fully-implicit manner. The expansions for the conductance terms are identical to those presented for the DC case (Lashgari et al., 2014).

$$q_{ELE} = \frac{\left[\left(E_{i+1,j,k} - E_{i,j,k}\right)\gamma_{i+\frac{1}{2},j,k}\right]^2}{\gamma_{i\to i+\frac{1}{2},j,k}} + \frac{\left[\left(E_{i,j,k} - E_{i-1,j,k}\right)\gamma_{i-\frac{1}{2},j,k}\right]^2}{\gamma_{i\to i-\frac{1}{2},j,k}} + \frac{\left[\left(E_{i,j+1,k} - E_{i,j,k}\right)\gamma_{i,j+\frac{1}{2},k}\right]^2}{\gamma_{i,j\to j+\frac{1}{2},k}}$$
$$+ \frac{\left[\left(E_{i,j,k} - E_{i,j-1,k}\right)\gamma_{i,j-\frac{1}{2},k}\right]^2}{\gamma_{i,j\to j-\frac{1}{2},k}} + \frac{\left[\left(E_{i,j,k+1} - E_{i,j,k}\right)\gamma_{i,j,k+\frac{1}{2}}\right]^2}{\gamma_{i,j,k\to k+\frac{1}{2}}}$$
$$+ \frac{\left[\left(E_{i,j,k} - E_{i,j,k-1}\right)\gamma_{i,j,k-\frac{1}{2}}\right]^2}{\gamma_{i,j,k\to k-\frac{1}{2}}}$$

Eq. 2-66

Where, γ_{ex}, γ_{ey}, and γ_{ez} are resistivities in x, y, and z directions, respectively and these are calculated for each grid-lock as

$$\gamma_{ex} = \sigma \frac{\Delta y \Delta z}{\Delta x}$$

Eq. 2-67

$$\gamma_{ey} = \sigma \frac{\Delta x \Delta z}{\Delta y}$$

Eq. 2-68

$$\gamma_{ez} = \sigma \frac{\Delta x \Delta y}{\Delta z}$$

Eq. 2-69

2.3.3 Electromagnetic heating

The four classical-electromagnetic equations in Maxwell's principle can be solved by appropriate transformations, and initial and boundary conditions. We consider a linear, isotropic reservoir with respect to electric conductivity, dielectric permittivity, and magnetic permeability, and the electromagnetic field distribution within a source free material is governed by Maxwell's equations Eq. 1-7 - Eq. 1-10 (Fanchi, 1990; Roussy and Pearce, 1995).

The following material constitutive relations are applied to Maxwell's equations above:

$$\vec{B} = \mu\vec{H}$$

Eq. 2-70

$$\vec{D} = \varepsilon\vec{E}$$

Eq. 2-71

$$\vec{J} = \sigma\vec{E}$$

Eq. 2-72

For time-harmonic fields, the instantaneous vector (time-domain) is related to the phasor vector (frequency-domain) by:

$$\frac{\partial\vec{E}}{\partial t} \leftrightarrow j\omega E$$

Eq. 2-73

$$\frac{\partial^2\vec{E}}{\partial t^2} \leftrightarrow (j\omega)^2 E$$

Eq. 2-74

$$\frac{\partial\vec{H}}{\partial t} \leftrightarrow j\omega H$$

Eq. 2-75

$$\frac{\partial^2\vec{H}}{\partial t^2} \leftrightarrow (j\omega)^2 H$$

Eq. 2-76

Thus, by substituting Eq. 2-70 to Eq. 2-76 into Eq. 1-7 to Eq. 1-10, we obtain:

$$\nabla \times \vec{E} = -j\omega\mu H$$

Eq. 2-77

$$\frac{1}{(\sigma + j\omega\varepsilon)} \nabla \times \vec{H} = E$$

Eq. 2-78

Taking curl on both sides of Eq. 2-78 yields:

$$\nabla \times \left[\frac{1}{(\sigma + j\omega\varepsilon)} \nabla \times H\right] = \nabla \times E$$

Eq. 2-79

Substituting Eq. 2-77 into Eq. 2-78 yields:

$$\nabla \times \left[\frac{1}{(\sigma + j\omega\varepsilon)} \nabla \times H\right] = -j\omega\mu H$$

Eq. 2-80

Eq. 2-80 is crucial to the calculation of EM wave propagation in oil sands. The variable of the magnetic field is solved for, and the distribution of the electric field can be obtained by the relationship for a linear dielectric material, as shown in Eq. 2-81. By the method of FDFD, Eq. 2-80 can be solved numerically and simultaneously with thermal oil reservoir modelling. The term $\frac{1}{(\sigma+j\omega\varepsilon)}$ including electrical conductivity and dielectric permittivity is treated by the arithmetic average of the neighboring two grid blocks. This appropriate approximation of dielectric properties provides accurate estimation of EM wave propagation, especially for a medium

exhibiting large variation in dielectric properties, such as water vaporization and steam condensation.

$$E = H\sqrt{\frac{j\omega\mu}{\sigma + j\omega\varepsilon}}$$

Eq. 2-81

Electric conductivity σ is a function of temperature, salinity and water saturation in a reservoir. In this study, the effect of salinity on conductivity is neglected in the calculation because the salinity is assumed as a constant under the initial condition in the process of simulation (Lashgari et al., 2016). To obtain the electric conductivity of the fluid-saturated reservoir, Archie's law is used to calculate the water phase conductivity in the reservoir with the exclusion of nonconductive oil, rock and gas, in Eq. 2-35 (Lashgari et al., 2016).

At high frequencies, polar molecules such as water try to align themselves with an alternating current when an EM wave passes through the reservoir. The molecules start to rotate, and the friction caused by movement of the molecules against each other generates heat to increase the reservoir temperature. The response of the reservoir, such as dielectric permittivity, can be described with a single but a complex parameter that represents both energy storage and loss of the applied wave (Abraham et al., 2016). This is given by:

$$\varepsilon = \varepsilon_r - j(\varepsilon_i + \frac{\sigma}{\omega})$$

Eq. 2-82

The energy loss can be traced to a fundamental mechanism rooted in charge conduction and dielectric polarization. At high frequencies, the time-averaged power dissipated per unit volume due to dielectric in a lossy medium is given according to Poynting's vector by (Davletbaev et al., 2010; Hossan and Dutta, 2012):

$$q_{RF} = \frac{1}{2}\omega\varepsilon_0\left(\varepsilon_i + \frac{\sigma}{\omega}\right)(|E|^2)$$

Eq. 2-83

2.4 Boundary conditions

Artificial boundary conditions with different types for the flow cell have been suggested over the years and all of them have the objective of providing as good an approximation of the real boundary conditions as possible. An important design criterion for the artificial boundary conditions is the conservation of flux in and out of the flow cell. For simplicity, the reservoir behaves as a closed calculation domain; in which leaking or an aquifer is not considered in this work (Dong, 2012).

2.4.1 Well Modelling

The mass and energy transfer through injectors and producers are handled in well models. The well models are usually expressed as constraint equations, depending on the type of well operation, and are coupled with the reservoir flow equations (Trimble and MacDonald, 1981; Huang 2012). In general, there is not a distributed mass source or sink in fluid flows in a 3D medium. As an approximation, the case where sources and sinks of a fluid are located at isolated points may be considered. Then these point sources and sinks can be surrounded

by small spheres that are excluded from the medium. The surface of these spheres can be treated as part of the boundary of the medium, and the mass flow rate per unit volume of each source or sink specifies the total flux through its surface (Chen et al., 2006; Chen 2007).

To investigate a wellbore model, the most commonly used wellbore model in the reservoir simulation processes: the sink/source well model is introduced first. If a bottom hole pressure $p_{bh}$is given, then Peaceman's well model is (Chen et al., 2006; Chen 2007).:

$$q = \frac{2\pi\rho k h_3}{\mu ln(r_e/r_w)}(p - p_{bh})$$

Eq. 2-84

where, h_3 reservoir thickness (or the height of the gridblock containing the well).

The equivalent radius r_e is the radius at which the steady state flowing pressure for the actual well equals the numerically computed pressure for the well cell. The above well model needs be extended in various directions, including to rectangular grids and incorporating gravity force effects, anisotropic reservoirs, skin effects, horizontal wells, and multiphase flows. Here I consider an extension of the model in Eq. 2-84 to the first four effects. The gravitational effects must be treated on the same footing as pressure gradient effects. The skin factor is a dimensionless number and accounts for the effect resulting from formation damage caused by drilling. With these effects for single-phase flow for an anisotropic permeability, the well model is extended to:

$$q = WI(p - p_{bh})$$

Eq. 2-85

In the non-square grid and anisotropic medium case, the equivalent radius r_e is (Peaceman, 1983)

$$r_e = \frac{0.14\left((k_{22}/k_{11})^{1/2}h_1^2 + (k_{11}/k_{22})^{1/2}h_2^2\right)^{1/2}}{0.5((k_{22}/k_{11})^{1/4} + (k_{11}/k_{22})^{1/4})}$$

Eq. 2-86

where, h_1 and h_2 are the x1- and x2-grid sizes of the grid block that contains the vertical well.

The well index is defined by:

$$WI = \frac{2\pi\rho h_3\sqrt{k_{11}k_{22}}}{\mu(ln(r_e/r_w) + s)}$$

Eq. 2-87

The effect of near-wellbore factors on well productivity or injectivity can be incorporated by using the skin factor ‘s’. Effects that can be treated in this manner include well damage, perforation impacts, partial penetration, fracturing, acidizing, and inclined (deviated) wells (Chen et al., 2006; Chen 2007).

Horizontal wells in either the x1- or the x2-coordinate direction use the same well model equations as vertical ones. Only the parameters related to the direction of the wellbore need to be modified. For example, the well index for a horizontal well parallel to the x1-direction is calculated:

$$WI = \frac{2\pi\rho h_1\sqrt{k_{22}k_{33}}}{\mu(ln(r_e/r_w) + s)}$$

Eq. 2-88

Accordingly, in the x1-direction the equivalent radius r_e is:

$$r_e = \frac{0.14\left((k_{33}/k_{22})^{1/2}h_2^2 + (k_{22}/k_{33})^{1/2}h_3^2\right)^{1/2}}{0.5((k_{33}/k_{22})^{1/4} + (k_{22}/k_{33})^{1/4})}$$

Eq. 2-89

A successful implementation of the horizontal well equations are based on the appropriate assumptions include the uniform grid spacing and permeability , the well is isolated (not near any other well), and it is not located close to any grid boundary (Chen 2007).

The equation of a vertical well derived for single-phase flow can be extended to multiphase flow, e.g., to a flow system of water, oil, and gas:

$$q = \frac{2\pi h_3\sqrt{k_{11}k_{22}}}{(ln(r_e/r_w) + s)}\frac{\rho_p}{\mu_p}\left(p_p - p_{bh}\right)$$

Eq. 2-90

Similarly, the equation of horizontal well derived for single-phase flow can be extended to multiphase flow, e.g., to a flow system of water, oil, and gas:

$$q = \frac{2\pi\rho h_1\sqrt{k_{22}k_{33}}}{\mu(ln(r_e/r_w) + s)}\frac{\rho_p}{\mu_p}\left(p_p - p_{bh}\right)$$

Eq. 2-91

2.4.2 Heat loss

In thermal recovery, the energy utilization necessitates careful evaluation of heat loss. The heat loss to the surroundings is the most important among various heat loss mechanisms (Huang 2012). A semi-analytical model assuming heat transfer to/from an infinite formation by

conduction is used to account for heat loss to overburden and underburden (Vinsome, P. K. W., Westerveld, 1980). This approach assumes a temperature profile at the base or cap rock as a function of time and distance from the reservoir interface (CMG STARS Manual, 2017).

$$T(t,z) = (T(t,0) + pz + qz^2)^{-z/d}$$

Eq. 2-92

The diffusion length is $d = \frac{\sqrt{\lambda}t}{2}$. This profile satisfies both T (t, 0) (grid block temperature) and T (t, ∞) = 0. p,q, and d are functions of time and can be determined by the boundary conditions (Dong, 2012). At the interface, according to Fourier's law, the profile must satisfy:

$$\frac{\partial \mathrm{T}\ (\mathrm{t},0)}{\partial t} = \lambda \frac{\partial^2 T(t,z)}{\partial z^2}\bigg|_{z=0}$$

Eq. 2-93

where, λ is assumed as:

$$\lambda = \frac{K_{tb}}{C_{pb}}$$

Eq. 2-94

In Eq. 2-94, C_{pb} and K_{tb} are the thermal capacity and the conductivity of overburden/underburden rock. The coefficients p and q are obtained at each time step in Eq. 2-95.

$$I^{n-1} = \big(T(t,0)\big)^{n-1}(d)^{n-1} + p^{n-1}((d)^{n-1})^2 + 2q^{n-1}((d)^{n-1})^3$$

Eq. 2-95

$$p = \frac{\frac{\lambda \Delta t^n \left(T(t,0)\right)^n}{(d)^n} + I^{n-1} - \frac{((d)^n)^3 \left(\left(T(t,0)\right)^n - \left(T(t,0)\right)^{n-1}\right)}{\lambda \Delta t^n}}{3((d)^n)^2 + \lambda \Delta t^n}$$

Eq. 2-96

$$q = \frac{2p^n (d)^n - \left(T(t,0)\right)^n + ((d)^n)^2 \frac{\left(T(t,0)\right)^n - \left(T(t,0)\right)^{n-1}}{\lambda \Delta t^n}}{2((d)^n)^2}$$

Eq. 2-97

The rate at which heat is lost from the block to the overburden/underburden is:

$$q_{LOSS} = -K_{tb} \left.\frac{\partial T}{\partial z}\right|_{z=0} = K_{tb} \left(\frac{T(t,0)}{d} - p\right)$$

Eq. 2-98

For the situation of z =0, the temperature of the reservoir equals the temperature of the control volume at the boundary. At the infinite length, the temperature of the location is equal to the initial reservoir reference condition.

The heat loss rate and its derivative with respect to temperature can be estimated and used directly in the energy conservation equation.

2.4.3 Heating Source and outer boundary conditions in electric heater process

As mentioned before, the electrical power of the rod is the known parameter, and the unknown is the temperature on the wellbore wall. For example, for a 500 m long horizontal well with electric

heater installed inside, the heating source can be expressed a total output power of 500 kW or 1 kW/m. For temperature control, the heater well operates on specified wellbore temperature T_{wspec} only. In each layer the heat rate is (CMG STARS Manual, 2017):

$$q_{hk} = I_{hk}\left(T_{wspec} - T_k\right)$$

Eq. 2-99

and the resulting q_{hk} varies. Note that in this case q_{hk} will be positive or negative, depending only on the relative values of T_{wspec} and T_k. If you wish to prevent heat transfer of a particular sign, controls must be used.

2.4.4 Current voltage source and outer boundary conditions in resistive heating process

Electric power can be applied to the model in two categories: constant specification on electric voltage and constant specification on input power (Killough and Gonzalez, 1986). The less realistic constant voltage case is, unfortunately, the simplest technique to implement in the numerical model. Constant voltage applied at an electrode simply becomes a quantity added to the accumulation portion of the electrical equations and a coefficient added to the diagonal that represents the unknown voltage:

$$0 = \Delta(\gamma_e \Delta E) + \gamma_{ewb}\left(E_{wb} - E_{xyz}\right)$$

Eq. 2-100

where, γ_{ewb} is electric conductance between finite difference cell and electrode, E_{wb} is specified electrode voltage, E_{xyz} is voltage at finite difference cell.

Specification of maximum input power level can be interpreted as a facility constraint on the electrical source and sink terms. Two approaches have been used for this constraint: explicit and fully implicit. For both approaches an initial estimate of the voltage at each of the electrodes is made by solving the equations for the total power applied to the model. These equations simply state that the power applied is equal to the sum of the product of the current times the applied voltage at each electrode (Killough and Gonzalez, 1986):

$$Power = \sum_{electrodes} (E_{wb}|I_{wb}|)$$

Eq. 2-101

$$I_{wb} = \gamma_{ewb}\left(E_{wb} - E_{xyz}\right)$$

Eq. 2-102

Near the electrode, the current flows radially. By analogy with fluid flow near a well, I_{wb} can be related to the electric potential at the electrode E_{wb}, and the average potential in the block E_{xyz} by (Glandt and Chia-Fu, 1992):

$$I_{wb} = \frac{2\pi\gamma_{ewb}L\left(E_{wb} - E_{xyz}\right)}{ln\left[\left(\frac{R_e}{R_w}\right) - 0.5\right]\Delta V}$$

Eq. 2-103

where, where L is the length of the electrode within the grid block, ΔV is the volume of the grid block, R_w is radius of the electrode and R_e is the equivalent radius determined by the size of the grid block.

Because a square uniform grid is used in this thesis of reservoir simulation, R_e is called the equivalent wellblock radius and is calculated using Peaceman's formula for a square uniform grid (Dogru, 2010):

$$R_e = \Delta x e^{-\frac{\pi}{2}}$$

Eq. 2-104

The unknown electrode voltages E_{xyz} are determined by solving the above quadratic equation in the single unknown E_{wb} since the amplitude of applied voltage is assumed to be the same for all electrodes.

In the case of explicit method, the E_{wb} calculated from Eq. 2-103 is used as a constant voltage specification for the iterations using the previous approach in Eq. 2-100 (Killough and Gonzalez, 1986).

An electrical boundary is a collection of block faces that are assumed to be at the same potential, and through which electric current flows into and out of the reservoir. Since a grid block's potential is referenced to the geometrical center of the block, there is a potential drop between a segment of electrical boundary and its host grid block. A boundary face may be external or internal to the grid (CMG STARS Manual, 2017). Each host block has an additional current term, corresponding to the electrical boundary, with a similar definition for geometric term and resistance. The (real or imaginary) current flow from block center i to boundary b is:

$$I_{i,b} = \gamma_i \left(E_i - E_{i,b}\right)$$

Eq. 2-105

In order to simulate the electrical current flow at the reservoir outer boundary accurately, the secondary boundary condition (Neumann condition) is used as, for example in x- direction:

$$\frac{\mathrm{dE}}{\mathrm{dx}} = f(x)$$

Eq. 2-106

2.4.5 Electromagnetic Wave Source and outer boundary conditions in Electromagnetic Heating process

The term q_{ELE} on the right side of Eq. 2-4 is the gain in heat content because of the power applied through the "photon" phase as discussed by Bird et al. (2002). This term can be obtained from a separate energy balance on the photon phase assuming steady-state since the mass of the photons is negligible (Carrizales, 2010). The mathematical formulation for this term can be also derived from the solution of Maxwell's equations or from the solution of the plane-wave radiation equation similar to the application of Lambert's law (Fanchi, 1990).

In a radial system, assuming that energy flows from the EM source in the radial direction only, the incident power is P_0 at the wellbore radius r_w can be written as:

$$P_0 = \frac{2\beta_0 h E_0^2}{\omega \mu_0 \delta} e^{-2\alpha_0 r_w}$$

Eq. 2-107

Solving for the electric field amplitude E_0 gives:

$$E_0 = \frac{P_0 \omega \mu_0 \delta}{2\beta_0 h} e^{2\alpha_0 r_w}$$

Eq. 2-108

$$\alpha_0 = \omega \sqrt{\frac{\mu_0 \varepsilon}{2}\left[\sqrt{1 + \left(\frac{\sigma}{\omega\varepsilon}\right)^2} - 1\right]}$$

Eq. 2-109

$$\beta_0 = \omega \sqrt{\frac{\mu_0 \varepsilon}{2}\left[\sqrt{1 + \left(\frac{\sigma}{\omega\varepsilon}\right)^2} + 1\right]}$$

Eq. 2-110

$$\delta^2 = \alpha_0^2 + \beta_0^2$$

Eq. 2-111

where, h is the thickness of irradiated zone.

One of the greatest challenges of the numerical modelling of EM waves by using Maxwell's equations is the accurate and efficient solution of EM wave interaction problems in open regions where spatial domain of the computed field is unbounded in one or more coordinate directions (Feng et al., 2015).

The perfectly matched layer (PML), which is an artificial medium, has been widely used to absorb incident EM waves omnidirectionally with virtually no reflection developed by split-field

(Bérenger, 1994). PML has been demonstrated to be the most effective for linear EM waves propagation regardless of incidence angle, and over a wide range of frequencies by lots of published articles (Katz et al., 1994; Andrew et al., 1995; Wittwer and Ziolkowski, 1996).

The PML was originally proposed for FDTD field computations in open spaces consisting of a stack of lossy layers with both electric and magnetic conductivities, the loss parameters being appropriately chosen in order to match the intrinsic impedances between the PML layers, while ensuring the waves inside the PML layers are absorbed without reflection (Yaich et al., 2018). Following Bérenger's original PML, variations are reported that the uniaxial PML (U-PML) (Sacks et al., 1995) and stretched PML (SC-PML) (Chew and Weedon, 1994; Rappaport, 1995; Mittra and Pekel, 1995) are the most popular for the solving Maxwell's equations by the method of FDTD, both resulting in similar numerical performance. Demonstration also shows that the using of stretched-coordinate PML (SC-PML) has significantly faster convergence speed than using the uniaxial PML (UPML) (Shin and Fan, 2012) and simple implementation in the corners and edges of PML resins (Chew and Weedon, 1994). To simply implement PML in dispersive and anisotropic materials, the nearly perfectly matched layer (NPML) is proposed by employing simple ordinary differential equations when the PML conductivity is spatially variant (Cummer, 2003).

In the current applications of PML in absorbing propagating electromagnetic waves, at least several layers have to be implemented in the PML with increase in electric conductivity as a geometric progression (Bérenger, 1996). The electric conductivity increases from the first PML layer connecting the computation domain to the latest one furthest to the domain to prevent

spurious reflection at PML interfaces. By using the PML for the solving of Maxwell's equations in frequency-domain, a 10-layer PML has been used for a typical case (Shin and Fan, 2012). The original PML was based the splitting of electromagnetic fields into uncoupled derivative directions (Bérenger, 1994). It was found that the split-field PML formulation is only weakly well-posed (Abarbanel and Gottlieb 1997) and numerical schemes based on this weakly well-posed PML would have undesirable instability under some circumstances (Saul and David, 1997).

In this chapter, the general frame of the single PML layer technique is pointed out on Figure 1. A plane EM wave source is located inside the computational domain, which is surrounded a PML with single layer in all directions. The Helmholtz's equation derived from original Maxwell's equations and the single PML layer formulation derived from SC-PML method are solved simultaneously by FDFD technique inside a computational domain and in the surrounded single PML layer, respectively.

According to Eq. 2-80, which is derived for the calculation of electromagnetic waves transmission in an oil sand reservoir, in two space dimensions this is equivalent to the TE version of Maxwell's equations (Singer and Turkel, 2004).

$$\frac{\partial}{\partial x}\left(\frac{S_y S_z}{S_x}\frac{1}{(\sigma + j\omega\varepsilon)}\frac{\partial H}{\partial x}\right) + \frac{\partial}{\partial y}\left(\frac{S_x S_z}{S_y}\frac{1}{(\sigma + j\omega\varepsilon)}\frac{\partial H}{\partial y}\right) + \frac{\partial}{\partial z}\left(\frac{S_x S_y}{S_z}\frac{1}{(\sigma + j\omega\varepsilon)}\frac{\partial H}{\partial z}\right)$$
$$= -j\omega\mu S_x S_y S_z H$$

Eq. 2-112

where, $S_x = \frac{1}{1-j\frac{\sigma_{PML,x}}{\omega\varepsilon}}$, $S_y = \frac{1}{1-j\frac{\sigma_{PML,y}}{\omega\varepsilon}}$ and $S_z = \frac{1}{1-j\frac{\sigma_{PML,z}}{\omega\varepsilon}}$. $\sigma_{PML,x}$, $\sigma_{PML,y}$ and $\sigma_{PML,z}$ are functions of only x, y and z respectively. When $\sigma_{PML,x} = \sigma_{PML,y} = \sigma_{PML,z} = 0$, this reduces to the Helmholtz equation (Eq. 2-80).

Similar to the implementation of PML by Bérenger in Figure 2.1, a basis of the PML is applied with adequate sets of parameters (σ_x,σ_x^*, σ_y,σ_y^*) in a 2D example, the EM wave transmission is perfect and reflectionless at a frequency and at any incident angle (Bérenger, 1994). For instance, according to Snell-Descartes law applied to an interface normal to y-axis, the impedance of the PML equals that of the computational domain and no reflection occurs when a plane wave propagates normally across the computational domain-PML interface. Moreover, if $\sigma_{x1} = \sigma_{x1}^* = 0$, then the propagating wave normal to AB-axis will not be absorbed. Similarly, if $\sigma_{y1} = \sigma_{y1}^* = 0$, then the propagating wave normal to AD-axis will also not be absorbed.

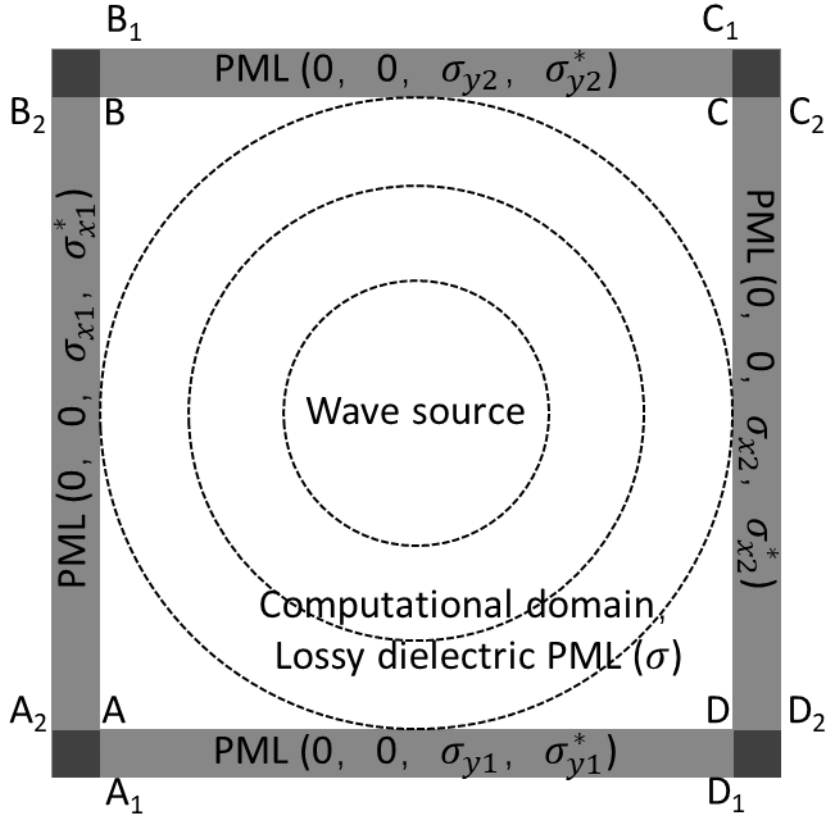

Figure 2.2 The single layer PML technique: Maxwell's equations and the PML formulations are solved by FDFD technique inside a computational domain and a PML layer, respectively. The computational domain is surrounded by a single PML layer whose properties have been predicted.

Calculations have been done for the validation of PML proposed in this thesis based on the background of pure water and saline water, as the plots of electric field magnitude in Figure 2.3 to Figure 2.4. The dielectric properties of water and saline water are summarized in Table 2.1, as well as applied frequency. The excellent agreement of numerical simulation results by using PML and the analytic solution (Eq. 2-113) demonstrate the feasibility of our novelty proposed method on appropriately absorbing electromagnetic waves at outer reservoir boundary.

$$E = E_0 e^{-\sqrt{j\omega\mu(\sigma+j\omega\varepsilon)}x}$$

Eq. 2-113

In this method, only one layer is added to the calculation domain, which is dramatically efficient in calculation compared to the original PML method, in which 10 to 15 layers are in need for the calculation.

Table 2.2 Dielectric properties of pure water and saline water for the calculation of PML

Sample	Electrical conductivity, S/m	Dielectric permittivity, $\varepsilon = \varepsilon_R - j\varepsilon_I$	Applied frequency
Pure water	0.0001	82.97-j8.84	10 MHz
Saline water	3.80	74.09-j55.20	10 MHz

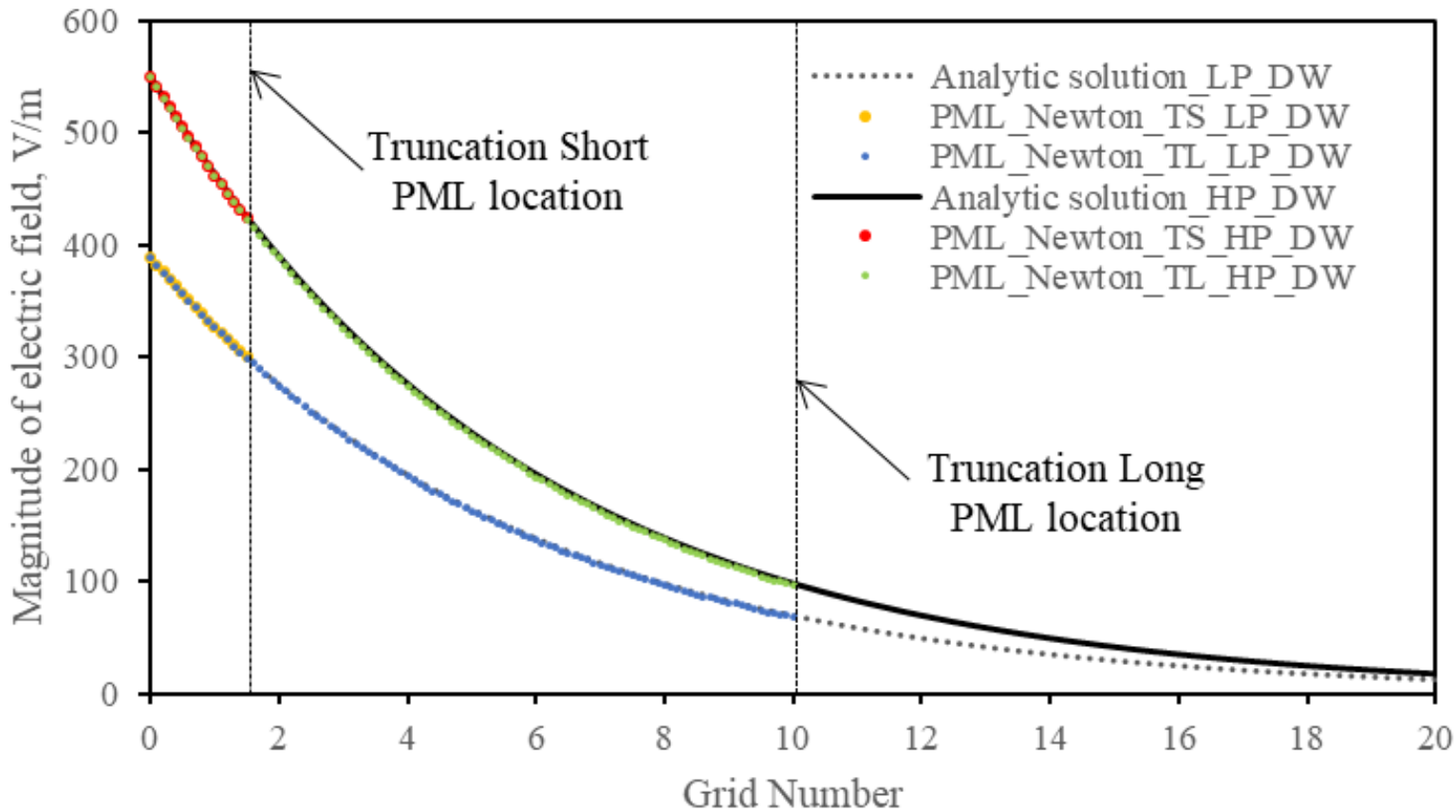

Figure 2.3 Calculation results of electric field magnitude by using PML, background is pure water (DW). Truncation locations are selected at a short one (TS) and a long one (TL) and the source power is selected at a high one (HP) and a low one (LP), respectively. Results are compared to analytic solutions.

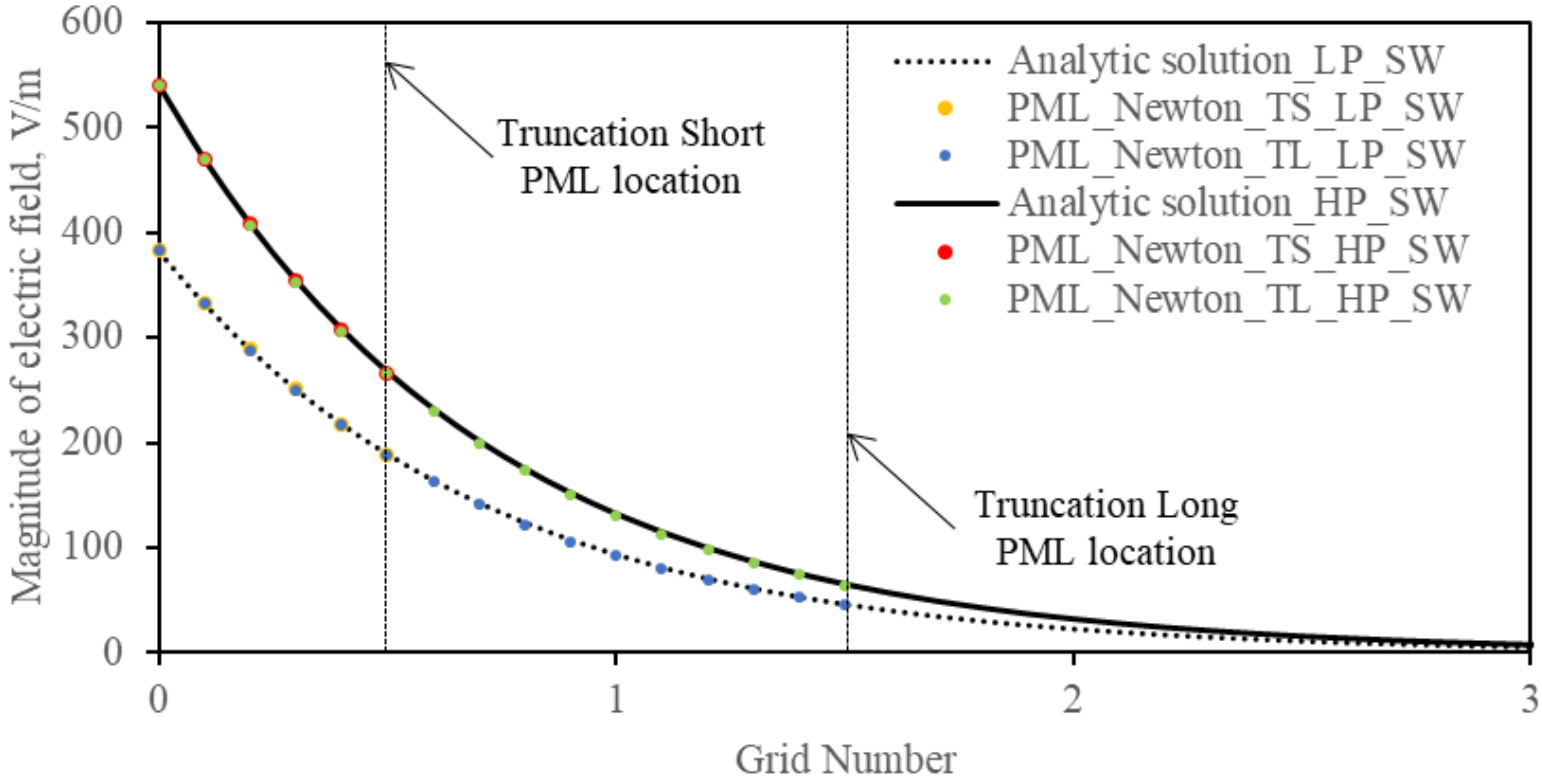

Figure 2.4 Calculation results of electric field magnitude by using PML, background is saline water (SW). Truncation locations are selected at a short one (TS) and a long one (TL) and the source power is selected at a high one (HP) and a low one (LP), respectively. Results are compared to analytic solutions.

Chapter 3 Numerical Methods

3.1 Discretization

The first and second order spatial derivatives are approximated by a central differential:

$$\frac{\partial f}{\partial x} \approx \frac{f_{i+1,j,k}^{n+1} - f_{i-1,j,k}^{n+1}}{2\Delta x}$$

Eq. 3-1

$$\frac{\partial}{\partial x}\left(T_s \frac{\partial f}{\partial x}\right) \approx \frac{T_{i+\frac{1}{2},j,k}^{n+1}\left(f_{i+1,j,k}^{n+1} - f_{i,j,k}^{n+1}\right) - T_{i-\frac{1}{2},j,k}^{n+1}\left(f_{i,j,k}^{n+1} - f_{i-1,j,k}^{n+1}\right)}{\Delta x^2}$$

Eq. 3-2

The discretization in time is approximated as:

$$\frac{\partial f}{\partial t} \approx \frac{f_{i,j,k}^{n+1} - f_{i,j,k}^{n}}{\Delta t}$$

Eq. 3-3

For the oil mass equation:

$$\frac{(\phi\rho_o S_o)^{n+1} - (\phi\rho_o S_o)^n}{\Delta t}$$

$$= \left(T_{f,ox}\right)_{i+1/2,j,k}^{n+1}\left(\frac{\Phi_{o,i+1,j,k}^{n+1} - \Phi_{o,i,j,k}^{n+1}}{\Delta x^2}\right) - \left(T_{f,ox}\right)_{i-1/2,j,k}^{n+1}\left(\frac{\Phi_{o,i,j,k}^{n+1} - \Phi_{o,i-1,j,k}^{n+1}}{\Delta x^2}\right)$$

$$+ \left(T_{f,oy}\right)_{i,j+1/2,k}^{n+1}\left(\frac{\Phi_{o,i,j+1,k}^{n+1} - \Phi_{o,i,j,k}^{n+1}}{\Delta y^2}\right) - \left(T_{f,oy}\right)_{i,j-1/2,k}^{n+1}\left(\frac{\Phi_{o,i,j,k}^{n+1} - \Phi_{o,i,j-1,k}^{n+1}}{\Delta y^2}\right)$$

$$+ \left(T_{f,oz}\right)_{i,j,k+1/2}^{n+1}\left(\frac{\Phi_{o,i,j,k+1}^{n+1} - \Phi_{o,i,j,k}^{n+1}}{\Delta z^2}\right) - \left(T_{f,oz}\right)_{i,j,k-1/2}^{n+1}\left(\frac{\Phi_{o,i,j,k}^{n+1} - \Phi_{o,i,j,k-1}^{n+1}}{\Delta z^2}\right)$$

$$+ q_o^{n+1}$$

Eq. 3-4

For the water/steam mass equation:

$$\frac{\left(\phi\rho_w S_w + \phi\rho_g S_g\right)^{n+1} - \left(\phi\rho_w S_w + \phi\rho_g S_g\right)^{n}}{\Delta t}$$

$$= \left(T_{f,wx}\right)^{n+1}_{i+\frac{1}{2},j,k}\left(\frac{\Phi^{n+1}_{w,i+1,j,k} - \Phi^{n+1}_{w,i,j,k}}{\Delta x^2}\right) - \left(T_{f,wx}\right)^{n+1}_{i-\frac{1}{2},j,k}\left(\frac{\Phi^{n+1}_{w,i,j,k} - \Phi^{n+1}_{w,i-1,j,k}}{\Delta x^2}\right)$$

$$+ \left(T_{f,wy}\right)^{n+1}_{i,j+\frac{1}{2},k}\left(\frac{\Phi^{n+1}_{w,i,j+1,k} - \Phi^{n+1}_{w,i,j,k}}{\Delta y^2}\right) - \left(T_{f,wy}\right)^{n+1}_{i,j-\frac{1}{2},k}\left(\frac{\Phi^{n+1}_{w,i,j,k} - \Phi^{n+1}_{w,i,j-1,k}}{\Delta y^2}\right)$$

$$+ \left(T_{f,wz}\right)^{n+1}_{i,j,k+\frac{1}{2}}\left(\frac{\Phi^{n+1}_{w,i,j,k+1} - \Phi^{n+1}_{w,i,j,k}}{\Delta z^2}\right) - \left(T_{f,wz}\right)^{n+1}_{i,j,k-\frac{1}{2}}\left(\frac{\Phi^{n+1}_{w,i,j,k} - \Phi^{n+1}_{w,i,j,k-1}}{\Delta z^2}\right)$$

$$+ \left(T_{f,gx}\right)^{n+1}_{i+\frac{1}{2},j,k}\left(\frac{\Phi^{n+1}_{g,i+1,j,k} - \Phi^{n+1}_{g,i,j,k}}{\Delta x^2}\right) - \left(T_{f,gx}\right)^{n+1}_{i-\frac{1}{2},j,k}\left(\frac{\Phi^{n+1}_{g,i,j,k} - \Phi^{n+1}_{g,i-1,j,k}}{\Delta x^2}\right)$$

$$+ \left(T_{f,gy}\right)^{n+1}_{i,j+\frac{1}{2},k}\left(\frac{\Phi^{n+1}_{g,i,j+1,k} - \Phi^{n+1}_{g,i,j,k}}{\Delta y^2}\right) - \left(T_{f,gy}\right)^{n+1}_{i,j-\frac{1}{2},k}\left(\frac{\Phi^{n+1}_{g,i,j,k} - \Phi^{n+1}_{g,i,j-1,k}}{\Delta y^2}\right)$$

$$+ \left(T_{f,gz}\right)^{n+1}_{i,j,k+\frac{1}{2}}\left(\frac{\Phi^{n+1}_{g,i,j,k+1} - \Phi^{n+1}_{g,i,j,k}}{\Delta z^2}\right) - \left(T_{f,gz}\right)^{n+1}_{i,j,k-\frac{1}{2}}\left(\frac{\Phi^{n+1}_{g,i,j,k} - \Phi^{n+1}_{g,i,j,k-1}}{\Delta z^2}\right)$$

$$+ q_w^{n+1} + q_g^{n+1}$$

Eq. 3-5

For the energy equation:

$$\frac{\begin{bmatrix}\left(\phi\rho_w S_w U_w + \phi\rho_g S_g U_g + \phi\rho_o S_o U_o + (1-\phi)U_r\right)^{n+1} \\ -\left(\phi\rho_w S_w U_w + \phi\rho_g S_g U_g + \phi\rho_o S_o U_o + (1-\phi)U_r\right)^{n}\end{bmatrix}}{\Delta t}$$

$$= \left(K_{eff}\right)^{n+1}_{i+1/2,j,k}\left(\frac{T^{n+1}_{i+1,j,k} - T^{n+1}_{i,j,k}}{\Delta x^2}\right) - \left(K_{eff}\right)^{n+1}_{i-\frac{1}{2},j,k}\left(\frac{T^{n+1}_{i,j,k} - T^{n+1}_{i-1,j,k}}{\Delta x^2}\right)$$

$$+ \left(K_{eff}\right)^{n+1}_{i,j+\frac{1}{2},k}\left(\frac{T^{n+1}_{i,j+1,k} - T^{n+1}_{i,j,k}}{\Delta x^2}\right) - \left(K_{eff}\right)^{n+1}_{i,j-\frac{1}{2},k}\left(\frac{T^{n+1}_{i,j,k} - T^{n+1}_{i,j-1,k}}{\Delta x^2}\right)$$

$$+ \left(K_{eff}\right)^{n+1}_{i,j,k+\frac{1}{2}}\left(\frac{T^{n+1}_{i,j,k+1} - T^{n+1}_{i,j,k}}{\Delta x^2}\right) - \left(K_{eff}\right)^{n+1}_{i,j,k-\frac{1}{2}}\left(\frac{T^{n+1}_{i,j,k} - T^{n+1}_{i,j,k-1}}{\Delta x^2}\right)$$

$$+ \left(H_w T_{f,wx}\right)^{n+1}_{i+\frac{1}{2},j,k}\left(\frac{\Phi^{n+1}_{w,i+1,j,k} - \Phi^{n+1}_{w,i,j,k}}{\Delta x^2}\right)$$

$$- \left(H_w T_{f,wx}\right)^{n+1}_{i-\frac{1}{2},j,k}\left(\frac{\Phi^{n+1}_{w,i,j,k} - \Phi^{n+1}_{w,i-1,j,k}}{\Delta x^2}\right)$$

$$+ \left(H_w T_{f,wy}\right)^{n+1}_{i,j+\frac{1}{2},k}\left(\frac{\Phi^{n+1}_{w,i,j+1,k} - \Phi^{n+1}_{w,i,j,k}}{\Delta y^2}\right)$$

$$- \left(H_w T_{f,wy}\right)^{n+1}_{i,j-\frac{1}{2},k}\left(\frac{\Phi^{n+1}_{w,i,j,k} - \Phi^{n+1}_{w,i,j-1,k}}{\Delta y^2}\right)$$

$$+ \left(H_w T_{f,wz}\right)^{n+1}_{i,j,k+\frac{1}{2}}\left(\frac{\Phi^{n+1}_{w,i,j,k+1} - \Phi^{n+1}_{w,i,j,k}}{\Delta z^2}\right)$$

$$- \left(H_w T_{f,wz}\right)^{n+1}_{i,j,k-\frac{1}{2}}\left(\frac{\Phi^{n+1}_{w,i,j,k} - \Phi^{n+1}_{w,i,j,k-1}}{\Delta z^2}\right)$$

$$+ \left(H_g T_{f,gx}\right)^{n+1}_{i+\frac{1}{2},j,k}\left(\frac{\Phi^{n+1}_{g,i+1,j,k} - \Phi^{n+1}_{g,i,j,k}}{\Delta x^2}\right) - \left(H_g T_{f,gx}\right)^{n+1}_{i-\frac{1}{2},j,k}\left(\frac{\Phi^{n+1}_{g,i,j,k} - \Phi^{n+1}_{g,i-1,j,k}}{\Delta x^2}\right)$$

$$+\left(H_g T_{f,gy}\right)_{i,j+\frac{1}{2},k}^{n+1}\left(\frac{\Phi_{g,i,j+1,k}^{n+1}-\Phi_{g,i,j,k}^{n+1}}{\Delta y^2}\right)-\left(H_g T_{f,gy}\right)_{i,j-\frac{1}{2},k}^{n+1}\left(\frac{\Phi_{g,i,j,k}^{n+1}-\Phi_{g,i,j-1,k}^{n+1}}{\Delta y^2}\right)$$

$$+\left(H_g T_{f,gz}\right)_{i,j,k+\frac{1}{2}}^{n+1}\left(\frac{\Phi_{g,i,j,k+1}^{n+1}-\Phi_{g,i,j,k}^{n+1}}{\Delta z^2}\right)-\left(H_g T_{f,gz}\right)_{i,j,k-\frac{1}{2}}^{n+1}\left(\frac{\Phi_{g,i,j,k}^{n+1}-\Phi_{g,i,j,k-1}^{n+1}}{\Delta z^2}\right)$$

$$+\left(H_o T_{f,ox}\right)_{i+\frac{1}{2},j,k}^{n+1}\left(\frac{\Phi_{o,i+1,j,k}^{n+1}-\Phi_{o,i,j,k}^{n+1}}{\Delta x^2}\right)-\left(H_o T_{f,ox}\right)_{i-\frac{1}{2},j,k}^{n+1}\left(\frac{\Phi_{o,i,j,k}^{n+1}-\Phi_{o,i-1,j,k}^{n+1}}{\Delta x^2}\right)$$

$$+\left(H_o T_{f,oy}\right)_{i,j+\frac{1}{2},k}^{n+1}\left(\frac{\Phi_{o,i,j+1,k}^{n+1}-\Phi_{o,i,j,k}^{n+1}}{\Delta y^2}\right)-\left(H_o T_{f,oy}\right)_{i,j-\frac{1}{2},k}^{n+1}\left(\frac{\Phi_{o,i,j,k}^{n+1}-\Phi_{o,i,j-1,k}^{n+1}}{\Delta y^2}\right)$$

$$+\left(H_o T_{f,oz}\right)_{i,j,k+\frac{1}{2}}^{n+1}\left(\frac{\Phi_{o,i,j,k+1}^{n+1}-\Phi_{o,i,j,k}^{n+1}}{\Delta z^2}\right)-\left(H_o T_{f,oz}\right)_{i,j,k-\frac{1}{2}}^{n+1}\left(\frac{\Phi_{o,i,j,k}^{n+1}-\Phi_{o,i,j,k-1}^{n+1}}{\Delta z^2}\right)$$

$$+q_{ssw}^{n+1}+q_{ssg}^{n+1}+q_{sso}^{n+1}+q_{ELE}^{n+1}-q_{LOSS}^{n+1}$$

Eq. 3-6

For resistive heating:

$$(\sigma_x)_{i+1/2,j,k}\left(\frac{\Psi_{i+1,j,k}-\Psi_{i,j,k}}{\Delta x^2}\right)-(\sigma_x)_{i-\frac{1}{2},j,k}\left(\frac{\Psi_{i,j,k}-\Psi_{i-1,j,k}}{\Delta x^2}\right)+(\sigma_y)_{i,j+\frac{1}{2},k}\left(\frac{\Psi_{i,j+1,k}-\Psi_{i,j,k}}{\Delta y^2}\right)$$
$$-(\sigma_y)_{i,j-\frac{1}{2},k}\left(\frac{\Psi_{i,j,k}-\Psi_{i,j-1,k}^{n}}{\Delta y^2}\right)+(\sigma_z)_{i,j,k+\frac{1}{2}}\left(\frac{\Psi_{i,j,k+1}-\Psi_{i,j,k}}{\Delta z^2}\right)$$
$$-(\sigma_z)_{i,j,k-\frac{1}{2}}\left(\frac{\Psi_{i,j,k}-\Psi_{i,j,k-1}}{\Delta z^2}\right)+J=0$$

Eq. 3-7

For electromagnetic heating:

$$\left(\frac{1}{(\sigma + j\omega\varepsilon)}\right)_{i+1/2,j,k}\left(\frac{H_{i+1,j,k} - H_{i,j,k}}{\Delta x^2}\right) - \left(\frac{1}{(\sigma + j\omega\varepsilon)}\right)_{i-\frac{1}{2},j,k}\left(\frac{H_{i,j,k} - H_{i-1,j,k}}{\Delta x^2}\right)$$
$$+\left(\frac{1}{(\sigma + j\omega\varepsilon)}\right)_{i,j+\frac{1}{2},k}\left(\frac{\mathrm{H}_{i,j+1,k} - \mathrm{H}_{i,j,k}}{\Delta y^2}\right) - \left(\frac{1}{(\sigma + j\omega\varepsilon)}\right)_{i,j-\frac{1}{2},k}\left(\frac{\mathrm{H}_{i,j,k} - \mathrm{H}_{i,j-1,k}}{\Delta y^2}\right)$$
$$+\left(\frac{1}{(\sigma + j\omega\varepsilon)}\right)_{i,j,k+\frac{1}{2}}\left(\frac{\mathrm{H}_{i,j,k+1} - \mathrm{H}_{i,j,k}}{\Delta z^2}\right) - \left(\frac{1}{(\sigma + j\omega\varepsilon)}\right)_{i,j,k-\frac{1}{2}}\left(\frac{\mathrm{H}_{i,j,k} - \mathrm{H}_{i,j,k-1}}{\Delta z^2}\right)$$
$$= -j\omega\mu\mathrm{H}_{i,j,k}$$

Eq. 3-8

3.2 Treatment of connections

Connections, expressed as transmissibility in reservoir simulation, are used in the present model to describe convection flow behaviours between control volumes. The flux term contains fluid properties, transmissibility and flow potential gradient.

For example, the transmissibility of phase p in the x1-direction is:

$$T_{p,i+\frac{1}{2},j,k} = \left(\frac{Ak}{h} x_{p,i}\rho_p k \frac{k_{rp}}{\mu_p}\right)_{i+\frac{1}{2},j,k}$$

Eq. 3-4

Eq. 3-4 contains the rock and grid properties $\frac{Ak}{h}$, the fluid property $\frac{x_{p,i}\rho_p}{\mu_p}$, and the rock/fluid property k_{rp}.

For the rock and grid properties, harmonic averaging is used for estimation of two adjacent grids:

$$\left(\frac{Ak}{h}\right)_{i+\frac{1}{2},j,k} = \frac{2\left(\frac{Ak}{h}\right)_{i,j,k}\left(\frac{Ak}{h}\right)_{i+1,j,k}}{\left(\frac{Ak}{h}\right)_{i,j,k} + \left(\frac{Ak}{h}\right)_{i+1,j,k}}$$

Eq. 3-5

For the fluid property, arithmetic averaging is used for estimation of two adjacent grids:

$$\left(\frac{x_{p,i}\rho_p}{\mu_p}\right)_{i+\frac{1}{2},j,k} = \frac{\left(\frac{x_{p,i}\rho_p}{\mu_p}\right)_{i,j,k} + \left(\frac{x_{p,i}\rho_p}{\mu_p}\right)_{i+1,j,k}}{2}$$

Eq. 3-6

For rock/fluid properties, upstream weighting technique is used for estimation of two adjacent grids from cell $i-1$ to cell i:

If $\Phi_{pi-1,j,k} > \Phi_{pi,j,k}$, $\left(k_{rp}\right)_{i+\frac{1}{2},j,k} = \left(k_{rp}\right)_{i-1,j,k}$; the flow of phase p is from block (i − 1, j, k) to block (i, j, k), where block (i−1, j, k) is the upstream block and block (i, j, k) is the downstream block for phase p.

If $\Phi_{pi-1,j,k} < \Phi_{pi,j,k}$, $\left(k_{rp}\right)_{i+\frac{1}{2},j,k} = \left(k_{rp}\right)_{i,j,k}$; the flow of phase p is from block (i , j, k) to block (i - 1, j, k), where block (i, j, k) is the upstream block and block (i - 1, j, k) is the downstream block for phase p.

In the process of electrical resistance heating, harmonic averaging is used for the estimation of electrical conductivity between two adjacent grids (Kabanov et al., 2018):

$$(\psi_i - \psi_{i+1})\sigma_{i+1/2,j,k} = \frac{(\psi_i - \psi_{i+1})}{\frac{1}{2\gamma_{e,i}} + \frac{1}{2\gamma_{e,i+1}}}$$

Eq. 3-7

$$(\gamma_e)_{i+1/2,j,k} = \frac{2(\gamma_e)_{i+1,j,k}(\gamma_e)_{i,j,k}}{(\gamma_e)_{i+1,j,k} + (\gamma_e)_{i,j,k}}$$

Eq. 3-8

This approximation of electric conductivity is similar to the average of absolute permeability in Eq. 3-8 that if one of the neighbouring grids has zero in electrical conductivity, there will not be electric current flow through these two grids.

In the process of EM heating, arithmetic averaging is used for the estimation of dielectric properties between two adjacent grids (Ji et al., 2019):

$$\left(\frac{1}{(\sigma + j\omega\varepsilon)}\right)_{i+1/2,j,k} = \frac{\left(\frac{1}{(\sigma + j\omega\varepsilon)}\right)_{i+1,j,k} + \left(\frac{1}{(\sigma + j\omega\varepsilon)}\right)_{i,j,k}}{2}$$

Eq. 3-9

3.3 Newton-Raphson method

The Newton-Raphson iteration is implemented in this work to solve the nonlinear equations include electrical phenomena in an oil reservoir. The Newton-Raphson method, invented by Isaac Newton and Joseph Raphson, is a powerful method for finding successive updates to roots. For a system with multi-equations and multi-variables, the Newton-Raphson method is expressed as:

$$[J]dV = -R$$

Eq. 3-10

where, J stands for a Jacobian matrix consisting of partial derivatives of the governing equations with respect to the independent variables, R indicates the residual vector and dV is the variables' difference gained from solving governing equations. To construct the Jacobian matrix, the derivative of each equation with respect to each independent variable needs to be calculated and assembled in the Jacobian matrix (Dong, 2012).

3.4 Grid and Jacobian Assembling

The grid in this simulation method is an assembly of control volumes, neighbours and wells. The control volumes and connections between neighbouring grids easily describe structured grids such as Cartesian grids (Dong, 2012).

For example, the assembling of a Jacobian matrix for a single equation system with single variable and discretized in a 5-grid system has the following configuration of non-zero values:

```
X X   X
X X X   X
  X X     X
X     X X   X
  X   X X X   X
    X   X X     X
        X     X X
          X   X X X
            X   X X
```

Figure 2.5 Jacobian structure of a single equation system with single variable and discretized in a 5-grid system

3.5 Time Step Control

Theoretically, in the method of fully implicit, the time step sizes of solving a linearized system are not limited. Because the phase change and the component appearance and disappearance are introduced in this simulation work, in the control volumes, it is necessary to control the time step to avoid convergence failure. The time step is calculated from relaxation methods (CMG STARS manual, 2017) as below:

$$\Delta t^{n+1} = \Delta t^{n} \frac{1.75DNORM(I)}{D(I)_{MAX}^{n} + 0.75DNORM(I)}$$

Eq. 3-11

where $D(I)_{MAX}^{n}$ is the maximum change value in P, T or Sp. DNORM is a pre-defined value for the different variables. Once a time step is lower than the minimal time step, the process will be terminated.

Chapter 4 Model Validation

4.1 Reservoir Model

The black-oil model contains three components: gas, oil and water and three phases: steam, oleic, aqueous. The steam component is allowed to appear in the gas and water phases, and the oil components can only show up in their own phase. A half reservoir 2D model with 20-m in lateral direction and 20-m in thickness with grid dimension of 1m×1m, as shown in Figure 5-1, is used in this thesis for a fast calculation.

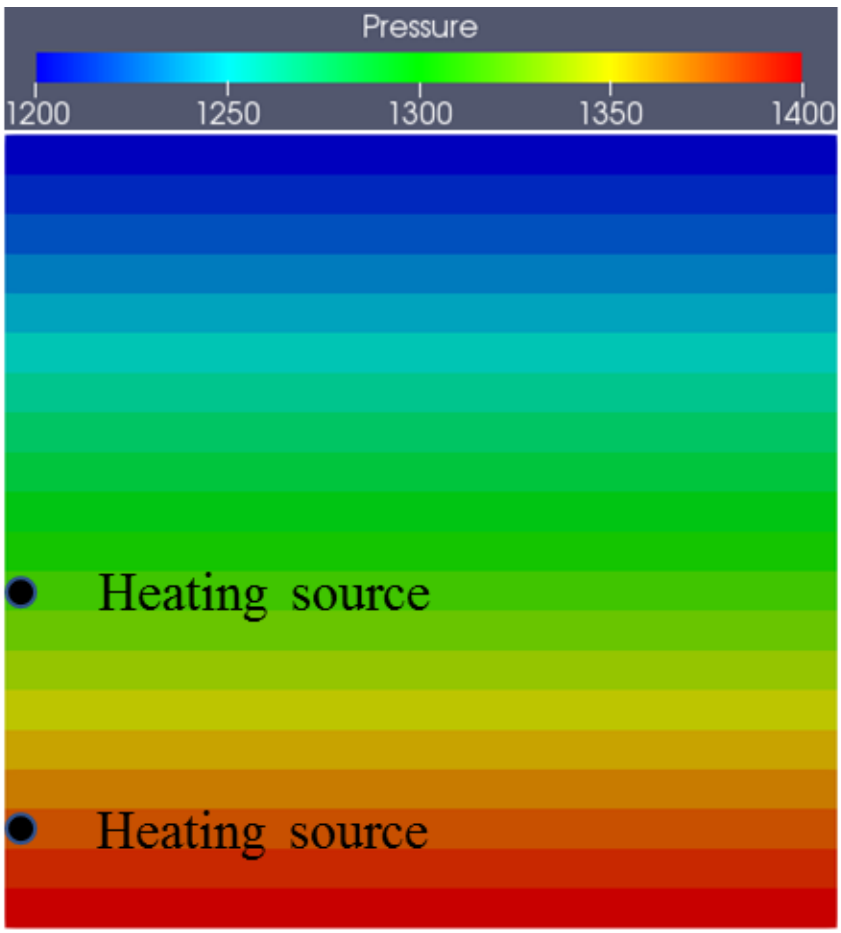

Figure 2.6 Illustration of half reservoir model with initial pressure distribution.

4.2 Initial Conditions

The current numerical code assumes that the reservoir is at a constant initial temperature with the already available distribution of water saturation, the oleic phase composition and the pressure at the reference point. Then, using a K-value based isothermal flash calculation the grid blocks are initialized. The initial properties are summarized in Table 4.1 to Table 4.3, and Figure 4.1.

Table 4.1 Characterization of Rock and Fluids

Items	Values
Vertical permeability, darcy	2.4
Horizontal permeability, darcy	4
Water heat capacity, C_w, kJ/(kg.℃)	4.2
Oil heat capacity, C_o, kJ/ (kg. ℃)	1.8
Sand matrix heat capacity, C_R, kJ/ (kg. ℃)	0.8
Oil sands thermal conductivity, K, W/(m.℃)	1.45
Sand density, ρ_R, kg/m^3	2400
Reference water density, $\rho_{w,ref}$, kg/m^3	1000
Reference oil density, $\rho_{o,ref}$, kg/m^3	1050
Reference porosity, ϕ_{ref}, fraction	0.3
Reference temperature, T_R, ℃	10
Reference pressure, P_R, Pa	1200×10^3
Water thermal expansion coefficient, β_w, 1/℃	0.207×10^{-3}
Oil thermal expansion coefficient, β_o, 1/℃	0.72×10^{-3}

Water compressibility, α_w, 1/Pa	4.58×10^{-10}
Oil compressibility, α_w, 1/Pa	1.5×10^{-10}
Oil sands compressibility, c, 1/Pa	1.0×10^{-9}

Table 4.2 Relative permeability of water-oil system

Sw	Krw	Kro
0	0	1
0.15	0	1
0.2	0.001	0.95
0.25	0.0016	0.84
0.3	0.0055	0.72
0.35	0.013	0.6
0.4	0.0254	0.47
0.45	0.044	0.35
0.5	0.0698	0.24
0.55	0.104	0.165
0.6	0.148	0.104
0.65	0.204	0.07
0.7	0.271	0.04
0.75	0.352	0.015
0.8	0.447	0
0.85	0.559	0
0.9	0.687	0
0.95	0.834	0
1	1	0

Table 4.3 Relative permeability of gas-oil system

Sg	Krg	Krog
1	1	0
0.85	1	0
0.8	0.95	0.0002
0.75	0.84	0.0016
0.7	0.72	0.0055
0.65	0.6	0.013
0.6	0.47	0.0254
0.55	0.35	0.044
0.5	0.248	0.0698
0.45	0.165	0.104
0.4	0.103	0.148
0.35	0.069	0.204
0.3	0.045	0.271
0.25	0.0288	0.352
0.2	0.0185	0.447
0.15	0.01	0.559
0.1	0	0.687
0.05	0	0.834
0	0	1

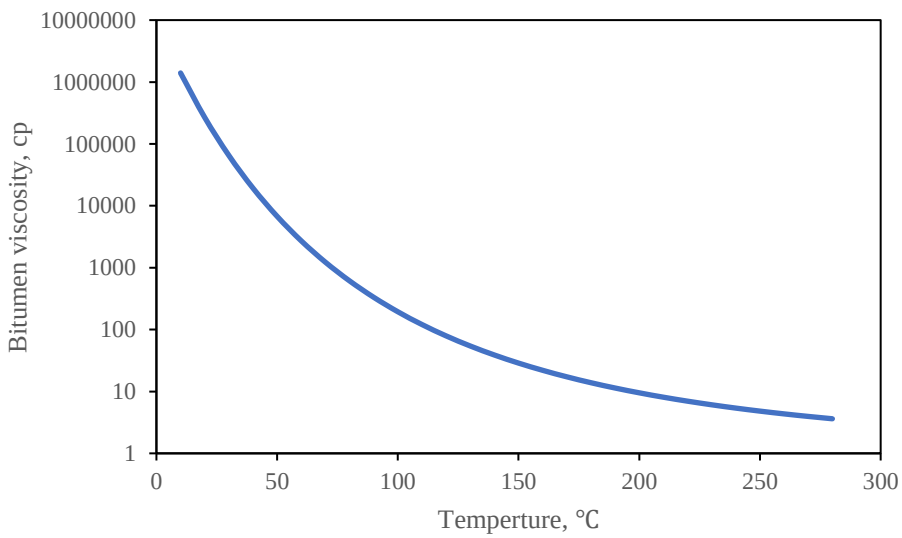

Figure 4.1 Oil viscosity versus temperature

4.2 Validation of Electric Heater process

The simulation results of electric heater processes were validated and verified by comparisons to available numerical solutions from CMG STARS.

The reservoir properties, as summarized in Table 4.1 to Table 4.3 and Figure 4.1, used for the model validation are same both in CMG STARS and this simulator developed in this thesis, except the fluid properties. In CMG STARS, default properties of fluids are used and the correlations as shown in section 2.2 are used in this thesis. For power control, the heater well operates on specified wellbore temperature T_{wspec} only as shown in Eq. 2-99. The function of electric heater in CMG STARS was conducted with maximum heating temperature (T_{wspec}) of 220 ℃ and 350 ℃, as well as the proposed simulator in this thesis. In order to obtain a more realistic simulation process,

Temperature and water saturation profiles of maximum heating source temperature of 220 ℃ and 350 ℃ are shown in Figure 4.2 to Figure 4.5, respectively. In general, comparisons of results were in good agreement in the two simulators. Producing almost the same temperature profiles demonstrates the accuracy of modelling heat transfer of the simulator proposed in this thesis. In addition, the water saturation profiles verify the feasibility of modelling in phase calculation and multi-phase flow of our proposed simulator.

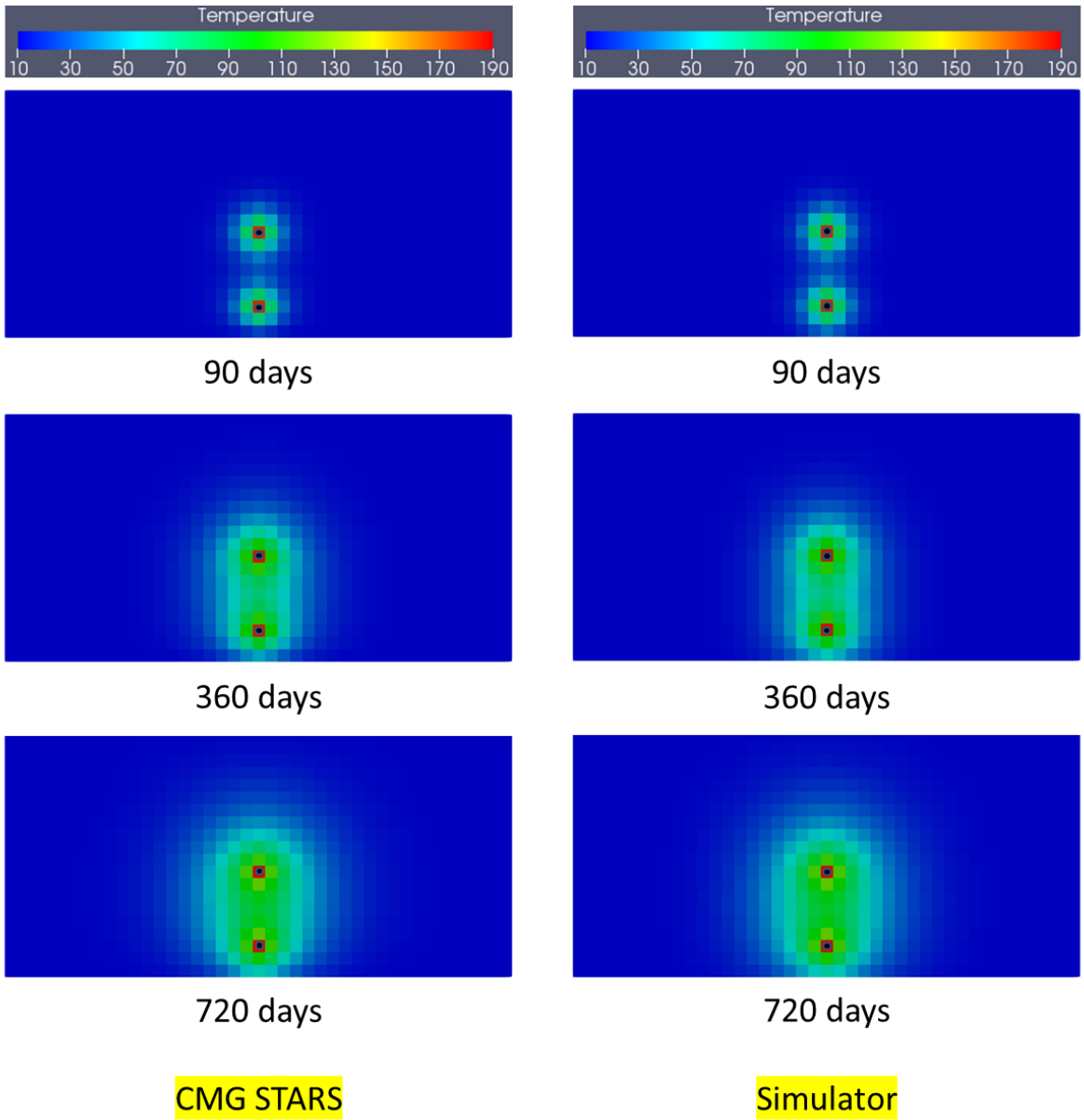

Figure 4.2 Comparison of temperature profiles by CMG STARS and the simulator in this thesis by maximum heating source temperature at 200 ℃. Time is selected at 90, 360 and 720 days.

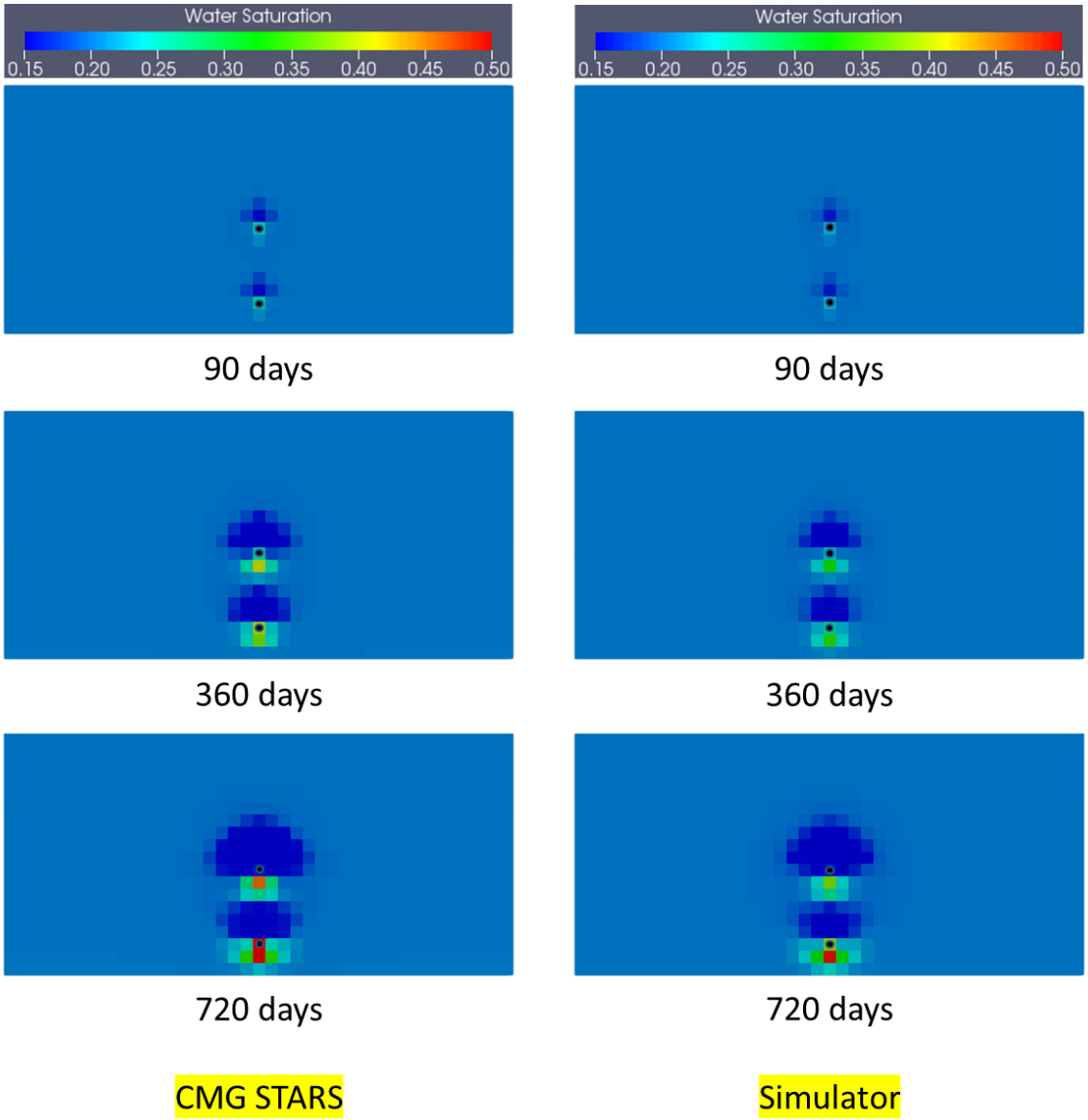

Figure 4.3 Comparison of water saturation profiles by CMG STARS and the simulator in this thesis by maximum heating source temperature at 200 ℃. Time is selected at 90, 360 and 720 days.

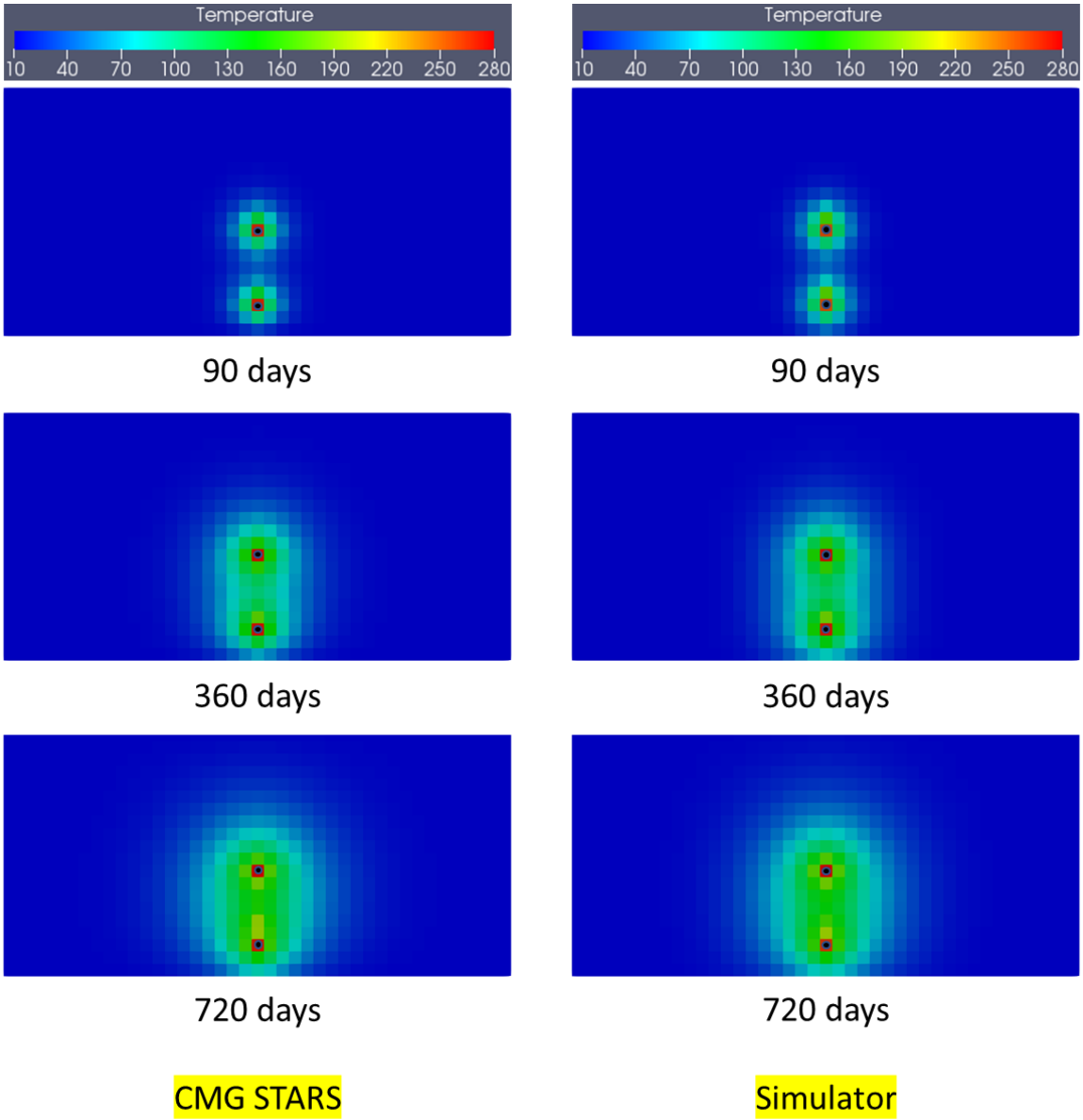

Figure 4.4 Comparison of temperature profiles by CMG STARS and the simulator in this thesis by maximum heating source temperature at 350 ℃. Time is selected at 90, 360 and 720 days.

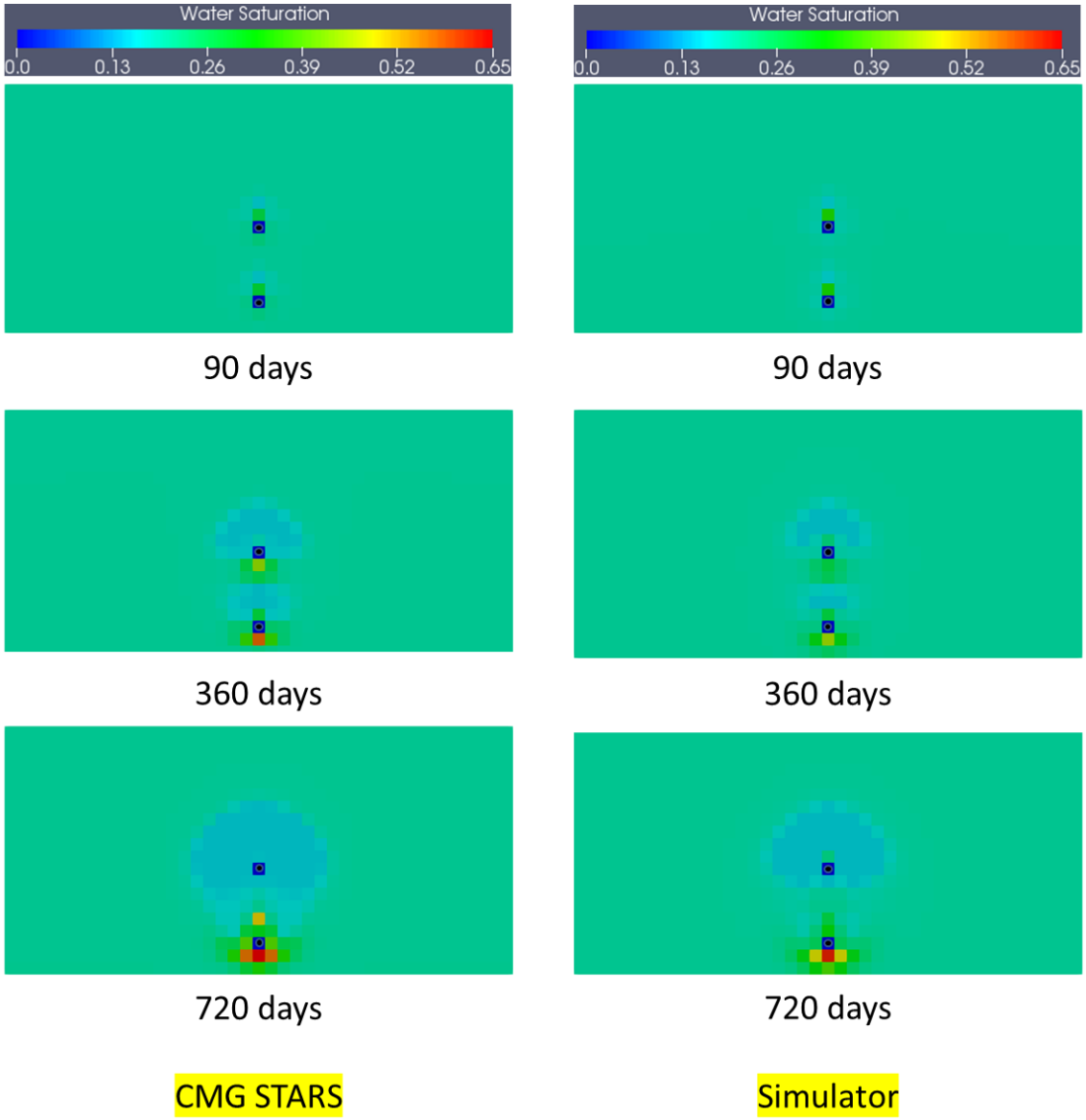

Figure 4.5 Comparison of water saturation profiles by CMG STARS and the simulator in this thesis by maximum heating source temperature at 350 ℃. Time is selected at 90, 360 and 720 days.

4.3 Validation of electrical resistance heating process

As mentioned before, the validation of fluids flow and heat transfer has been done in section 4.2. the validation of modelling electrical resistance heating process is conducted by the comparison of electrical potential between numerical simulation results and analytic solution (Killough and Gonzalez, 1986):

$$I_{wb}\frac{2\pi\gamma_{ewb}L\left(E_{wb}-E_{xyz}\right)}{ln\left[\left(\frac{R_e}{R_w}\right)-0.5\right]\Delta V}$$

Eq. 4-1

$$E_r = E_{wb} - I_{wb}\cdot ln\left(\frac{r}{R_w}\right)\frac{1}{2\pi\gamma_{ewb}L}$$

Eq. 4-2

The plots of electrical field potential of numerical solution and analytic solution with source voltage of 220 V are shown in Figure 4.6. The good agreement in electrical potential of was found of the two simulation approaches and the validation of the proposed simulator was conducted.

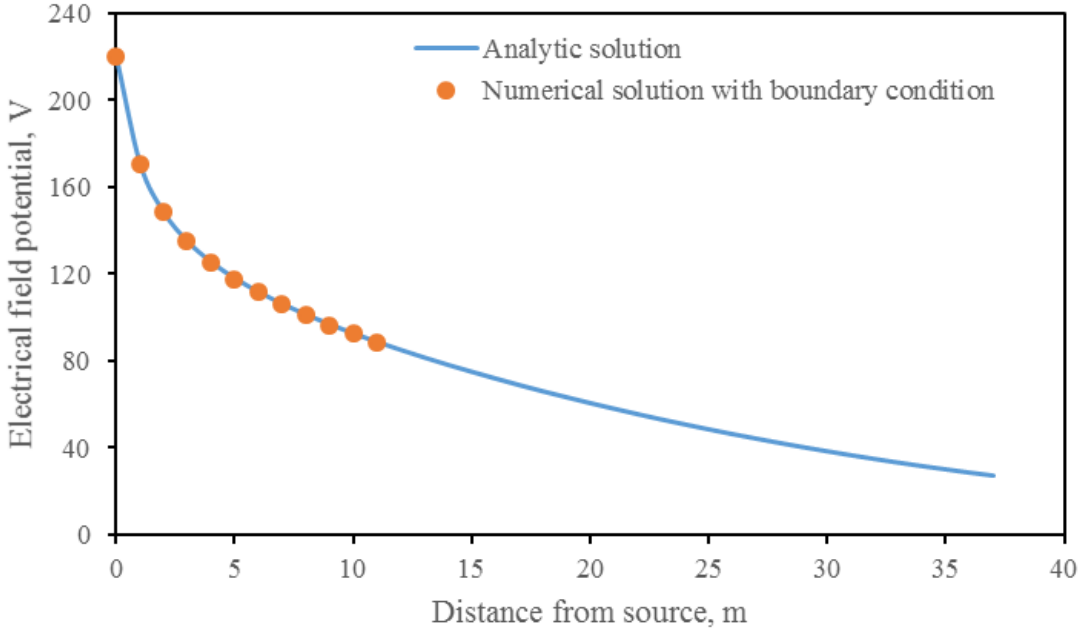

Figure 4.6 The results of electrical field potential of analytic solution and simulator in this thesis.

4.4 Validation of electromagnetic heating process

The simulation results by using Helmholtz's equation for the magnetic field proposed in this study are first compared to published analytical solutions for a homogeneous dielectric medium. By combining Maxwell's equations in a frequency domain, a 1D plane wave in a lossy medium can be analytically expressed by Eq. 4-3 (Saeedfar et al., 2016). Figure 4.7 shows the comparisons of spatial electric field distributions between the numerical solution in the proposed model and the analytical solution in Eq. 4-3. The good agreement of numerical and analytical results demonstrates the accuracy of the proposed numerical model on EM wave propagation estimation. By the method of finite differences (Chen, 1994), a grid size must be smaller than the wavelength of the system in which the frequency domain Maxwell's equations are discretized (Shin, 2013). In the finite difference time domain calculations, a grid size of l/20 is used for

calculation accuracy (Fu and Sun, 1999). In the finite difference frequency domain scheme, to accurately approximate spatial derivatives by finite difference, the grid size inside an EM medium should be smaller than 1/15 of the wavelength (Shin and Fan, 2012). In this study under scheme of finite difference frequency domain, grid size determination is related to EM source frequency, implying that high frequency waves owning short wavelength is simulated at small grids and low frequency wave having long wavelength is calculated at large grids. As shown in Figure 4.7 to obtain a high agreement level of the analytical and numerical solutions in the results of electric field distribution, EM waves in the radio-frequency band of 1.0×10^{8}, 1.0×10^{7} and 1.0×10^{6} Hz are simulated at the grid sizes of 0.1, 1.0 and 1.0 m, respectively.

$$E = E_0 e^{-\sqrt{j\omega\mu(\sigma+j\omega\varepsilon)}x}$$

Eq. 4-3

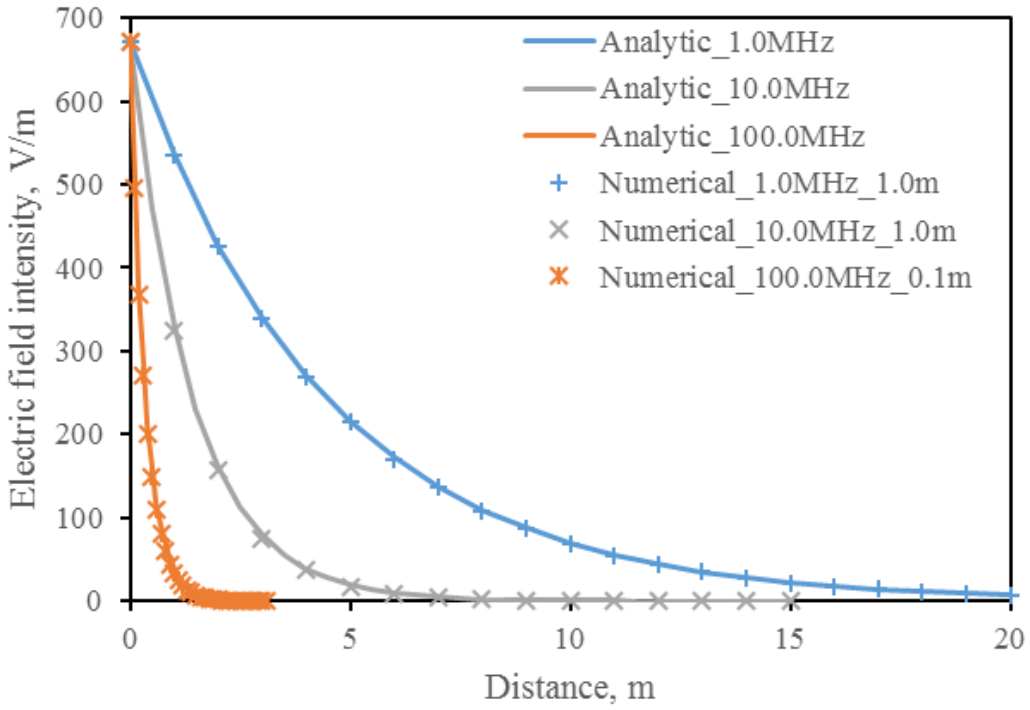

Figure 4.7 Comparison of electric field intensity distribution by analytic solution and numerical model in homogeneous media.

The second approach of model validation is estimation of electric field distributions in inhomogeneous media, in which dielectric properties are space-dependent. Simulation results of using Helmholtz's equation for the magnetic field proposed in this study are compared to those previously using Helmholtz's equation for the electric field by Yee's method. A gridding system was proposed by Yee (1966) involving staggered electric and magnetic fields in space by a half grid cell. In recent decades, Yee's method has been widely applied for solutions of EM waves in inhomogeneous media (Teixeira, 2008). In EM heating, a high power of an EM source can cause vaporization of in-situ water resulting in the development of a steam chamber near the source in a reservoir (Sadeghi et al., 2017a). In the direction from the EM source to outer reservoir, water saturation, which mainly controls the values of electric conductivity and dielectric permittivity,

varies gradually at the steam chamber boundary, as shown in Figure 4.8 to Figure 4.10. The simulation results of Figure 4.8 to Figure 4.10 show that there is excellent agreement of electric field distributions between the Helmholtz equation for the magnetic fields proposed in this study and by Yee's method, in the frequency range from 1.0×10^6 to 1.0×10^8 Hz. In addition, the large differences of electric field distributions from Helmholtz's equation for the electric field method (Eq. 1-1) and Helmholtz's equation for the magnetic field method (Eq. 2-79) show that the previously used Eq. 1-1 is not suitable for EM wave estimation in an inhomogeneous medium.

In Yee's method, both variables of the electric component and magnetic component are solved for simultaneously, while the solely magnetic component is solved for in the method of Helmholtz's equation for the magnetic field (Eq. 2-79) proposed in this study. Thus, the novel equation derived from Maxwell's equations in this study has the advantages of lower memory requirement and faster calculations over Yee's method.

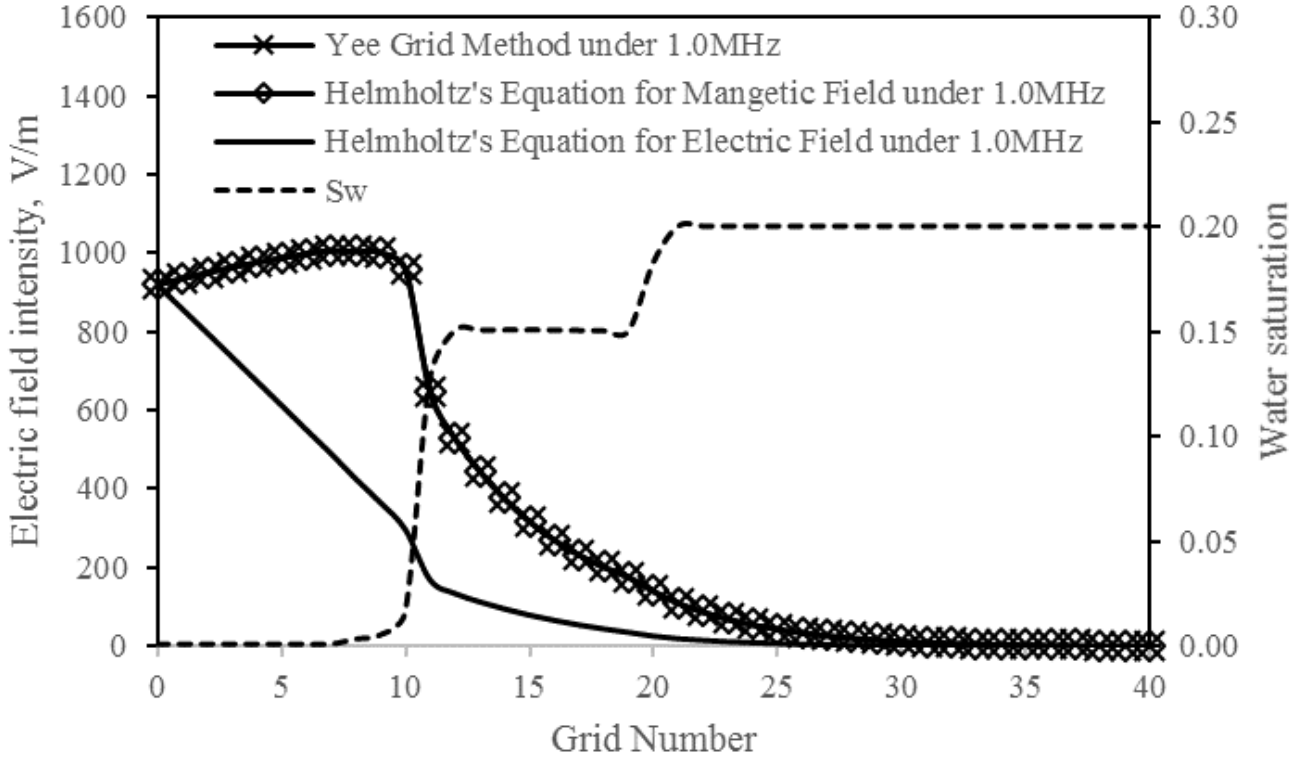

Figure 4.8 Profiles of electric field distribution versus distance under various water saturations by Yee's method, Helmholtz's equation for electric field (Eq. 1-1) and Helmholtz's equation for magnetic field (Eq. 2-79) in this work for an inhomogeneous medium. (a) is electric field distribution under EM source frequency of 1.0 MHz.

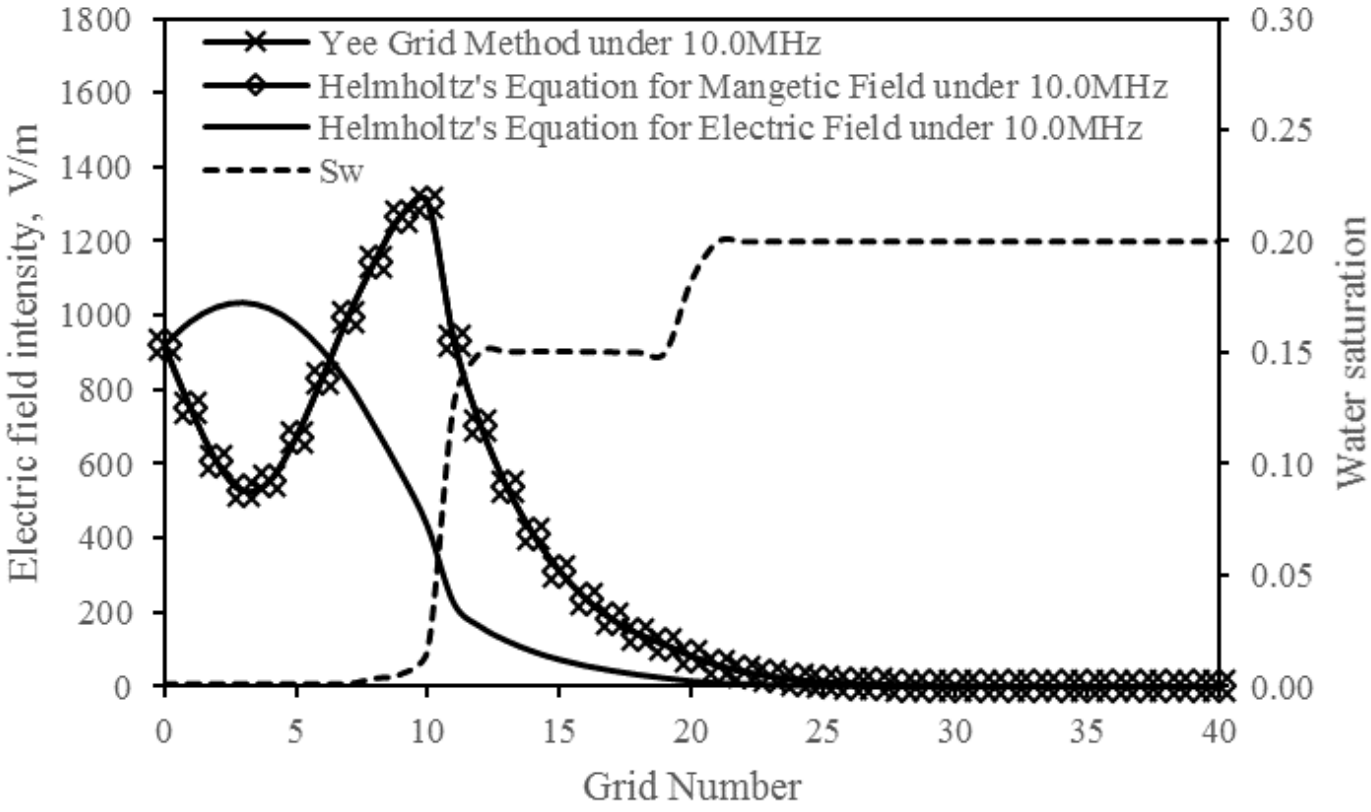

Figure 4.9 Profiles of electric field distribution versus distance under various water saturations by Yee's method, Helmholtz's equation for electric field (Eq. 1-1) and Helmholtz's equation for magnetic field (Eq. 2-79) in this work for an inhomogeneous medium. (a) is electric field distribution under EM source frequency of 10.0 MHz.

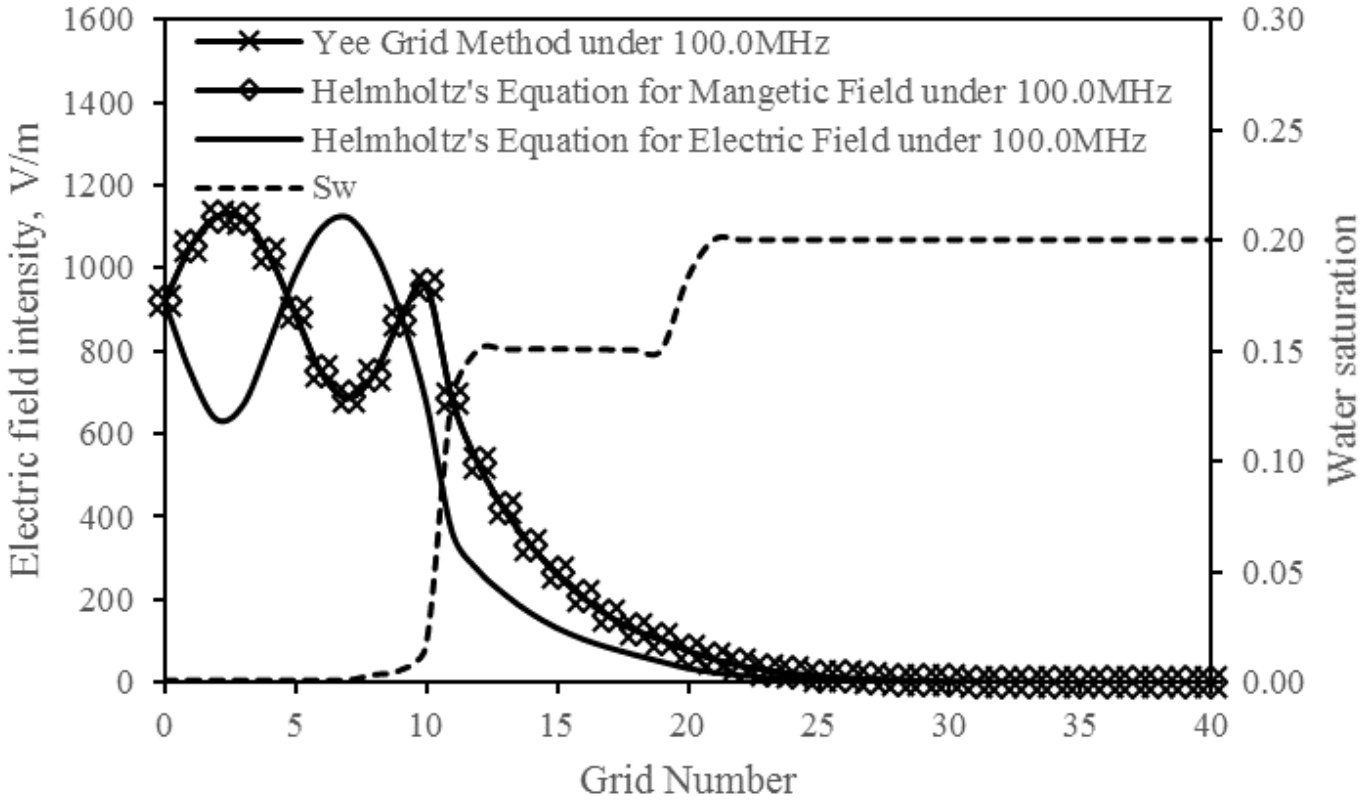

Figure 4.10 Profiles of electric field distribution versus distance under various water saturations by Yee's method, Helmholtz's equation for electric field (Eq. 1-1) and Helmholtz's equation for magnetic field (Eq. 2-79) in this work for an inhomogeneous medium. (a) is electric field distribution under EM source frequency of 100.0 MHz.

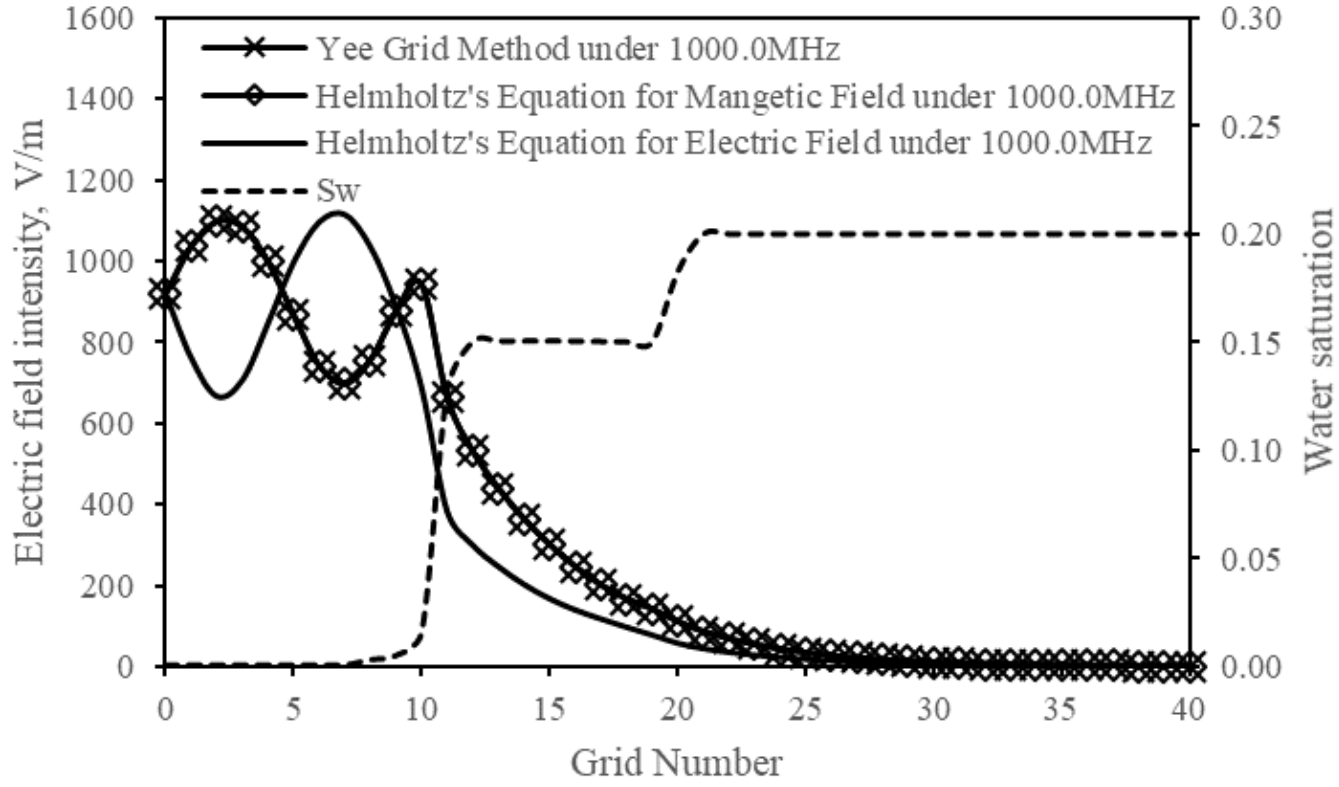

Figure 4.11 Profiles of electric field distribution versus distance under various water saturations by Yee's method, Helmholtz's equation for electric field (Eq. 1-1) and Helmholtz's equation for magnetic field (Eq. 2-79) in this work for an inhomogeneous medium. (a) is electric field distribution under EM source frequency of 1000.0 MHz.

Chapter 5 Simulation Results and Discussions

5.1 Cases of electric heater process

The reservoir properties, as summarized in Table 4.1 to Table 4.3 and Figure 4.1, are used for the simulation of the application of electric heater in oil sands reservoir. Reservoir model is same to the model used in the validation cases in section 4.1. The input power of electric heater is in the value of W/m.

First, the effect of continuous heating by electric heater in wellbore on depletion is studied. The horizontal well is located at left of reservoir in the lateral direction and 2 m above the bottom of the formation. The producer operates under a constant flowing bottom-hole pressure (BHP) (Rangel-German, et al., 2004), as described in Table 5.1 to Table 5.3.

An electric heater is implemented in the horizontal well.

Seven cases are considered:

Case 1-1: A constant heating source at 500 W/m of the electric heater is used in a horizontal well. Heating is conducted for 90 days with well shut-in to find out heat transfer and distribution results.

Case 1-2: A constant heating source at 1000 W/m of the electric heater is used in a horizontal well. Heating is conducted for 90 days with well shut-in to conduct the comparison to case 1 in the view of heating source power.

Case 1-3: A constant heating source at 1000 W/m of the electric heater is used in a horizontal well. Heating is conducted for 10 years with well constrained at minimum BHP at 1200 kPa.

Case 1-4: A constant heating source at 1000 W/m of the electric heater is used in a horizontal well. Heating is conducted for 10 years with well constrained at minimum BHP at 1000 kPa. Oil production performance is compared between Case 3 and Case 4.

Case 1-5: Due to the primary heat conduction in the process of heating by electric heater, the relatively slow heat transfer limits the heated-up area in the vicinity of wellbore. The feasibility of using cyclic heating and production is estimated. In this method, electric heater turned on with wellbore shut-in in a first period (1 month). Then, the wellbore is open for production within next period (1 month) under constraint of minimum BHP and heating is continuous. After the first cycle is finished, the operation continues to the next cycle with the same operation sequence.

Case 1-6: All the operation parameters are same to Case 1-5 except for the periods of heating cycle. The time period of heating with well shut-in has been extended to 2-month and the period of production is unchanged at 2-month.

Table 5.1 Application of electric heater by a single horizonal well under continuous heating

#	Heating Source	Well Pattern	Production well Constraint	Operation Time
Case 1-1	Power (500 W/m)	Single Horizontal Well	Shut-in	90 days
Case 1-2	Power (1000 W/m)	Single Horizontal Well	Shut-in	90 days
Case 1-3	Power (1000 W/m)	Single Horizontal Well	Minimum BHP (1200 kPa)	8 years
Case 1-4	Power (1000 W/m)	Single Horizontal Well	Minimum BHP (1000 kPa)	8 years

Table 5.2 Application of electric heater by a single horizonal well under cyclic heating and production

#	Heating Source	Well Pattern	Well Constraint while Heating	Well Constraint while Producing	Heating Cycle interval	Production Cycle interval	Operation Time
Case 1-5	Power (1000 W/m)	Single Horizontal Well	Shut-in	Minimum BHP (1000 kPa)	1-month	1-month (with heating)	8 years
Case 1-6	Power (1000 W/m)	Single Horizontal Well	Shut-in	Minimum BHP (1000 kPa)	2-month	2-month (with heating)	8 years

5.1.1 Effect of input power

Case 1 and Case 2 are conducted, and simulation results are compared to find out the effect of input power on the heating performance of electric heater process. Simulation results of temperature and water saturation at day 90 are shown in Figure 5.1.

Temperature profiles show the higher input power can heat up relatively larger area in the vicinity of wellbore and higher temperature at the wellbore. Due to the nature of primary heat conduction in electric heater process, high input power enables the larger amount of heat accumulated in the area close to the wellbore under high temperature without delivering the heat further to cold reservoir.

The distribution of water saturations of the two cases show that water is vaporized into steam and the condensate is accumulated above the wellbore, where temperature is below the saturation steam temperature.

The simulation results in this part provide the comment that the application of electric heater is favorable for pre-heating in the process of oil sands recovery but because of its limitations in heating distance by heat conduction, it may not be best as a full bitumen recovery process.

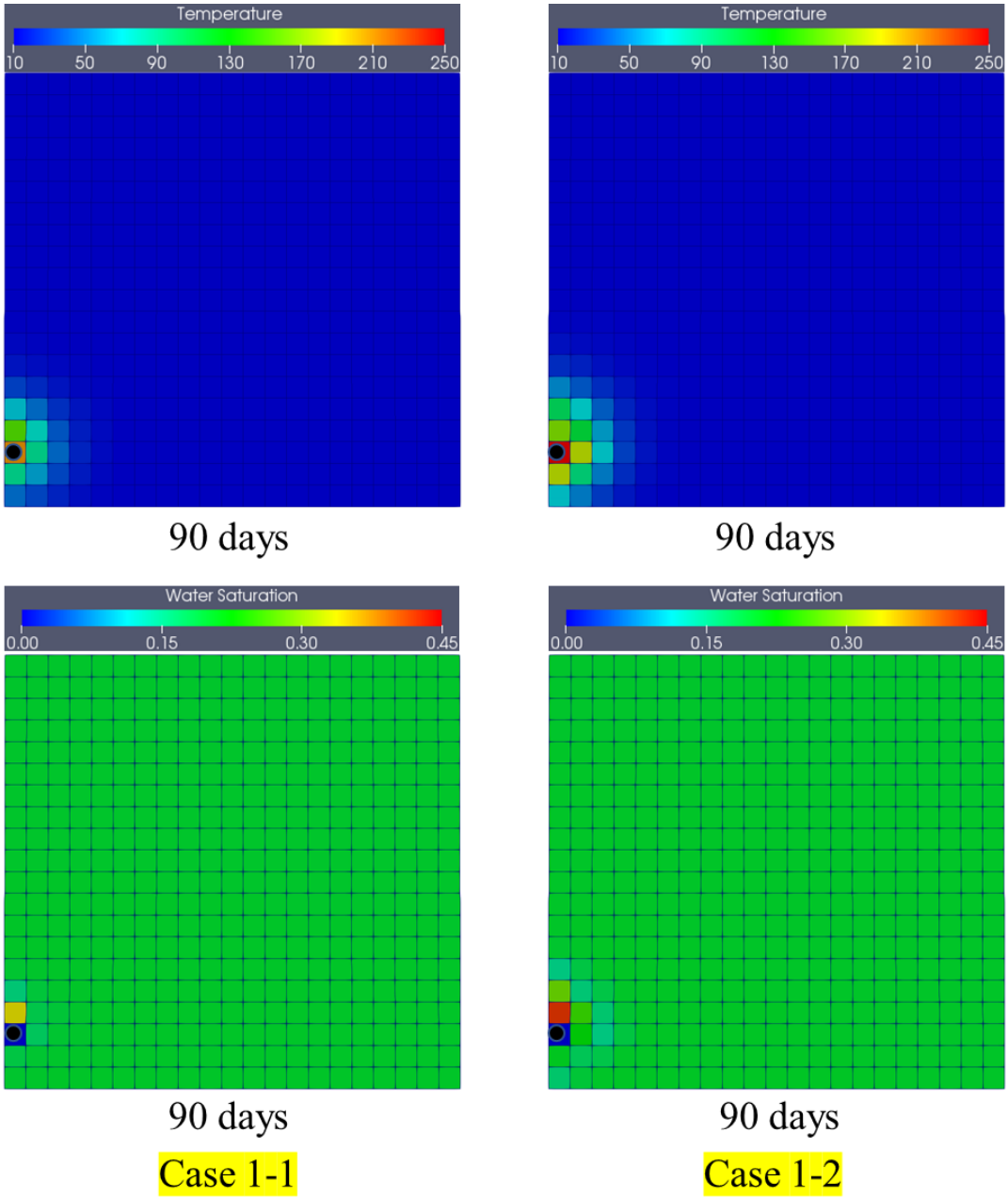

Figure 5.1 Temperature (℃) and water saturation profiles under heating by electric heater of Case 1-1 and Case 1-2.

5.1.2 Application of a single horizontal well with continuous production

The oil production is simulated of heating by the electric heater in wellbore. Simulation results of temperature and water saturation profiles are shown in Figure 5.2. In addition, curves of the amount of cumulative produced oil are plotted in Figure 5.3.

Heating is conducted continuously by 8 years to find out the feasibility of recover oil sands reservoir by electric heater at wellbore. At end of year 8, only a small part (4 – 5m) of area in the vicinity of wellbore is heated up above 100 ℃ as the temperature profiles shown in Figure 5.2. due to the primary heat condition in the process of heating by electric heater, there is similar temperature distributions of Case 1-3 and Case 1-4. It is also found that much amount of heat is delivered above the wellbore by the relatively high temperature profiles. The density difference of vapor and liquid results in counter-current flow in vertical direction. Steam flowing upwards delivers much heat above the wellbore by heat convection, which is largely faster than heat conduction.

In Case 1-3, the wellbore is constrained at a minimum BHP of 1200 kPa and the constraint is 1000 kPa in Case 1-4. The difference in well constraint in pressure results in relatively high amount of water accumulated below wellbore in Case 1-3 than the amount in Case 1-4 because of low pressure difference for liquid production at wellbore in Case 1-3. Figure 5.3 also shows that the low-pressure difference restricts the amount of oil production by the curves of cumulative oil production in Case 1-3 and Case 1-4.

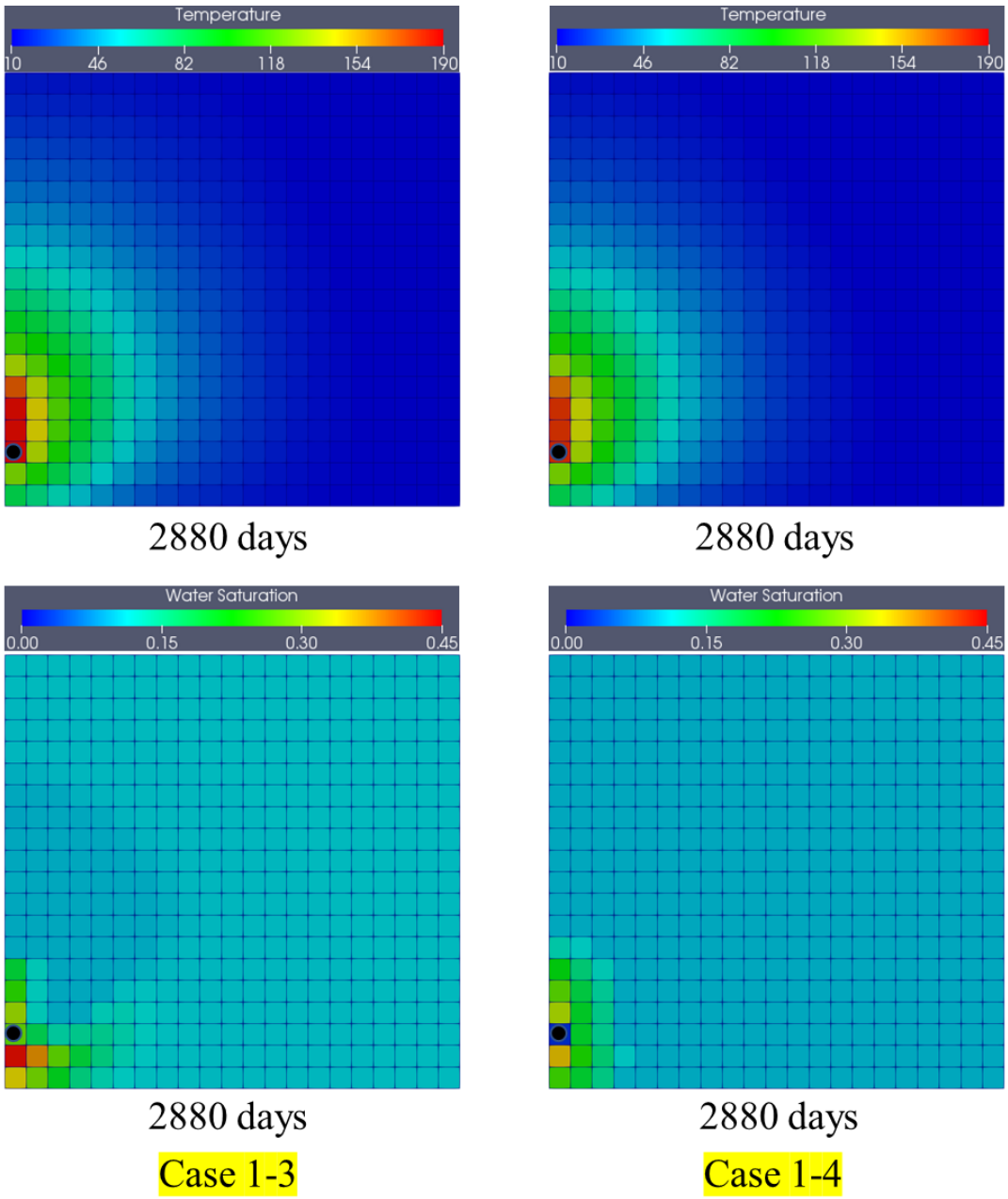

Figure 5.2 Temperature (℃) and water saturation profiles under heating by electric heater of Case 1-3 and Case 1-4.

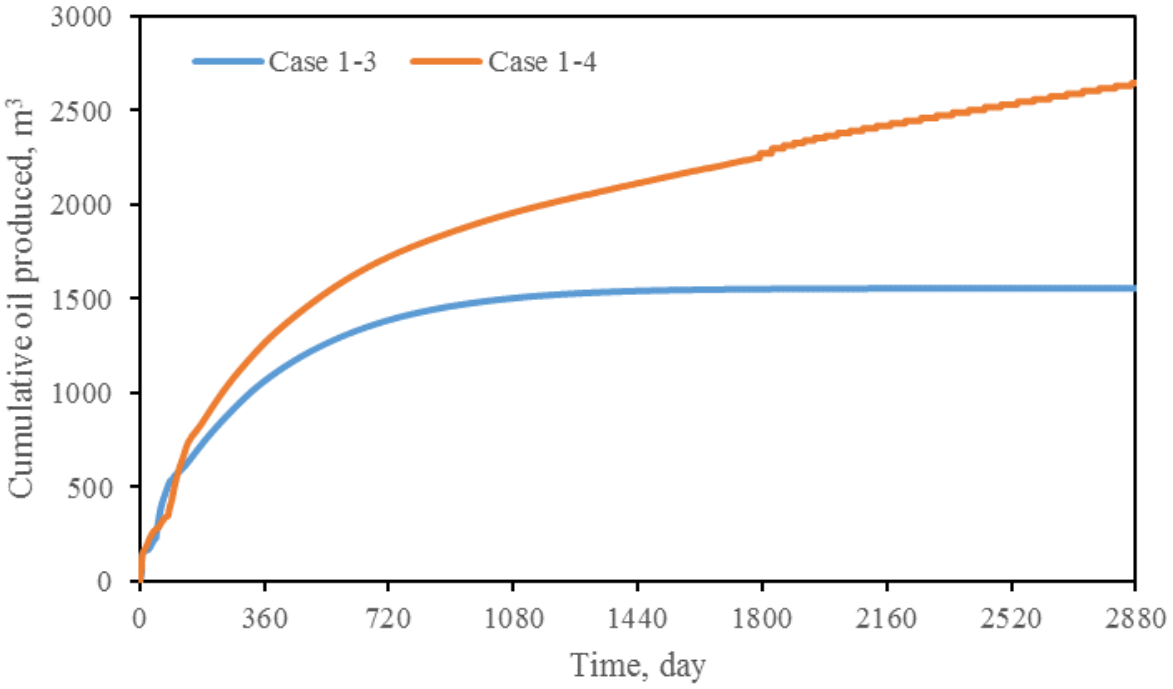

Figure 5.3 Cumulative oil produced of Case 1-3 and Case 1-4.

5.1.3 Application of a single horizontal well under cyclic heating and production

The application of a single horizontal well with continuous production is found limited in recovery oil sands reservoir by the restricted heating area, as shown in section 5.1.2. In this part, the feasibility of using cyclic heating and production is estimated. In this method, heating by electric heater is conducted with wellbore shut-in in a first period. Then, wellbore is open for production and heating is continuous. On one hand, continuous heating during production period can prevent significant drop in temperature in the vicinity of wellbore. On the other hand, the same amount of energy utilized is same compared to the cases in section 5.1.2.

The curves of cumulative oil produced in Figure 5.4 show that by application of cyclic heating and production can produce more oil when compared to the curves in Figure 5.3, in which oil is

continuously produced. The period of well shut-in stores heat inside the reservoir without production and this approach enlarges the heated-up area in reservoir. In the period of production, the high temperature oil with low viscosity can be produced to surface quickly. By the comparison of curves in Figure 5.4, it is shown relatively low constraint on BHP can produce more oil in Case 1-6 compared to Case 1-5.

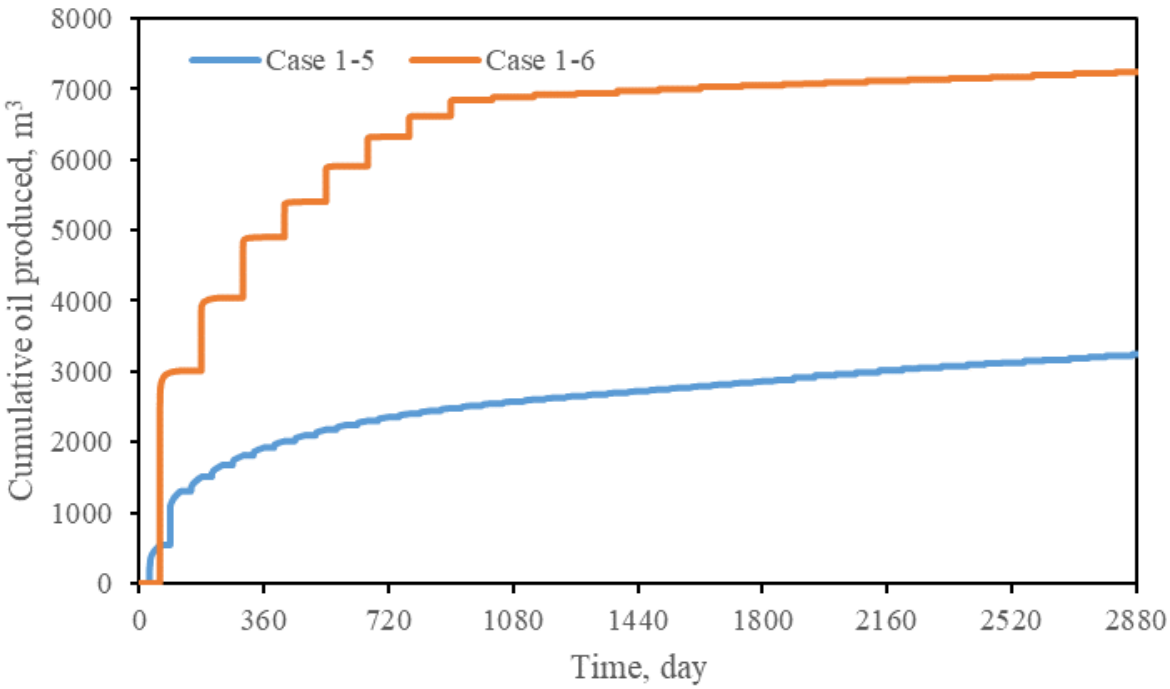

Figure 5.4 Cumulative oil produced of Case 1-5 and Case 1-6.

5.2 Cases of electrical resistance heating process

The reservoir properties, as summarized in Table 4.1 to Table 4.3 and Figure 4.1, are used for the simulation of the application of electric heater in oil sands reservoir. Reservoir model is same to the model used in the validation cases in section 4.1. The voltage applied at the electrode represents power input of electrical resistance heating and the energy dissipated in oil sands reservoir depends on the electrical properties of a reservoir.

Cases (Table 5.3) of Joule heating using the resistive heating process have been developed and executed. Comparisons in heating and production performance are also provided for variations in voltage at electrode, salinity electrical conductivity, and reservoir properties, such as water saturation. Scenarios are presented for finding potential application methods of resistive heating processes.

Case 2-1: In this case, electrical potential of 220 Voltage is used for heating source at the electrode to heat the reservoir electrically for 90 days, and wellbore is shut-in. The electrical conductivity of the saline water is 1.0 S/m.

Case 2-2: In this case, electrical potential of 220 Voltage is used for heating source at the electrode to heat the reservoir electrically for 90 days, and wellbore is shut-in. The electrical conductivity of the saline water is 2.0 S/m.

Case 2-3: In this case, electrical potential of 110 Voltage is used for heating source at the electrode to heat the reservoir electrically for 90 days, and wellbore is shut-in. The electrical conductivity of the saline water is 2.0 S/m.

Case 2-4: In this case, electrical potential of 220 Voltage is used for heating source at the electrode to heat the reservoir electrically for 2800 days (8 years), and wellbore is open for production with a minimum BHP at 1200 kPa. The electrical conductivity of the saline water is 2.0 S/m.

Case 2-5: In this case, electrical potential of 220 Voltage is used for heating source at the electrode to heat the reservoir electrically for 2800 days (8 years), and wellbore is open for production with a minimum BHP at 1000 kPa. The electrical conductivity of the saline water is 2.0 S/m.

Case 2-6: In this case, electrical potential of 220 Voltage is used for heating source at the electrode to heat the reservoir electrically for 2800 days (8 years), and wellbore is open for production with a minimum BHP at 1000 kPa. The electrical conductivity of the saline water is 2.0 S/m. Because water is the dominant material for transmitting electrical current and heat generation, the heating source is controlled under the condition without water vaporization. In other words, heating source is turned off once there is water vaporized into steam in oil sands reservoir.

Case 2-7: In this case, electrical potential of 220 Voltage is used for heating source at the electrode to heat the reservoir electrically for 2800 days (8 years), and wellbore is open for production with a minimum BHP at 1000 kPa. The well with an electrode implemented inside is drilled in a water zone, which is at the bottom of the reservoir.

Table 5.3 Application of electrical resistive heating by a single horizonal well under continuous heating

#	Electrode Voltage	Water Electrical Conductivity	Well Pattern	Production well Constraint	Operation Time
Case 2-1	220 V	1 S/m	Single Horizontal Well	Shut-in	90 days
Case 2-2	220 V	2 S/m	Single Horizontal Well	Shut-in	90 days
Case 2-3	110 V	2 S/m	Single Horizontal Well	Shut-in	90 days
Case 2-4	220 V	2 S/m	Single Horizontal Well	Minimum BHP (1200 kPa)	8 years
Case 2-5	220 V	2 S/m	Single Horizontal Well	Minimum BHP (1000 kPa)	8 years

5.2.1 Effect of Saline Water Electrical Conductivity and Applied Voltage at Electrodes

Case 2-1 to Case 2-3 are conducted to find out the effect of salinity electrical conductivity and applied voltage on heating performance of resistive heating process. High salinity electrical conductivity can transmit electrical current further to cold oil sands and the high voltage applied at the electrode provides larger electrical potential between the electrode and reservoir, which would be beneficial for heat generation.

Simulation results of temperature, water saturation and electrical potential are shown in Figure 5.5 for Case 2-1 to Case 2-3 at the end of 90 days.

By comparison of Case 2-1 and Case 2-2 in temperature profiles, it is found that high electrical conductivity of salinity in reservoir provides a relatively larger heated-up area around the wellbore in Case 2-2, when compared to the results in Case 2-1 with low electrical conductivity of salinity. According to Eq. 2-59, the heat generation rate under resistive heating is positively proportional to the value of electrical conductivity of reservoir. Thus, reservoir with higher salinity and therefore higher high electrical conductivity enables faster heat generation under the application of resistive heating. In Case 2-3, due to the low level of applied electrical voltage at the electrode, there is limited heated area.

The results of water saturations as shown in Figure 5.5 provide the information that water would be vaporized under resistive heating. In both Case 2-1 and Case 2-2, extremely low water saturation (below 0.001) is found in the grid, where the electrode is implemented. As a result, according to Eq. 3-8, low electrical conductivity by low water saturation impedes electrical current flow further to reservoir. Comparison of Case 2-1 and Case 2-3 shows that there are

similar distributions of electrical potential of the two cases, even though the applied voltage is 220 V in Case 2-1 and the voltage is 110 V in Case 2-3. This is the result of low water saturation by vaporization in Case 2-1, which impedes electrical current flow near the electrode, and relatively high water saturation, which enables electrical current flow out, in Case 2-3.

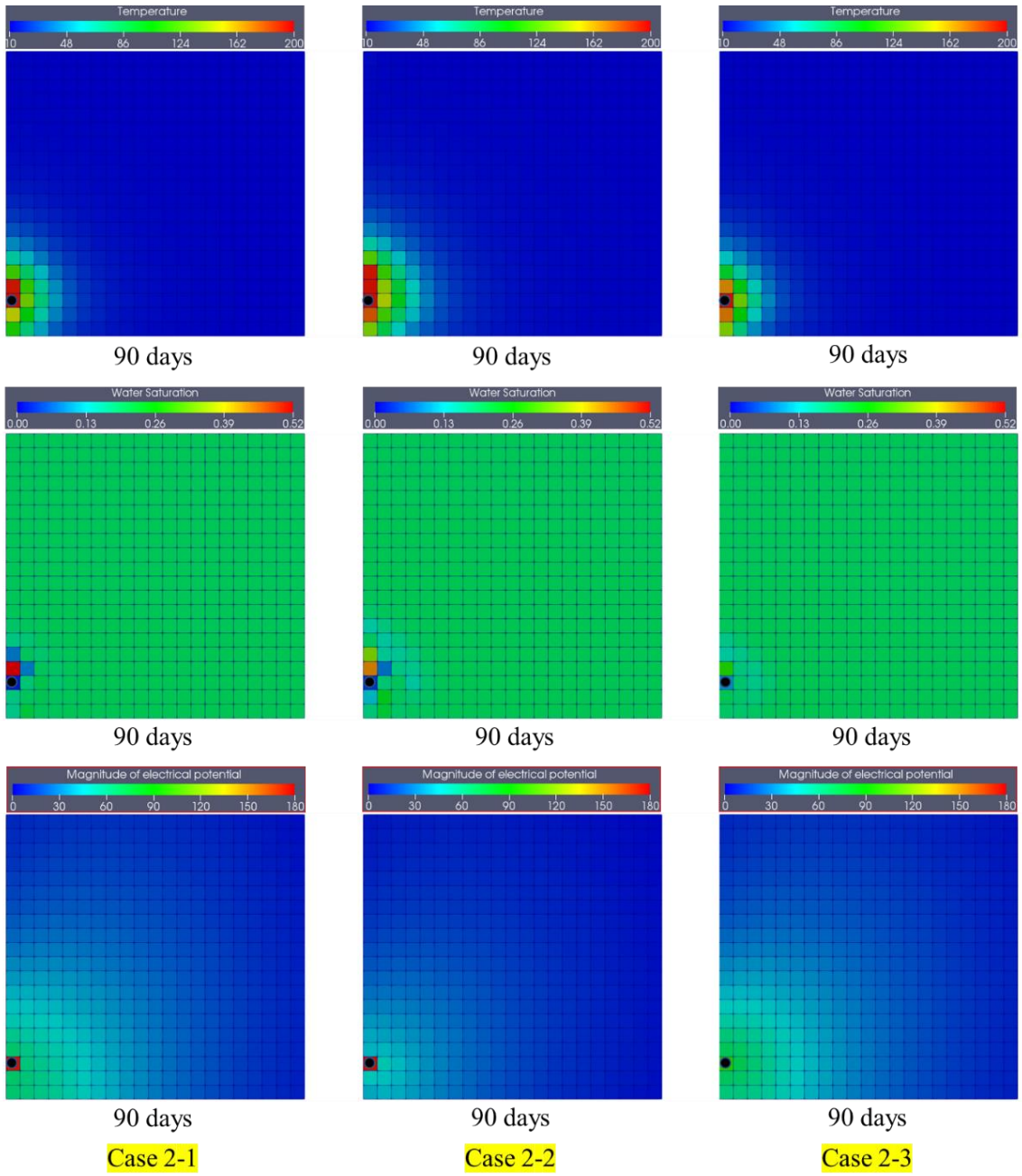

Figure 5.5 Temperature (℃), water saturation and electrical potential (voltage) profiles under resistive heating of Case 2-1, Case 2-2 and Case 2-3, at 90 days.

5.2.2 Application of a single horizontal well under continuous production

The oil production is simulated for resistive heating process with a single horizontal well. Simulation results of Case 2-4 and Case 2-5 regarding temperature and water saturation profiles are shown in Figure 5.6. In addition, curves of the cumulative produced oil are plotted in Figure 5.7. The only difference between Case 2-4 and Case 2-5 is the minimum BHP at the wellbore which affects oil production.

At the end of 2880 days (8 years), the heated-up area by resistive heating remains limited around the wellbore. Similar results to Case 2-1 in electrical potential are found in Case 2-4 and Case 2-5. Due to the vaporization of water by in-situ heat generation in resistive heating process, the electrical current is mostly restricted to the vicinity of the wellbore, and the resulting electrical potential is shown in Figure 5.6. Without transmission of electrical current further to oil sands, the heat is mainly transferred by conduction in lateral direction, once the water is mostly vaporized to steam at the location of electrode implementation. The further growth of heated-up area in Case 2-4 in vertical direction, compared to the result of Case 2-5, is the result of heat convection by steam flow upwards. In Case 2-4, the high minimum BHP maintains heat in the reservoir, which enlarges the heated-up zone in the vertical direction.

Curves of cumulative oil produced as shown in Figure 5.7 demonstrate that the low minimum BHP at wellbore (Case 2-5) enables more oil produced to surface when compared to Case 2-4, in which the minimum BHP is high. There are time periods during which oil production rates are higher than the other time periods for both Case 2-4 and Case 2-5. From 220 days to 300 days in Case 2-4, oil rate is significantly high as shown by the shape of the cumulative oil production

curve. In Case 2-5, this period is found from 400 days to 580 days. The reason is still unclear and needs to be evaluated more thoroughly in future work.

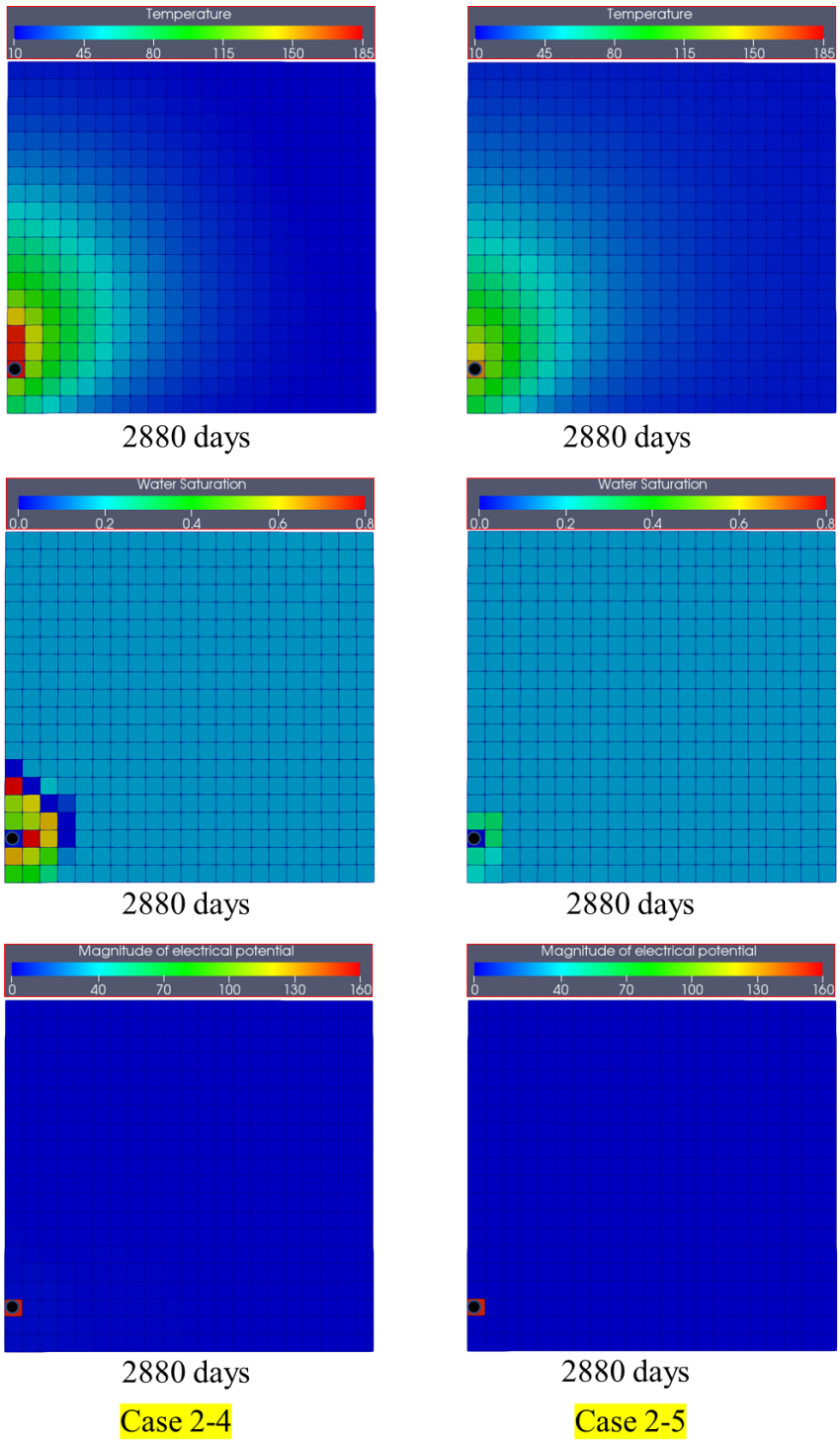

Figure 5.6 Temperature (℃), water saturation and electrical potential (voltage) profiles under resistive heating of Case 2-4 and Case 2-5, at 2880 days (8 years).

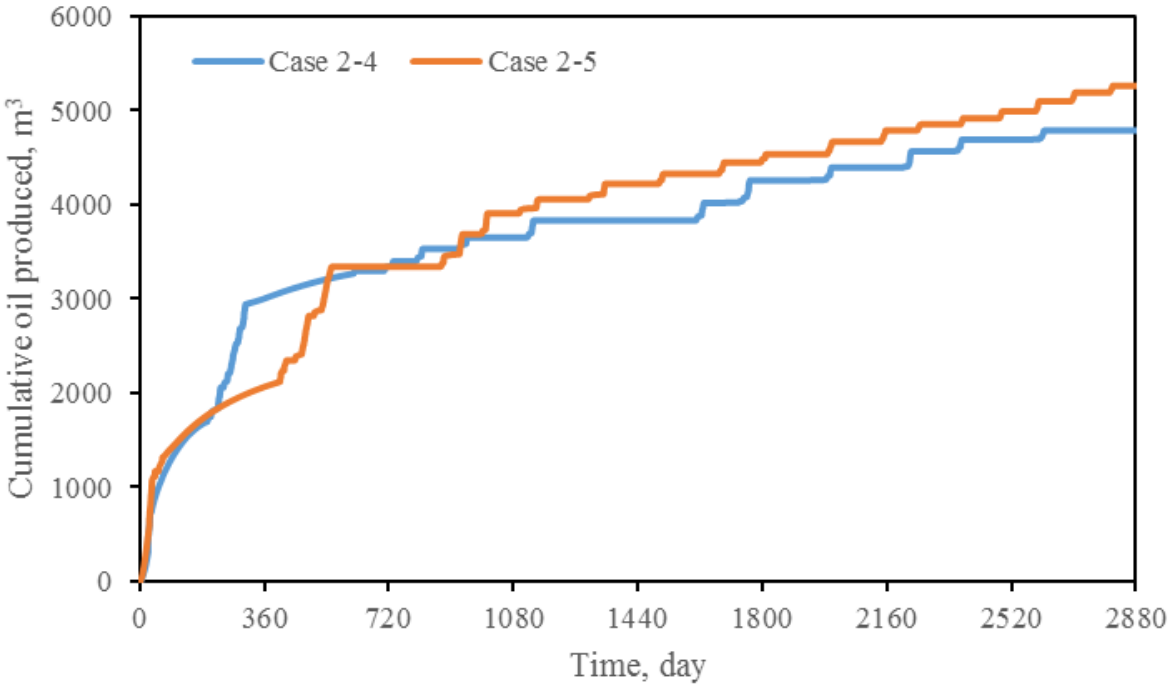

Figure 5.7 Cumulative oil produced of Case 2-4 and Case 2-5.

5.3 Cases of electromagnetic heating process

The reservoir properties, as summarized in Table 4.1 to Table 4.3 and Figure 4.1, are used for the simulation of the application of electric heater in oil sands reservoir. Reservoir model is same to the model used in the validation cases in section 4.1. The power input at an antenna is converted to the magnitude of electric field for the calculation of electromagnetic wave propagation in oil sands reservoir.

Cases (Table 5.4 to Table 5.7) of reservoir heating by propagation of electromagnetic waves have been developed and executed. Comparisons in heating and production performance are also provided for variations in wave source frequency, power, and reservoir properties. Scenarios are presented for finding potential application methods of EM heating processes. The formation of a

desiccated zone above an antenna is critical to EM heating process success, and this finding is confirmed under EM heating by the model and simulated cases. The method of properly averaging dielectric properties at neighbouring grid blocks is found to be effective in modelling of EM wave transmission. This is important because oil sands reservoirs contain inhomogeneous media where the local dielectric permittivity is determined by fluid saturations and compositions.

Nine cases were prepared for the evaluation of electromagnetic heating in oil sands reservoir:

Case 3-1: To investigate EM heating performance in an oil sands reservoir, a single horizontal well with implementation of an EM source antenna inside is drilled 2 m above the bottom of the reservoir. The heating source wave is selected with frequency of 1.0 MHz and power of 1.0 kW/m. Well is shut-in for 90 days to find out heat transfer and distribution results under variations in output power and frequency at the antenna.

Case 3-2: Operation parameters are same as in Case 3-1 except the heating power is increased to 2.0 kW/m.

Case 3-3: The frequency of electromagnetic wave is 10.0 MHz, which is 10 times the value used in Case 3-1 and Case 3-2. The output power at the antenna is 1.0 kW/m with the well shut-in.

Case 3-4: In this case, both output power and frequency of the source electromagnetic wave are set at the higher levels of 2.0 kW/m and 10.0 MHz, respectively.

Case 3-5: After the Comparison of output power and frequency provided by antenna in Case 3-1 to Case 3-4, the power is set at 1.0 kW/m to match the capability of equipment at surface, and the frequency of 10.0 MHz is found capable of fast heat generation. Production at the wellbore is constrained by a minimum Bottom-Hole-Pressure (BHP) of 1200 kPa.

Case 3-6: Operation parameters are the same as Case 3-5 except the minimum BHP has been reduced to 1000 kPa to determine its effect on oil production performance.

Case 3-7: The feasibility of using cyclic heating and production is evaluated for electromagnetic heating. In this method, heating is conducted with wellbore shut-in in a first period (1 month). Then, the wellbore is open for production within next period (1 month) under constraint of minimum BHP and heating is continuous. After the first cycle is finished, the operation continues to the next cycle with the same operation sequence.

Case 3-8: All the operation parameters are same to Case 3-7 except the periods of heating cycle. The time period of heating with well shut-in has been extended to 2-month and the period of production is unchanged at 1-month.

Case 3-9: A well-pair is used in this case to mimic the process of SAGD. A heating source at 1000 W/m and 1.0 MHz at the antenna is used in both the two horizontal wells for pre-heating during the first 90 days. Heating is continuous at the upper well and the lower well is alternated to a production well with a constraint of minimum BHP at 1000 kPa.

Table 5.4 Application of electromagnetic heating by a single horizonal well without production

#	Source Frequency	Heating Source	Grid Size	Well Pattern	Well Constraint	Operation Time
Case 3-1	1.0 MHz	Power (1.0 kW/m)	1.0 m	Single Horizontal Well	Shut-in	90 days
Case 3-2	1.0 MHz	Power (2.0 kW/m)	1.0 m	Single Horizontal Well	Shut-in	90 days
Case 3-3	10.0 MHz	Power (1.0 kW/m)	1.0 m	Single Horizontal Well	Shut-in	90 days
Case 3-4	10.0 MHz	Power (2.0 kW/m)	1.0 m	Single Horizontal Well	Shut-in	90 days

Table 5.5 Application of electromagnetic heating by a single horizonal well with continuous production

#	Source Frequency	Heating Source	Grid Size	Well Pattern	Production well Constraint	Operation Time
Case 3-5	10.0 MHz	Power (1.0 kW/m)	1.0 m	Single Horizontal Well	Minimum BHP (1200 kPa)	8 years
Case 3-6	10.0 MHz	Power (1.0 kW/m)	1.0 m	Single Horizontal Well	Minimum BHP (1000 kPa)	8 years

Table 5.6 Application of electromagnetic heating by a single horizonal well cyclic heating and production

#	Source Frequency	Heating Source, Power (kW/m)	Grid Size	Well Pattern	Production well Constraint	Heating Cycle interval	Production Cycle interval	Operation Time
Case 3-7	10.0 MHz	Power (1.0 kW/m)	1.0 m	Single Horizontal Well	Minimum BHP (1000 kPa)	1-month (with heating)	1-month (with heating)	8 years
Case 3-8	10.0 MHz	Power (1.0 kW/m)	1.0 m	Single Horizontal Well	Minimum BHP (1000 kPa)	2-month (with heating)	2-month (with heating)	8 years

Table 5.7 Application of electromagnetic heating by a well-pair

#	Heating Source	Source Frequency	Grid Size	Well Pattern	Upper well Constraint	Lower well Constraint	Operation Time
Case 3-9	Power (1.0 kW/m)	10.0 MHz	1.0 m	Well-pair	Shut-in for Heating	Shut-in for Pre-heating (90 days) + Minimum BHP (1000 kPa)	12 years

5.3.1 Evaluation of Power and Frequency at Source

Cases for applications of EM heating with a power source of 1.0 kW/m and 2.0 kW/m were built as shown in Table 5.4. Four simulation cases, as shown in Table 5.6, were conducted by the variations in EM source frequency of 1.0 MHz and 10.0 MHz, respectively. Well is shut-in without production to find out the capability of heating reservoir by electromagnetic waves.

At the end of 90 days, properties including temperature, water saturation and magnitude of electric field have been shown in Figure 5.8.

The difference between Case 3-1 and Case 3-2 is the input power. Simulation results show that by the increase in power from 1.0 kW/m to 2.0 kW/m, the heated-up area is enlarged under the comparison of temperature profiles. High output power at an antenna excites high value of electric field intensity locally and the high magnitude of electric field can generate a larger amount of heat by radiation.

In Case 3-3 and Case 3-4, the frequency of electromagnetic wave source has been increased to 10.0 MHz. After 90 days, temperature profiles for the two cases show that high EM source frequency (10.0 MHz) has the potential to heat up a relatively larger area of the reservoir than the low frequency cases (1.0 MHz). Because the heat generation rate is positively proportional to the wave frequency, the relatively slow heat generation of Case 3-1 and Case 3-2 cannot provide adequate energy to offset the heat transfer by conduction to the surrounding formations. Thus, there is faster in-situ heat generation from use of high frequency waves than is the case for the low frequency. Correspondingly, the desiccated zone with water saturation below 0.001 is, in Case 3-4 with the highest power and applied frequency, the largest of the cases at the end of 90 days.

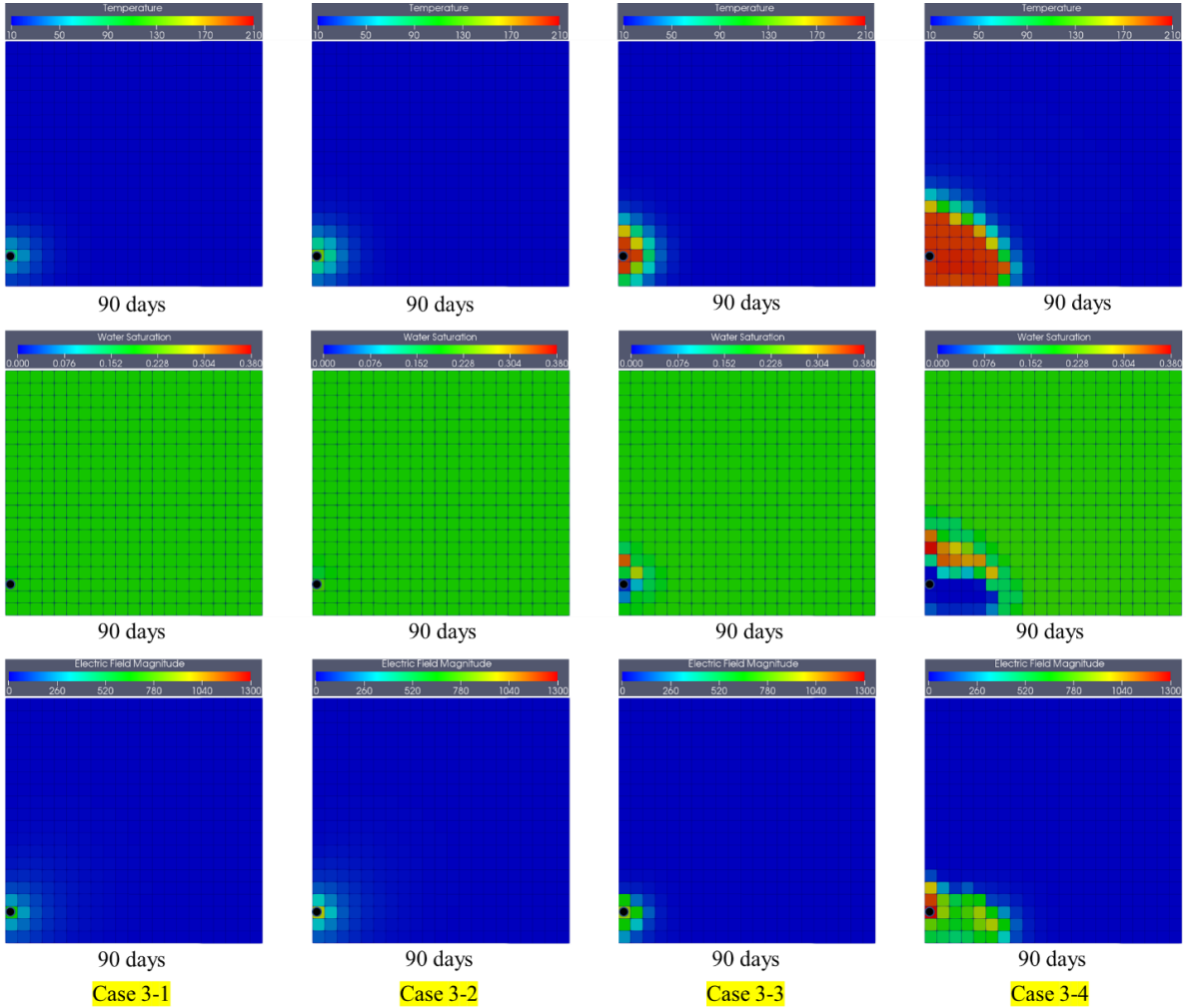

Figure 5.8 Temperature (℃), water saturation and magnitude of electric field (V/m) profiles under heating by electromagnetic waves of Case 3-1 to Case 3-4.

5.3.2 Application of a single horizontal well under continuous production

By EM heating, the oil near the wellbore is heated up, driven to the wellbore by gravity and produced to the surface. Cases for applications of EM heating with a power source of 1 kW/m were built by using typical fluids and reservoir properties of oil sands reservoirs in Alberta, Canada (Sadeghi et al., 2017b). Four simulation cases, as shown in Table 5.7 and Table 5.8, were conducted by varying well pattern and well constraints, respectively. Production at the wellbore is constrained by a minimum Bottom-Hole-Pressure (BHP).

Figure 5.9 shows the profiles of temperature, water saturation and electric field intensity at a cross-section view of Cases 3-5 to Case 3-6. Results of these three cases are drawn at 2880 days (8 years).

At the end of 2880 days, temperature profiles of the two cases show that the heated-up area is restricted by the continuous fluids production at the well. By gravity, the in-situ generated steam flows upwards and touches cold oil sands above the antenna. Then, condensate is formed by the steam cooling to below saturated steam temperature at reservoir pressure. Because the dominant dielectric lossy material in the oil sands reservoir is water, it absorbs the most energy and attenuates EM waves significantly. The water saturation and electric field intensity drawn in both Figure 5.9 demonstrate that the accumulated condensate at the top of the desiccated zone largely impedes EM wave propagation. As a result, EM wave propagates only in the vicinity of wellbore without further touching cold oil sands.

Curves of cumulative oil production are plotted in Figure 5.10 in the cases summarized in Table 5.7. The amount of produced oil from the wellbore is largely impacted by the difference between BHP and reservoir pressure. The wellbore is constrained at a minimum pressure of 1200 kPa

(Case 3-5) and 1000 kPa (Case 3-6). Oil production is triggered by a pressure increase under heating. Because the in-situ pressure can be largely increased by vaporization under heat generation, the amounts of produced oil in the Case 3-6 under low BHP is significantly higher than the amounts with a high BHP in Case 3-5. Oil production shown in Figure 5.10 in Case 5 provides the information that the enlarged pressure difference between the wellbore and reservoir can benefit the oil production rate.

In Case 3-5, due to the low-pressure difference of wellbore and the local grid, which is potential of liquid production at the wellbore, condensate accumulation around the wellbore limits its EM wave penetration in oil sands, which is critical to heat generation and heat transfer.

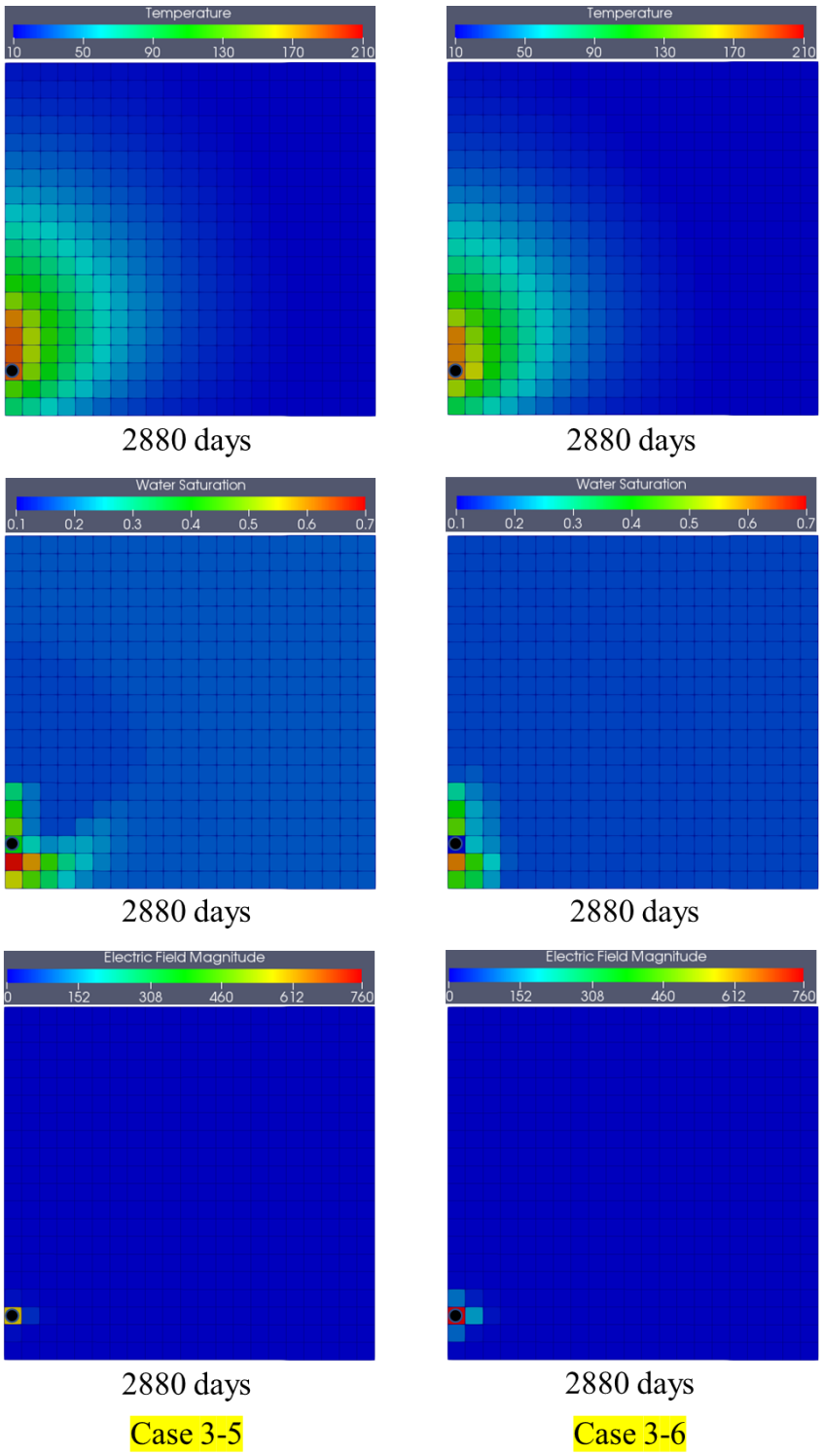

Figure 5.9 Temperature (℃), water saturation and magnitude of electric field (V/m) profiles under heating by electromagnetic waves of Case 3-5 to Case 3-6.

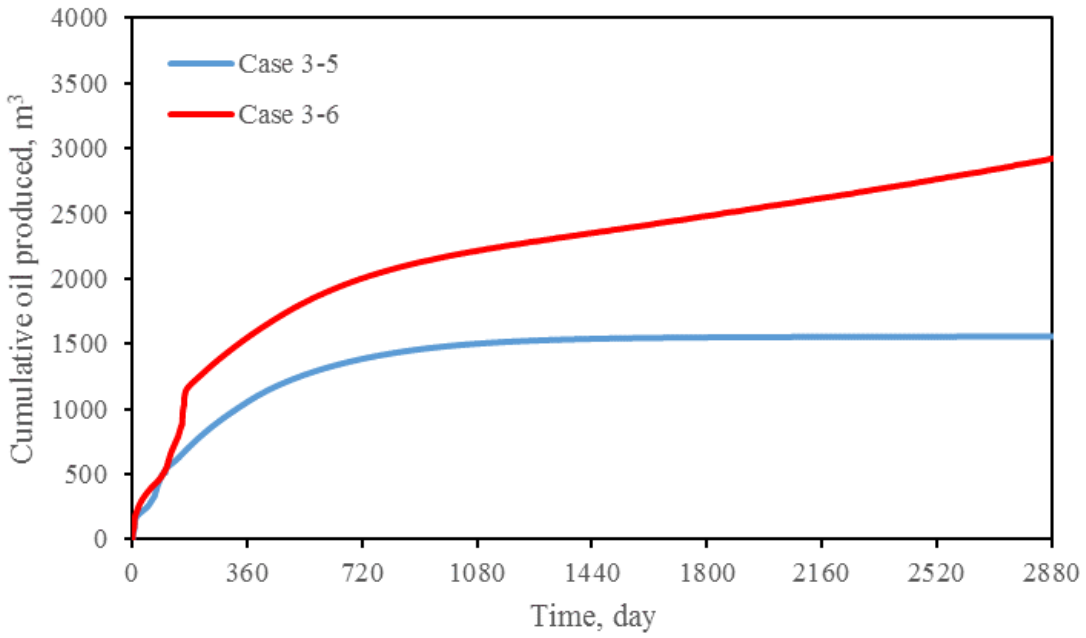

Figure 5.10 Cumulative oil produced by electromagnetic heating of Case 3-5 and Case 3-6.

5.3.3 Application of a single horizontal well under cyclic Heating and production

The application of a single horizontal well with continuous production is found limited in recovery oil sands reservoir by the restricted heating area. In this part, the feasibility of using cyclic heating and production is evaluated. In this method, heating by electric heater is conducted with wellbore shut-in in a first period. Then, wellbore is open for production and heating is continuous.

The curves of cumulative oil produced in Figure 5.11 show that by application of cyclic heating and production can produce more amount of oil when compared to the curves in Figure 5.10, in which oil is continuously produced. The period of well shut-in stores the heat inside reservoir without production and this approach enlarges the heated-up area in reservoir. In the period of production, the high temperature oil with low viscosity can be produced to surface quickly. By

the comparison of curves in Figure 5.11, it is shown relatively low constraint on BHP can produce a larger amount of oil in Case 3-8 than the amount in Case 3-7.

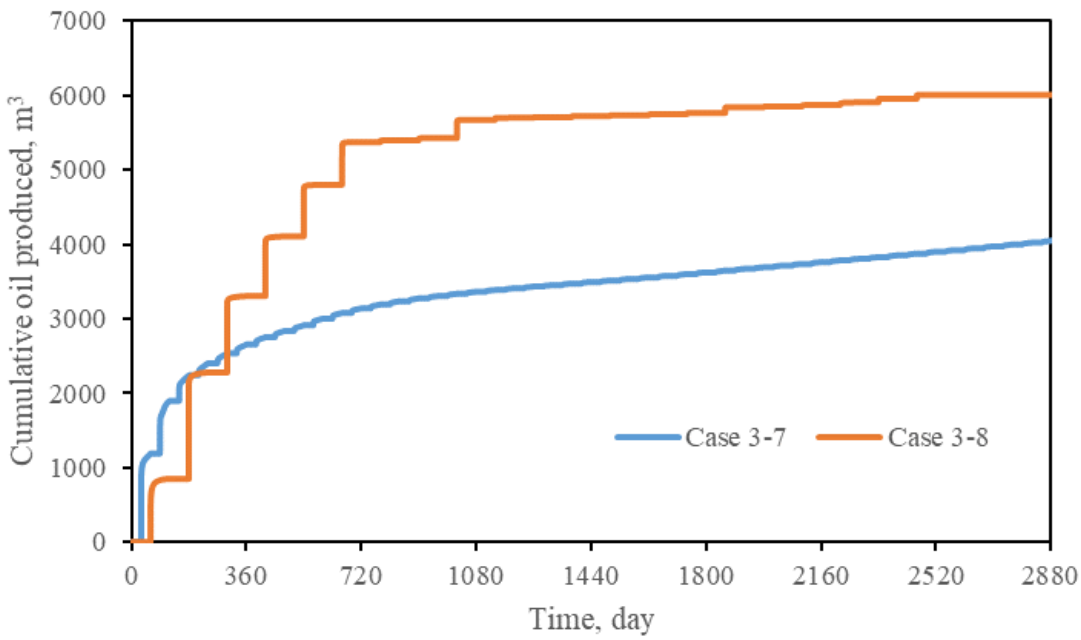

Figure 5.11 Cumulative oil produced by electromagnetic heating of Case 3-7 and Case 3-8.

5.3.4 Application of a horizontal well-pair

A well-pair is used in this study to mimic the process of SAGD, in which steam is injected in a reservoir from an upper horizontal well and heated fluids are produced at a lower horizontal well to the surface. In this section, a horizontal well-pair is implemented in a reservoir with the same configuration as in SAGD. Antennas are placed inside both wellbores for preheating. EM heating is conducted at the first three months without production to achieve heat communication between the two wells. Then, EM heating is only applied at the upper horizontal well with production at the lower well at the same time. An EM source at a frequency of 10.0 MHz is chosen because of

the apparent developed desiccated zone, which is regarded as crucial to EM heating success, as shown in Figure 5.8. Case operations are summarized in Table 5.9. Figure 5.12 shows profiles of temperature, water saturation and electric field intensity in the cases by application of a horizontal well-pair in the oil sands reservoir. At the end of 90 days, heat communication between the two wells is established when the temperature at the middle point of the well-pair is around 80℃. Simulation results show that, as the heating time progresses, a desiccated zone has been established above the well-pair at the end of both 1800 days (5 years) and 2880 days (8 years). The comparison of water saturation in Figures 5.11 shows that, with a well-pair, the desiccated zone tends to develop vertically. The combination of an upper heating well and a lower production well enables heated fluids flowing downwards by gravity and leaving space for EM wave penetration further upwards. At the end of 2880 days (8 years), the vertical development of the desiccated zone seems to have ceased due to much accumulation of condensate at the top.

In Figure 5.13, Case 3-9 results show a significant increase in the amount of produced oil than in Case 3-8, in which only a single horizontal well is applied. Due to 5 m separation between the upper well with the EM source and the lower well for production, the relatively low pressure at the lower production by a well constraint of a minimum BHP enables fluid flow downwards without accumulation in the vicinity of the upper well, compared to Case 3-8. Thus, there is potential for the EM wave propagating further to cold oil sands through a desiccated zone with extremely low water saturation.

By the analysis of heating and production performance in the cases, it is found that the development of a desiccated zone is related to EM source frequency and this has a major effect

on the oil production rate. A medium level EM wave frequency, such as in Case 3-9, is necessary to make wave penetrating further to the oil sands reservoir and establishment of a desiccated zone by generating heat. In addition, a relatively moderate oil production rate can maintain the heat in the reservoir to prevent the desiccated zone shrinkage by steam condensation.

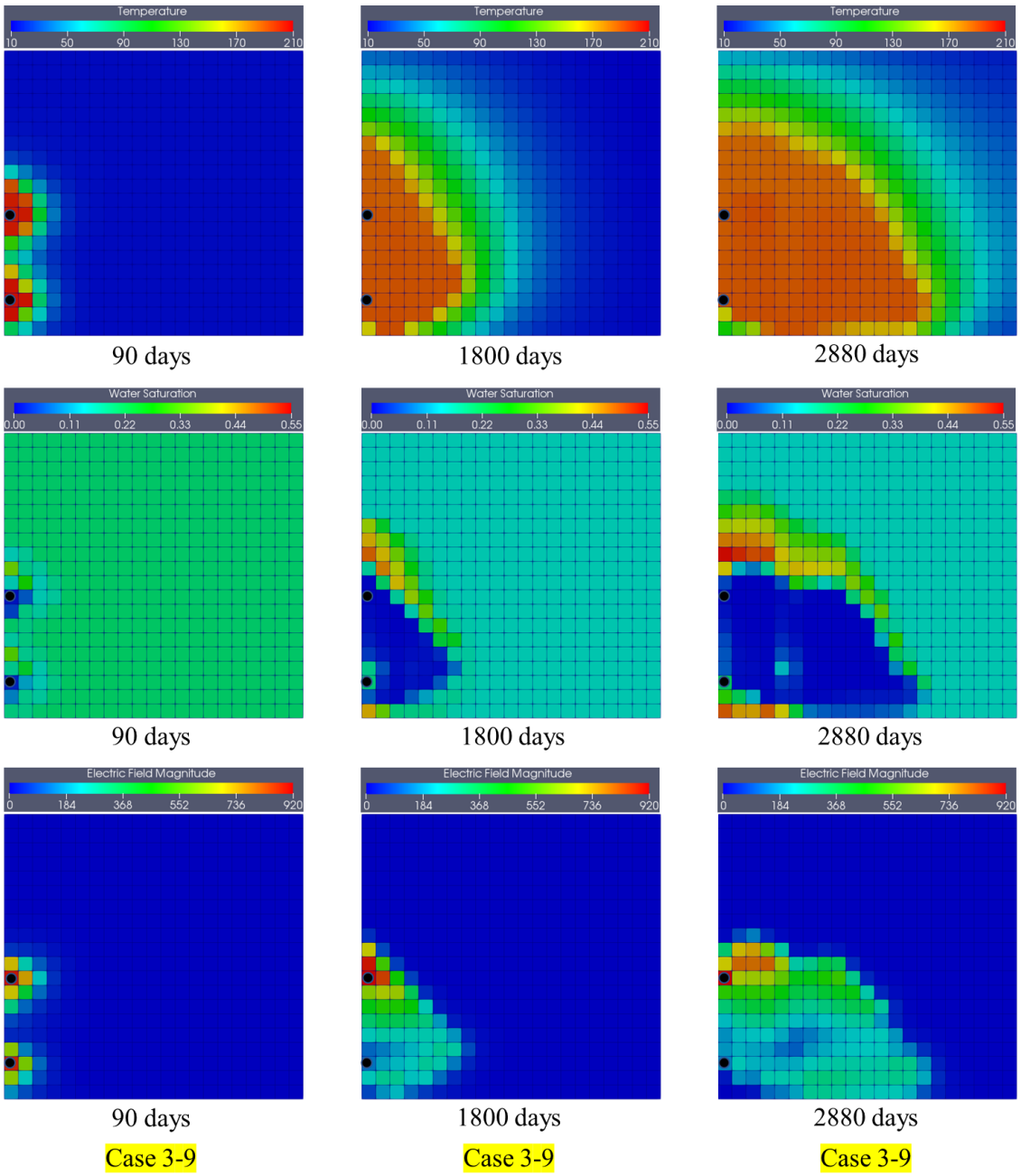

Figure 5.12 Temperature (℃), water saturation and magnitude of electric field (V/m) profiles under heating by electromagnetic waves of Case 3-9 at 90 days, 1800 days and 2880 days.

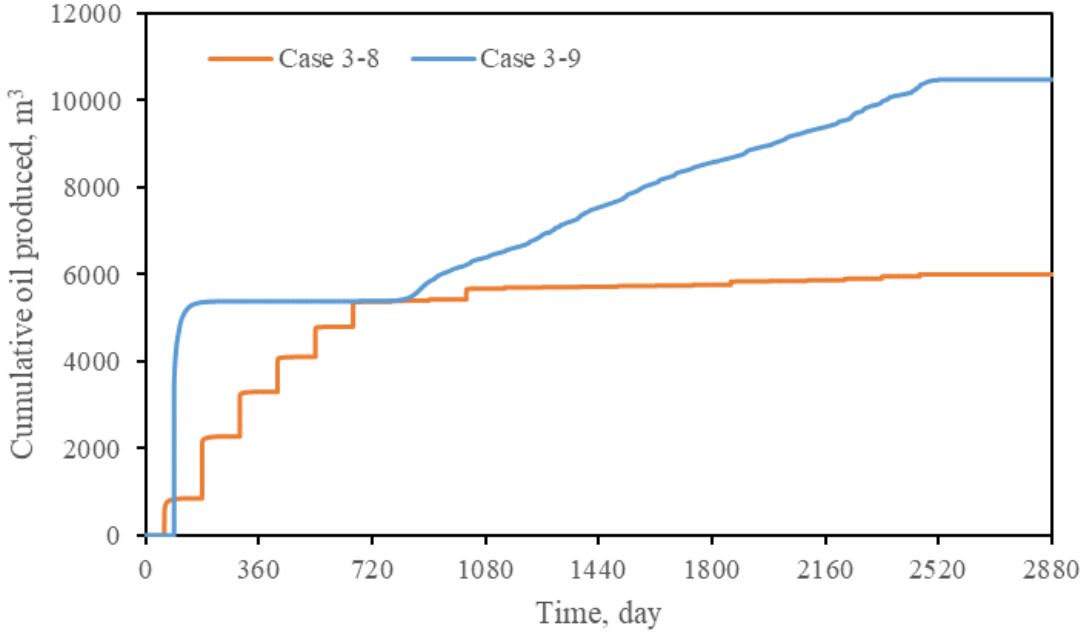

Figure 5.13 Cumulative oil produced by electromagnetic heating of Case 3-8 and Case 3-9.

Chapter 6 Comparison of Electrical Heating Processes

This chapter presents a critical comparison of electrical heating methods, including electric heater, electrical resistive heating and electromagnetic heating, for oil sands reservoirs. Based on the proposed numerical simulation techniques in this thesis, the results are summarized and compared. Mechanism studies of electrical heating processes were conducted to achieve a better understanding of these processes and provide theoretical support for future studies. Energy dissipation and heat transfer in the reservoir are discussed. The model developed and the comparative analysis of different methods of electrical heating assisted oil production provided by this work provides a useful tool for making reservoir development decisions and for designing process operating plans.

6.1 Heat generation mechanism

The mechanism of heat generation of the three electrical heating processes, namely electric heater, electrical resistive heating and electromagnetic heating vary according to the underlying process physics. The simulation results in the previous chapters provide straightforward illustrations of the heat generation in the three heating processes.

In the process of heating by electric heater, the electric current flows through the electrode only, and thus generates heat in the wellbore by Joule heating. That means that the electrode itself is the source of heat. Practically, this could be also a hot tube, for example purged with steam or hot water, not released into the reservoir. So, the dissipation of energy into the reservoir depends on thermal contact of the heater to the reservoir and also on thermal conduction through the reservoir, as shown in Figure 5.1 which illustrates the temperature profiles under heating by an electric heater. The higher the reservoir thermal conduction the higher the differential

temperature is between the heater source and a remote point in a reservoir. As the temperature at the remote point increases, the thermal energy flow decreases meaning that less thermal power can be brought into the reservoir as process operation time elapses. Disadvantageous is the tight drilling space required due to reliance on thermal conduction. Also, heaters require a high temperature in order to produce a large temperature differential to drive the heat transfer. This high temperature can cause thermal contact issues due to drying out of the reservoir close to the heater surface (Wacker et al., 2011) and also the potential formation of a zone of thermal cracking of the oil forming solid coke.

Electrical resistive heating uses the reservoir as a resistance, where the current goes through conductive paths (McGee and Vermeulen, 2000). In this process, electrical current can flow between electrical potential sources (wells) and generate the Joule heating. Therefore, the regions around the electrodes in (or around) the wells are heated to high temperatures. In this process electrical conductivity plays a very important role as shown in Figure 5.5. In order to increase efficiency of this type of heating process, the presence of optimum saline water saturation is an important design consideration.

Electromagnetic heating has the source of energy in the form of electromagnetic waves at the antenna implemented in a reservoir. Under radiation, energy is converted to heat as a result of frictional effect of polar molecules (such as, for instance, water molecule) which oscillate in applied EM field (Bogdanov et al., 2011). Heat can be generated as long as the electromagnetic waves can effectively penetrate the reservoir. Methods for enlarging the penetration depth of electromagnetic waves into a reservoir are critical for achieving successful reservoir heating under electromagnetic wave radiation.

6.2 Effect of vaporization on energy dissipation

Water and steam are considered as critical to the processes of electrical heating. In electric heater process, water and steam are regarded as the fluids which can deliver heat further to cold oil sands reservoir. In electrical resistive heating process, electrical conductivity of water is relatively high compared to rock and hydrocarbon phases and this leads to an increase in the electrical current density in water phase. Therefore, the most generation of heat takes place in the water phase. In the process of electromagnetic heating, water is the primary material to absorb energy from electromagnetic waves.

In this part, the effect of water vaporization and steam condensation is discussed for the three electrical heating processes. Under the heating by electric heater, local vaporization of water enables generated steam flow upwards to heat up the reservoir in vertical direction. Water vaporization is found beneficial to heat transfer in the vertical direction, as shown in Figure 5.2.

In electrical resistive heating process, since steam is essentially a non-conductive, it disconnects the conductive paths near the electrodes where the temperature declines sharply until steam condenses and again electrical conductivity increases in the presence of condensed water, as shown in Figure 6.2. In Figure 6.1, the cross-section of an oil sands reservoir has been shown with a line from left heating source to right reservoir boundary. In Figure 6.2, simulation results of water saturation and electrical potential are plotted along the line (Figure 6.1). At the end of day 1, when water is not vaporized into steam under short heating time, electrical voltage has its highest value at the location of electrode and decreases gradually to the right reservoir boundary. However, at the end of day 2880 (8 year), by heat generation according to Joule effect, local water at the location of electrode implementation is vaporized. As a result, the local electrical

conductivity is significantly reduced, which impedes electrical current flow outwards to oil sands reservoir, as shown by the curve of electrical voltage at end of day 2880. Thus, this process should be designed to keep the temperature below the boiling point by circulating water. This can prevent the evaporation leading to an increase in the process efficiency.

In contrast, the vaporization of water provides benefits to the process of electromagnetic heating. Evaporation of connate water in the vicinity of the EM antenna results in a desiccated zone leading to a drastic reduction in the absorption coefficient of the media and thereby deeper penetration of electromagnetic waves, as shown in Figure 6.3. Properties including magnitude of electric field and water saturation are plotted in the direction (Figure 6.1) from the heating source to right reservoir boundary. At the time of day 1, with initial water saturation of 0.2, the magnitude of electric field decreases gradually by the power law. With the continuation in heating by electromagnetic wave radiation, vaporization of water enables electromagnetic waves to penetrate further into cold oil sands and heat up the reservoir. These advantages of electromagnetic heating suggest that application of electromagnetic heating of oil sands is technically promising.

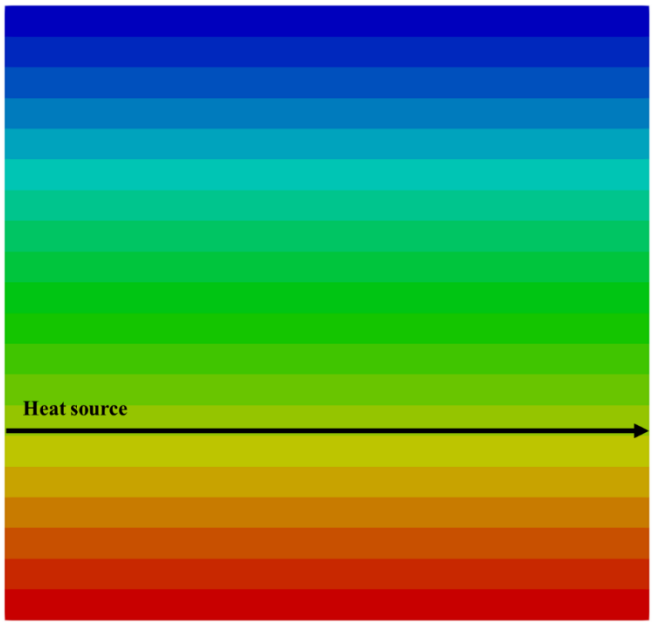

Figure 6.1 Illustration of the location from left heating source to right reservoir boundary in view of cross-section.

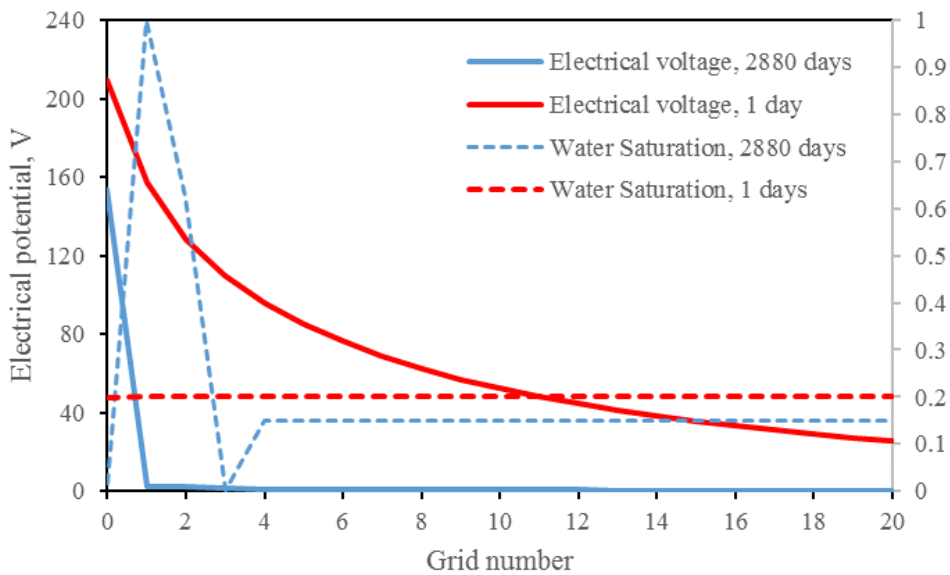

Figure 6.2 Distributions of water saturation and electrical potential in the lateral direction from electrode to right reservoir boundary at day 1 and day 2880, Case 2-4.

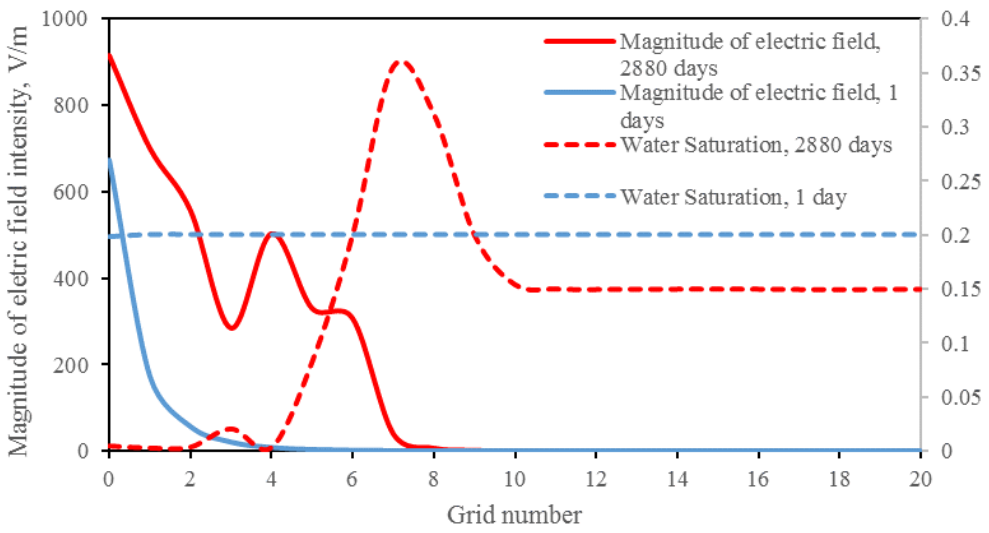

Figure 6.3 Distributions of water saturation and magnitude of electric field in the lateral direction from electrode to right reservoir boundary at day 1 and day 2880, Case 3-9.

6.3 Oil Production performance

A comparison of the amount cumulative oil produced has been conducted of Case 1-6, Case 2-5 and Case 3-9. In Case 1-6, electric heater is used for heating a reservoir. Electrical current is introduced in reservoir to generate heat according to electrical resistance heating in Case 2-5. An antenna is implemented in a reservoir in Case 3-9 to generate heat by the method of electromagnetic heating. Plots of cumulative oil production curves in Figure 6.4 demonstrate the capability of electromagnetic heating in recovery of oil sands reservoir. A desiccated zone, in which water saturation is extremely low, provides possibility of electromagnetic waves penetrating further cold oil sands and generating heat. Consequently, a greater amount of oil can be produced by the method of electromagnetic heating than the other two methods.

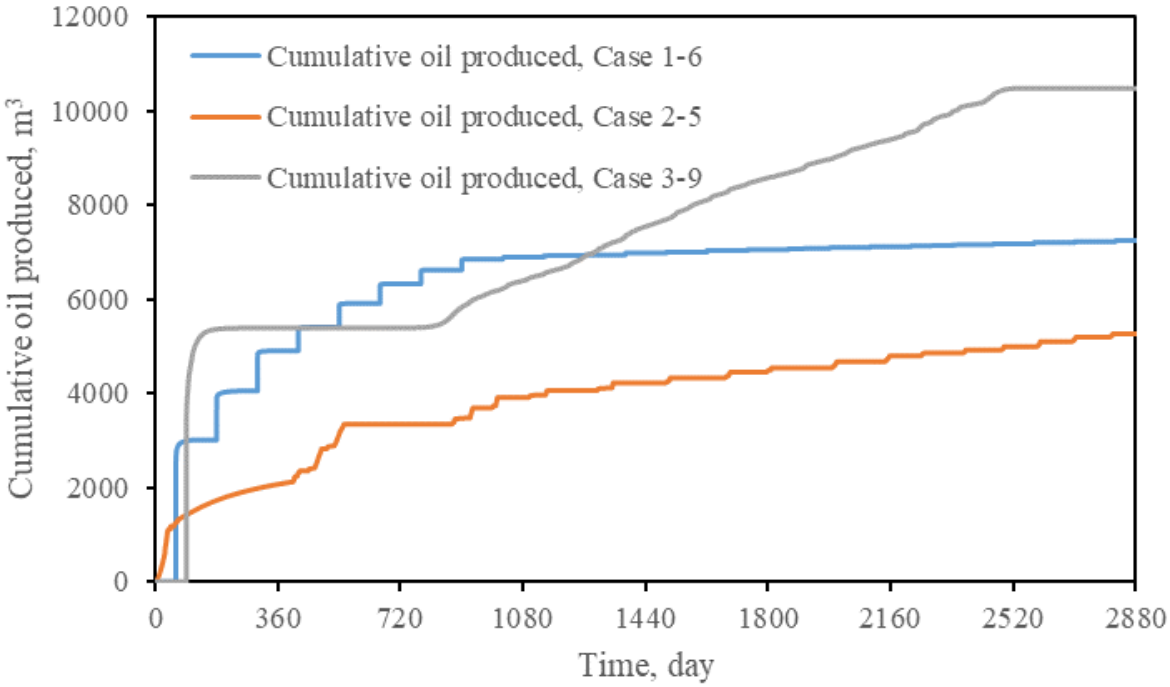

Figure 6.4 Comparison of cumulative oil produced of the three electrical heating processes. Case 1-6 applies electric heater, Case 2-5 applies electrical resistance heating and Case 3-9 uses electromagnetic heating.

Chapter 7 Conclusions and Recommendations

7.1 Conclusions

In the following, the contributions of this thesis are described in a brief:

- Formulation of the problem: mass balance equations for compositional flow, energy balance, electrical energy dissipation and heat generation terms for the above electrical heating processes.
- A fully implicit numerical simulator: new simulator handles the three electrical heating processes accurately with regard to their physical mechanisms.
- Treatment of boundary conditions: appropriate boundary conditions have been proposed in both internal boundary, such as voltage at electrode in electrical resistance heating and power at antenna in electromagnetic heating, and external boundary, such as applications of electrical current estimation at reservoir boundary in electrical resistance heating and PML at reservoir boundary in electromagnetic heating.
- Simulation results: results are provided by executing the new simulator and the validation has been done through comparisons to CMG STARS in phase calculation and multi-phase flow, and comparisons to analytic solutions in electrical energy dissipation.
- Evaluation of the important and controlling process parameters: parameter sensitivity study allowing assessment of where there is a need for basic oil sands electrical property data collection.
- Comparative simulations: a range of comparative simulations at field scale of the three methods and understating the physics and determining which method offers the best performance for typical oil sands parameters.

7.1.1 A Single Simulator of Electrical Heating

A single simulator that is capable of modelling all electrical heating processes for heavy oil and oil sands thermal recovery has been developed in this thesis. In this fully implicit numerical simulator, simultaneous modelling thermal oil reservoirs and electrical energy dissipations has been developed and validated. By using the law of Ampere balance, electrical current flow in oil sands reservoir has been rigorously simulated. Using derivations from Maxwell's equations, a simple and high accuracy method has been proposed for the estimation of electromagnetic wave distributions in inhomogeneous media, such as oil sands reservoirs in which saturations and temperature are dynamic parameters under a heating process.

In addition, the necessity of using two simulators, one for the electrical heating (especially in the case of EM heating) and one for the phase behaviour and multiphase fluid flow, is avoided by application of this single simulator developed in this thesis. The computational overhead and complexity of swapping data back and forth between two simulators has been omitted. Also, it has not been possible until now to model all three electrical heating processes in a single model and deliverables in this thesis enable a direct comparison of the different methods to be made.

7.1.2 Techniques in Modelling of Electrical Heating Processes

Formulations involved in electrical current flow in reservoir in the process of electrical resistance heating and electromagnetic wave propagation in oil reservoir in electromagnetic heating have been provided in this thesis. With consideration of extremely low electrical conductivity under water vaporization of a grid on calculation of electrical current flow in the simulation model, an appropriate averaging method in electrical conductivity between neighbouring grids has been

proposed in this thesis. Furthermore, an estimation of electrical current at reservoir outer boundary can be used to mimic the electrical current flow in an infinity domain. By the derivations from Maxwell's equations, a simple and high accuracy method has been proposed for the estimation of EM wave distributions in inhomogeneous media, such as oil sands reservoirs in which saturations and temperature are dynamic parameters under a heating process. Combination of the newly derived formulation of electromagnetic wave propagation and method of PML, an efficient method has been provided in this thesis in the absorption of EM wave at reservoir outer boundaries.

7.1.3 Comparative Analysis of Electrical Heating Methods

Comparative studies show that water vaporization under application of electrical heaters can accelerate the heat transfer in vertical direction by counter-current flow of steam and liquids. Existence of water phase is critical for electrical current flow in reservoir because water is the dominant conductive material in an oil reservoir. Vaporization of water under Joule effect by electrical current flow would impede electrical current flow further to cold oil sands. In contrast, in the process of electromagnetic heating, water vaporization in the vicinity of wellbore (containing antennas) enables the transmission of electromagnetic waves further to cold oil sands. Because water is the dominant dielectric material to absorb electromagnetic waves, evaporation of connate water in the vicinity of the electromagnetic antenna results in a desiccated zone leading to a drastic reduction in the energy reduction of electromagnetic waves and thereby deeper penetration of electromagnetic waves.

The feasibility of electrical heating methods for oil sands recovery has been tested by scenarios of a single horizontal well and a horizontal well-pair. Simulation results showed that a desiccated

zone, which is regarded crucial to a successful electrical heating process, can be established under electrical heating in the reservoir and heated oil will be produced to the surface. A moderate level of electromagnetic wave frequency and an oil production rate constraint are beneficial to a desiccated zone development.

7.2 Recommendations for Future Work

In this thesis, a deep understanding of electrical heating processes, with respect of theoretical analysis and potential applications, has been provided by the methods of numerical simulation. While the developed numerical simulator provides available tools for studying problems related to electrical heating methods for oil sands recovery techniques, there are still some problems involving modelling techniques and related applications of electrical heating, which are in need to be evaluated and solved in the future work.

These problems are considered in the areas of future work. A brief description of these problems is presented in the follows.

7.2.1 Effect of Electro-Osmosis on Wettability

Helmholtz double layer is formed, in water saturated rocks, by the attractive forces between the electrically negative surfaces of minerals and the positive poles of water molecules and positive ions, in aqueous solution (connate waters). This electrical double layer is divided into two electrochemical regions: a region of fixed water molecules and cations and a more mobile region of loosely bound cations and water molecules. In the application of electrical resistance heating, the mobile layer migrates under electrical current flow in oil reservoir, in the direction of the electrical field. This motion of the water molecules and cations within the mobile layer drags the

water molecules, cations, anions, and other fluids, in the free fluid, along with it, enlarges the effective pore throat diameter allowing flow of both wetting and non-wetting fluids (Hill et al., 2008). Thus, the alternations in wettability by electrical current flow will be added in the future reservoir simulator with efficient simulation technique.

7.2.2 Asphaltic Crude Rheology under Irradiation

Concerns have been raised regarding irreversible alternations of crude oil properties in the process of electromagnetic heating. Explosion of oil sands to microwaves generates the necessary heat to decompose bitumen to yield a crude oil and distilled kerogen. The asphaltene precipitation process was explained by the formation of a film-type oil, whose viscosity is higher than that of the original oil, on the surface of pore channels (Kovaleva et al., 2010a). The thickness of film in some cases is comparable to the radius of pore channels, resulting in a decreasing cross-section of pore channels, and thereby, their permeability. The base of the film-type oil is adsorptive layers of asphaltene-resin substances, which are polar components changing the molecular structure of the solid surface; these present the basis for the formation of an oil boundary layer. Thus, this effect of changes in crude oil rheology on the fluid flow in oil reservoir should be considered and the technique of modelling this process has to be delicately evaluated.

7.2.3 Water Injection to Improve Application of Electric Heater

The idea of cold water injection at moderate rate proposed by Mcgee and Vermeulen in 2007 can be utilized to achieve two purposes: (1) limit the temperature of ‘hot spots’ near the electric heater to prevent failure in equipment; (2) increase the convective heat transfer around the

electrodes by flow of vaporize steam in the vicinity of the electrodes. However, the injection of cold water in reservoir will result in additional cost of investment in infrastructure at surface. Future study will be done to evaluate the effect of cold water injection on the oil production by application of electric heater.

7.2.4 Solvent/gas Injection to Improve Electrical Heating Processes

Solvent/gas injection could be an approach to improve the performance of electrical heating process with two fold benefits: maintain the pressure of reservoir by filling the void space left by the removed oil, and help to reduce oil viscosity by solvent dissolution in oil (Rangel-German, 2004). It is possible to inject gas phase to improve oil production performance in electrical heating processes and the injection strategies will be discussed in the future.

7.2.5 Optimization of Electrical Heating by Sensitivity Analysis of Operation Parameter

The electrical heating processes can be further optimized in terms of operation parameters. Such as frequency, power and well configuration in electromagnetic heating. All of the methods could be tested for SAGD-type well pairs to obtain a continuous oil production and high recovery factor.

References

Abarbanel, S., & Gottlieb, D. (1997). *A mathematical analysis of the PML method*. Journal of Computational Physics, 134(2), 357-363.

Abernethy, E. R. (1976). *Production increase of heavy oils by electromagnetic heating. Journal of Canadian Petroleum Technology*, 15(03).

Abraham, T., Afacan, A., Dhandharia, P., & Thundat, T. (2016). *Conduction and dielectric relaxation mechanisms in athabasca oil sands with application to electrical heating*. Energy & Fuels, 30(7), 5630-5642.

Akfhampour, K. H. (1985). *A novel approach to solving downhole fluid flow problems by use of an electric heating system*. IEEE IAS Petroleum and Chemical Industry Committee Houston, 12.

Alomair, O. A., Alarouj, M. A., Althenayyan, A. A., Al Saleh, A. H., Almohammad, H., Altahoo, Y. & Alshammari, Y. (2012, January). *Improving heavy oil recovery by unconventional thermal methods*. In SPE Kuwait International Petroleum Conference and Exhibition. Society of Petroleum Engineers.

Amba, S. A., Chilingar, G. V., & Beeson, C. M. (1964). *Use of direct electrical current for increasing the flow rate of reservoir fluids during petroleum recovery*. Journal of Canadian Petroleum Technology, 3(01), 8-14.

Andrew, W. V., Balanis, C. A., & Tirkas, P. A. (1995). *A comparison of the Berenger perfectly matched layer and the Lindman higher-order ABC's for the FDTD method*. IEEE Microwave and guided wave letters, 5(6), 192-194.

Archie GE. (1942). *The electrical resistivity log as an aid in determining some reservoir characteristics.* Transactions of the AIME. 146(01):54-61.

Ayappa, K. G. (1997). *Modelling transport processes during microwave heating: A review*. Reviews in chemical engineering, 13(2), 1-69.

Aziz, K., & Settari, A. (1979). *Petroleum reservoir simulation*. Applied Science Publishers, London, 135-139.

Baylor, B. A., Maggard, J. B., & Waftenbarger, R. A. (1990). Improved calculation of oil production response to electrical resistance heating (ERH). In SPE Annual Technical Conference and Exhibition. Society of Petroleum Engineers.

Bera, A., & Babadagli, T. (2015). *Status of electromagnetic heating for enhanced heavy oil/bitumen recovery and future prospects: A review*. Applied Energy, 151, 206-226.

Bientinesi, M., Petarca, L., Cerutti, A., Bandinelli, M., De Simoni, M., Manotti, M., & Maddinelli, G. (2013). *A radiofrequency/microwave heating method for thermal heavy oil recovery based on a novel tight-shell conceptual design*. Journal of Petroleum Science and Engineering, 107, 18-30.

Bird, R.B., Steward, W.E. and Lightfoot, E.N. (2002). *Transport Phenomena*. New York City: John Wiley & Sons, Inc. 506-507.

Bogdanov, I., Cambon, S., & Prinet, C. (2014, December). *Analysis of heavy oil production by radio-frequency heating*. In SPE International Heavy Oil Conference and Exhibition. Society of Petroleum Engineers.

Bogdanov, I., Torres, J. A., Akhlaghi, H., & Kamp, A. M. (2011). *The influence of salt concentration in injected water on low-frequency electrical-heating-assisted bitumen recovery*. SPE Journal, 16(03).

Bogdanov, I., Torres, J., Kamp, A. M., & Corre, B. (2011, January). *Comparative analysis of electromagnetic methods for heavy oil recovery.* In SPE Heavy Oil Conference and Exhibition. Society of Petroleum Engineers.

Bogdanov, I., Torres, J., & Corre, B. (2012, January). *Numerical simulation of electromagnetic driven heavy oil recovery.* In SPE Improved Oil Recovery Symposium. Society of Petroleum Engineers.

Bridges, J., Taflove, A., & Snow, R. (1979). *U.S. Patent No. 4,140,180.* Washington, DC: U.S. Patent and Trademark Office.

Butler, R. M., & Yee, C. T. (2002). P*rogress in the in-situ recovery of heavy oils and bitumen*. Journal of Canadian Petroleum Technology, 41(01).

Carrizales, M. A., Lake, L. W., & Johns, R. T. (2008, January). *Production improvement of heavy-oil recovery by using electromagnetic heating*. In SPE annual technical conference and exhibition. Society of Petroleum Engineers.

Carrizales, M., & Lake, L. W. (2009, October). *Two-dimensional COMSOL simulation of heavy-oil recovery by electromagnetic heating.* In COMSOL Conference held in Boston, Massachusetts, USA (pp. 10-13).

Carrizales, M. A. (2010). *Recovery of stranded heavy oil by electromagnetic heating* (Doctoral dissertation). The University of Texas at Austin.

Carrizales, M. A., Lake, L. W., & Johns, R. T. (2010, January). *Multiphase fluid flow simulation of heavy oil recovery by electromagnetic heating*. In SPE Improved Oil Recovery Symposium. Society of Petroleum Engineers.

Chakma, A., & Jha, K. N. (1992, January). *Heavy-oil recovery from thin pay zones by electromagnetic heating.* In SPE Annual Technical Conference and Exhibition. Society of Petroleum Engineers.

Chen, Z. (1994). *BDM mixed methods for a nonlinear elliptic problem.* Journal of computational and applied mathematics, 53(2), 207-223.

Chen, L. F., Ong, C. K., Neo, C. P., Varadan, V. V., & Varadan, V. K. (2004). *Microwave electronics: measurement and materials characterization*. John Wiley & Sons.

Chen, Z. (2007). *Reservoir simulation: mathematical techniques in oil recovery* (Vol. 77). Siam.

Chew, W. C., & Weedon, W. H. (1994). *A 3D perfectly matched medium from modified Maxwell's equations with stretched coordinates*. Microwave and optical technology letters, 7(13), 599-604.

Chhetri, A. B., & Islam, M. R. (2008). *A critical review of electromagnetic heating for enhanced oil recovery*. Petroleum Science and Technology, 26(14), 1619-1631.

Chute, F. S., & Vermeulen, F. E. (1990). *Physical modeling of systems involving electromagnetic heating of materials*. IEEE Transactions on Education, 33(2), 190-197.

Chute, F. S., Vermeulen, F. E., Cervenan, M. R., & McVea, F. J. (1979*). Electrical properties of Athabasca oil sands*. Canadian Journal of Earth Sciences, 16(10), 2009-2021.

Crookston, R. B., Culham, W. E., & Chen, W. H. (1979). *A numerical simulation model for thermal recovery processes*. Society of Petroleum Engineers Journal, 19(01), 37-58.

Cummer, S. A. (2003). *A simple, nearly perfectly matched layer for general electromagnetic media.* IEEE microwave and wireless components letters, 13(3), 128-130.

Das, S. K. (2008, January). *Electro magnetic heating in viscous oil reservoir.* In International Thermal Operations and Heavy Oil Symposium. Society of Petroleum Engineers.

Davison, R. J. (1995). *Electromagnetic stimulation of Lloydminster heavy oil reservoirs: field test results.* Journal of Canadian Petroleum Technology, 34(04).

Davison, R. J. (1992, January). *Electromagnetic Stimulation of Lloydminster Heavy Oil Reservoirs*. In Technical Meeting/Petroleum Conference of The South Saskatchewan Section. Petroleum Society of Canada.

Davletbaev, A. Y., Kovaleva, L. A., & Nasyrov, N. M. (2008). *Numerical simulation of injection of a solvent into a production well under electromagnetic action.* Fluid Dynamics, 43(4), 583-589.

Davletbaev, A., Kovaleva, L., Babadagli, T., & Minnigalimov, R. (2010, October). *Heavy oil and bitumen recovery using radiofrequency electromagnetic irradiation and electrical heating: Theoretical analysis and field scale observations*. In Canadian Unconventional Resources and International Petroleum Conference.

Davletbaev, A., Kovaleva, L., & Babadagli, T. (2011). *Mathematical modeling and field application of heavy oil recovery by Radio-Frequency Electromagnetic stimulation.* Journal of petroleum science and engineering, 78(3-4), 646-653.

Debye, P. J. W. (1929). *Polar molecules*. Chemical Catalog Company, Incorporated.

Dogru, A. H. (2010). Equivalent Wellblock Radius for Partially Perforated Vertical Wells--Part I: Anisotropic Reservoirs with Uniform Grids. SPE Journal, 15(04), 1-028.

Depew, M. C., Lem, S., & Wan, J. K. S. (1991). *Microwve induced catalytic decomposition of some Alberta oil sands and bitumens*. Research on chemical intermediates, 16(3), 213-223.

Dong, C. (2012). *An integrated multi-component reservoir-wellbore thermal model.* PhD Thesis. University of Calgary.

El-Feky, S. A. H. (1977). *Theoretical and experimental investigation of oil recovery by the electrothermic technique.* PhD Dissertation. University of Missouri-Rolla.

Eskandari, S., Jaghargh, E. M., & Rasaei, M. R. (2014*). 2D Numerical Simulation and Analysis of Microwave Heating in Heavy Oil Reservoirs.* Energy Sources, Part A: Recovery, Utilization, and Environmental Effects, 36(18), 1961-1971.

Eskandari, S., Jalalalhosseini, S. M., & Mortezazadeh, E. (2015). *Microwave heating as an enhanced oil recovery method—potentials and effective parameters*. Energy Sources, Part A: Recovery, Utilization, and Environmental Effects, 37(7), 742-749.

Fanchi, J. R. (1990, January*). Feasibility of reservoir heating by electromagnetic irradiation. In SPE Annual Technical Conference and Exhibition*. Society of Petroleum Engineers.

Feng, N., Yue, Y., Zhu, C., Wan, L., & Liu, Q. H. (2015). *Second-order PML: Optimal choice of nth-order PML for truncating FDTD domains*. Journal of Computational Physics, 285, 71-83.

Fisher, S. T. (1980). *Processing of solid fossil-fuel deposits by electrical induction heating.* IEEE Transactions on industrial electronics and control instrumentation, (1), 19-26.

Fu, Q., Sun, W. B., & Yang, P. (1999). *Modeling of scattering and absorption by nonspherical cirrus ice particles at thermal infrared wavelengths.* Journal of the atmospheric sciences, 56(16), 2937-2947.

Gasbarri, S., Diaz, A., & Guzman, M. (2011, January). *Evaluation of electric heating on recovery factors in extra heavy oil reservoirs.* In SPE Heavy Oil Conference and Exhibition. Society of Petroleum Engineers.

Ghannadi, S., Irani, M., & Chalaturnyk, R. J. (2014, June). *Induction and Radio Frequency Heating Strategies for Steam-Assisted Gravity Drainage Start-Up Phase*. In SPE Heavy Oil Conference-Canada. Society of Petroleum Engineers.

Glandt, C. A., & Chia-Fu, H. (1992, January). Electric Preheating in Low-Injectivity Tar Sand Deposits. In SPE/DOE Enhanced Oil Recovery Symposium. Society of Petroleum Engineers.

Godard, A., & Rey-Bethbeder, F. (2011, January). *Radio frequency heating, oil sand recovery improvement*. In SPE Heavy Oil Conference and Exhibition. Society of Petroleum Engineers.

Greff, J., & Babadagli, T. (2013). *Use of nano-metal particles as catalyst under electromagnetic heating for in-situ heavy oil recovery.* Journal of Petroleum Science and Engineering, 112, 258-265.

Gunal, O. G., & Islam, M. R. (2000). *Alteration of asphaltic crude rheology with electromagnetic and ultrasonic irradiation.* Journal of Petroleum Science and Engineering, 26(1-4), 263-272.

Harding, T. G., Zanon, S., Imran, M., & Kerr, R. K. (2016, June). *In-situ reflux: an improved in-situ recovery method for oil sands.* In SPE Canada Heavy Oil Technical Conference. Society of Petroleum Engineers.

Harvey, A. H., Arnold, M. D., & El-Feky, S. A. (1979). *Selective electric reservoir heating.* Journal of Canadian Petroleum Technology, 18(03).

Harvey, H. A., & Arnold, M. D. (1980). *Estimation of heat distribution in selective electric reservoir heating.* Journal of Petroleum Technology, 32(06), 965-968.

Hasanvand, M. Z., & Golparvar, A. (2014). *A critical review of improved oil recovery by electromagnetic heating.* Petroleum Science and Technology, 32(6), 631-637.

Hascakir, B., Acar, C., & Akin, S. (2009). *Microwave-assisted heavy oil production: an experimental approach*. Energy & Fuels, 23(12), 6033-6039.

Hascakir, B., Babadagli, T., & Akin, S. (2010). *Field-scale analysis of heavy-oil recovery by electrical heating*. SPE Reservoir Evaluation & Engineering, 13(1), PP-131.

Hiebert, A. D., Vermeulen, F. E., Chute, F. S., & Capjack, C. E. (1986). *Numerical simulation results for the electrical heating of Athabasca oil-sand formations*. SPE reservoir engineering, 1(01), 76-84.

Hill, D. G., Chilingar, G. V., & Wittle, J. K. (2008, January). *Direct current electrical enhanced oil recovery in heavy-oil reservoirs to improve recovery, reduce water cut, and reduce H2S production while increasing API gravity*. In SPE Western Regional and Pacific Section AAPG Joint Meeting. Society of Petroleum Engineers.

Hossan, M. R., & Dutta, P. (2012). *Effects of temperature dependent properties in electromagnetic heating*. International journal of heat and mass transfer, 55(13-14), 3412-3422.

Huang, C. K. (2009). *Development of a general thermal oil reservoir simulator under a modularized framework.* Dissertation Abstracts International, 70(03).

Islam, M. R., & Wadadar, S. S. (1991, January). *Enhanced oil recovery of Ugnu tar sands of Alaska using electromagnetic heating with horizontal wells*. In International Arctic Technology Conference. Society of Petroleum Engineers.

Ivory, J., Frauenfeld, T., & Jossy, C. (2010). *Thermal solvent reflux and thermal solvent hybrid experiments*. Journal of Canadian Petroleum Technology, 49(02), 23-31.

Jackson, C. (2002, January). *Upgrading a heavy oil using variable frequency microwave energy.* In SPE International Thermal Operations and Heavy Oil Symposium and International Horizontal Well Technology Conference. Society of Petroleum Engineers.

Jha, A. K., Joshi, N., & Singh, A. (2011, January). *Applicability and assessment of micro-wave assisted gravity drainage (MWAGD) applications in Mehsana heavy oil field, India.* In SPE

Jha, K. N., & Chakma, A. (1999). *Heavy-oil recovery from thin pay zones by electromagnetic heating.* Energy Sources, 21(1-2), 63-73. Heavy Oil Conference and Exhibition. Society of Petroleum Engineers.

Ji, D., Harding, T., Chen, Z., Dong, M., & Liu, H. (2019, March). *Modelling of Electromagnetic Heating Process and its Applications in Oil Sands Reservoirs*. In SPE Reservoir Simulation Conference. Society of Petroleum Engineers.

Kasevich, R. S., Price, S. L., Faust, D. L., & Fontaine, M. F. (1994, January). *Pilot testing of a radio frequency heating system for enhanced oil recovery from diatomaceous earth*. In SPE Annual Technical Conference and Exhibition. Society of Petroleum Engineers.

Kasevich, R. S., Price, S. L., & Albertson, A. (1997, January). *Numerical modeling of radio frequency heating process for enhanced oil production.* In SPE Western Regional Meeting. Society of Petroleum Engineers.

Katterbauer, K., Hoteit, I., & Sun, S. (2015*). History matching of electromagnetically heated reservoirs incorporating full-wavefield seismic and electromagnetic imaging*. SPE Journal, 20(05), 923-941.

Katz, D. S., Thiele, E. T., & Taflove, A. (1994). *Validation and extension to three dimensions of the Berenger PML absorbing boundary condition for FD-TD meshes*. IEEE microwave and guided wave letters, 4(8), 268-270.

Killough, J. E., & Gonzalez, J. A. (1986, January). *A fully-implicit model for electrically enhanced oil recovery.* In SPE Annual Technical Conference and Exhibition. Society of Petroleum Engineers.

Kim, E. S. (1987). *Reservoir simulation of in situ electromagnetic heating of heavy oils*. Texas A and M Univ., College Station (USA).

Koch, A., Sotskiy, S., Mustafina, D., & Danov, V. (2013, June*). Mechanism of heavy oil recovery driven by electromagnetic inductive heating*. In SPE Heavy Oil Conference-Canada. Society of Petroleum Engineers.

Koolman, M., Huber, N., Diehl, D., & Wacker, B. (2008, January). *Electromagnetic heating method to improve steam assisted gravity drainage.* In International Thermal Operations and Heavy Oil Symposium. Society of Petroleum Engineers.

Kovaleva, L., Davletbaev, A., Babadagli, T., & Stepanova, Z. (2010a). *Effects of electrical and radio-frequency electromagnetic heating on the mass-transfer process during miscible injection for heavy-oil recovery*. Energy & fuels, 25(2), 482-486.

Kovaleva, L., Davletbaev, A., & Minnigalimov, R. (2010b). *Recoveries of Heavy Oil and Bitumen Techniques with the Radio Frequency Electromagnetic Irradiation (Russian*). In SPE Russian Oil and Gas Conference and Exhibition. Society of Petroleum Engineers.

Lashgari, H., Delshad, M., Sepehrnoori, K., & De Rouffignac, E. P. (2014, June). *Development of Electrical Joule"s Heating Simulation for Heavy Oil Reservoirs*. In SPE Heavy Oil Conference-Canada. Society of Petroleum Engineers.

Lashgari, H. R., Sepehrnoori, K., & Delshad, M. (2016). *A four-phase chemical/gas model in an implicit-pressure/explicit-concentration reservoir simulator.* SPE Journal, 21(04), 1-086.

Linkewich Z. (2014). *Fundamentals of radio frequency heating and the eseieh process.* Presentation at UPTECH Upstream Oil & Gas Summit. Lake Louise, Alberta, Canada. September 21-23.

Maggard, J. B., & Wattenbarger, R. A. (1991, August). *Factors affecting the efficiency of electrical resistance heating patterns.* In Proc., Fifth UNITAR/UNDP Conference on Heavy Crudes and Tar Sands, Caracas (Vol. 3, pp. 519-530).

McGee, B. C. W., Vermeulen, F. E., & Yu, L. (1999). *Field test of electrical heating with horizontal and vertical wells.* Journal of Canadian Petroleum Technology, 38(03).

McGee, B. C., & Vermeulen, F. E. (2007). *The mechanisms of electrical heating for the recovery of bitumen from oil sands. J*ournal of canadian petroleum technology, 46(01).

McGee, B. C. W., McDonald, C. W., & Little, L. (2008, January). *Electro-Thermal Dynamic Stripping Process-Integrating Environmentalism with Bitumen Production.* In International Thermal Operations and Heavy Oil Symposium. Society of Petroleum Engineers.

McGee, B. C. W., & Donaldson, R. D. (2009, January). *Heat transfer fundamentals for electro-thermal heating of oil reservoirs.* In Canadian International Petroleum Conference. Petroleum Society of Canada.

McPherson, R. G., Stanton, F. S., & Vermeulen, F. E. (1985). *Recovery of Athabasca bitumen with the electromagnetic flood (EMF) process.* Journal of Canadian Petroleum Technology, 24(01).

Meissner, T., & Wentz, F. J. (2004). *The complex dielectric constant of pure and sea water from microwave satellite observations.* IEEE Transactions on Geoscience and remote Sensing, 42(9), 1836-1849.

Meyer, R. F., Attanasi, E. D., & Freeman, P. A. (2007). *Heavy oil and natural bitumen resources in geological basins of the world (No. 2007-1084).* US Geological Survey.

Mittra, R., & Pekel, U. (1995). *A new look at the perfectly matched layer (PML) concept for the reflectionless absorption of electromagnetic waves*. IEEE Microwave and Guided Wave Letters, 5(3), 84-86.

Moini, B., & Edmunds, N. (2013). Quantifying heat requirements for SAGD startup phase: Steam injection, electrical heating. Journal of Canadian Petroleum Technology, 52(02), 89-94.

Mukhametshina, A., & Martynova, E. (2013). *Electromagnetic heating of heavy oil and bitumen: a review of experimental studies and field applications.* Journal of Petroleum Engineering, 2013.

Nigmatulin, R. I., Sayakhov, F. L., & Kovaleva, L. A. (2001, March). *Cross transport phenomena in disperse systems interacting with a high-frequency electromagnetic field*. In Doklady Physics (Vol. 46, No. 3, pp. 215-218). MAIK Nauka/Interperiodica.

Okassa, F. D., Godi, A., De Simoni, M., Manotti, M., & Maddinelli, G. (2010, January). *A nonconventional EOR technology using RF/MW heating coupled with a new patented well/reservoir interface*. In SPE Annual Technical Conference and Exhibition. Society of Petroleum Engineers.

Ovalles, C., Fonseca, A., Lara, A., Alvarado, V., Urrecheaga, K., Ranson, A., & Mendoza, H. (2002, January). *Opportunities of downhole dielectric heating in venezuela: three case studies involving medium, heavy and extra-heavy crude oil reservoirs*. In SPE International Thermal Operations and Heavy Oil Symposium and International Horizontal Well Technology Conference. Society of Petroleum Engineers.

Pasalic, D., Vaca, P., & Okoniewski, M. (2014, August). *Modeling of EM assisted oil recovery.* In 2014 International Conference on Electromagnetics in Advanced Applications (ICEAA) (pp. 620-623). IEEE.

Peaceman, D. W. (1983). *Interpretation of well-block pressures in numerical reservoir simulation with nonsquare grid blocks and anisotropic permeability*. Society of Petroleum Engineers Journal, 23(03), 531-543.

Pearce, D. C., Hulse, W. H., & Walker, J. W. (1973). *The application of the theory of heterogeneous dielectrics to low surface area soil systems.* IEEE Transactions on Geoscience Electronics, 11(4), 167-170.

Pizarro, J. O. S., & Trevisan, O. V. (1990). *Electrical heating of oil reservoirs: numerical simulation and field test results.* Journal of Petroleum Technology, 42(10), 1-320.

Rangel-German, E. R., Schembre, J., Sandberg, C., & Kovscek, A. R. (2004). *Electrical-heating-assisted recovery for heavy oil*. Journal of Petroleum Science and Engineering, 45(3-4), 213-231.

Rappaport, C. M. (1995). *Perfectly matched absorbing boundary conditions based on anisotropic lossy mapping of space.* IEEE Microwave and Guided Wave Letters, 5(3), 90-92.

Rehman, M. M., Meribout, M. (2012). *Conventional versus electrical enhanced oil recovery: a review*. Journal of Petroleum Exploration and Production Technology, 2(4), 157-167.

Ritchey, H. W. (1956). *U.S. Patent No. 2,757,738.* Washington, DC: U.S. Patent and Trademark Office.

Rodriguez, R. F., Bashbush, J. L., & Rincon, A. C. (2008, January). *Feasibility of using electrical downhole heaters in Faja heavy oil reservoirs*. In International Thermal Operations and Heavy Oil Symposium. Society of Petroleum Engineers.

Roussy, G., & Pearce, J. A. (1998, May). *Foundations And Industrial Applications Of Microwaves And Radio Frequency Fields*. Physical And Chemical Processes. In Proceedings of the 6th International Conference on Optimization of Electrical and Electronic Equipments (Vol. 1, pp. 115-116). IEEE.

Sacks, Z. S., Kingsland, D. M., Lee, R., & Lee, J. F. (1995). *A perfectly matched anisotropic absorber for use as an absorbing boundary condition*. IEEE transactions on Antennas and Propagation, 43(12), 1460-1463.

Sadeghi, A., Hassanzadeh, H., & Harding, T. G. (2017). *Modeling of desiccated zone development during electromagnetic heating of oil sands.* Journal of Petroleum Science and Engineering, 154, 163-171.

Saeedfar, A., Lawton, D., & Osadetz, K. (2016, June*). Directional RF Heating for Heavy Oil Recovery Using Antenna Array Beam-Forming.* In SPE Canada Heavy Oil Technical Conference. Society of Petroleum Engineers.

Sahni, A., Kumar, M., & Knapp, R. B. (2000). *Electromagnetic heating methods for heavy oil reservoirs (No. UCRL-JC-138802).* Lawrence Livermore National Lab., CA (US).

Sayakhov, F. L., Babalyan, G. A., & Chistyakov, S. I. (1970). *On the high-frequency heating bottomhole zone*. Neft. Khoz, 12, 49-66.

Shin, W., & Fan, S. (2012). *Choice of the perfectly matched layer boundary condition for frequency-domain Maxwell's equations solvers*. Journal of Computational Physics, 231(8), 3406-3431.

Shokrlu, Y. H., & Babadagli, T. (2011, January). *Transportation and interaction of nano and micro size metal particles injected to improve thermal recovery of heavy-oil.* In SPE Annual Technical Conference and Exhibition. Society of Petroleum Engineers.

Sierra, R., Tripathy, B., Bridges, J. E., & Ali, S. M. (2001, January). *Promising progress in field application of reservoir electrical heating methods.* In SPE International Thermal Operations and Heavy Oil Symposium. Society of Petroleum Engineers.

Singer, I., & Turkel, E. (2004). *A perfectly matched layer for the Helmholtz equation in a semi-infinite strip.* Journal of Computational Physics, 201(2), 439-465.

Soliman, M. Y. (1997). *Approximate solutions for flow of oil heated using microwaves.* Journal of Petroleum Science and Engineering, 18(1-2), 93-100.

Sresty, G. C., Snow, R. H., & Bridges, J. E. (1984). *U.S. Patent No. 4,485,869.* Washington, DC: U.S. Patent and Trademark Office.

Sresty, G. C., Dev, H., Snow, R. H., & Bridges, J. E. (1986). *Recovery of bitumen from tar sand deposits with the radio frequency process.* SPE Reservoir Engineering, 1(01), 85-94.

Stone, H. L. (1973). *Estimation of three-phase relative permeability and residual oil data*. Journal of Canadian Petroleum Technology, 12(04), 53-61.

Stroemich, C. P., Vermeulen, F. E., Chute, F. S., & Sumbar, E. (1990). *Wellbore Power Transmission for In-Situ Electrical Heating.* AOSTRA Journal of Research, 6(4), 273-294.

Swiech, W. M., Taylor, S. E., & Zeng, H. (2013, June). *Dielectric Behaviour of Synthetic Oil Sands*. In SPE Heavy Oil Conference-Canada. Society of Petroleum Engineers.

Sumbar, E., Chute, S., & Vermeulen, F. (1992*). Electromagnetic in-situ heating of heavy oil reservoirs to increase production rates*. Journal of microwave power and electromagnetic energy, 27(2), 67-74.

Sutton, W. H., & Johnson, W. E. (1980). *U.S. Patent No. 4,219,361*. Washington, DC: U.S. Patent and Trademark Office.

Teixeira, F. L. (2008*). Time-domain finite-difference and finite-element methods for Maxwell equations in complex media*. IEEE Transactions on Antennas and Propagation, 56(8), 2150-2166.

Todd, J. C., & Howell, E. P. (1978). *Numerical Simulation of in-situ electrical heating to increase oil mobility*. Journal of Canadian Petroleum Technology, 17(02).

Trimble, R. H., & McDonald, A. E. (1981). Corp. *A Strongly Coupled, Fully Implicit, Three-Dimensional, Three-Phase Well Coning Model.* Society of Petroleum Engineers.

Vermeulen, F. E., & Chute, F. S. (1983). *Electromagnetic techniques in the in-situ recovery of heavy oils.* Journal of microwave power, 18(1), 15-29.

Vermeulen, F., & McGee, B. (2000). *In-situ electromagnetic heating for hydrocarbon recovery and environmental remediation.* Journal of Canadian Petroleum Technology, 39(08).

Vinsome, P. K. W., & Westerveld, J. (1980*). A simple method for predicting cap and base rock heat losses in'thermal reservoir simulators.* Journal of Canadian Petroleum Technology, 19(03).

Wacker, B., Karmeileopardus, D., Trautmann, B., Helget, A., & Torlak, M. (2011, January). *Electromagnetic Heating for In-situ Production of heavy oil and bitumen Reservoirs.* In Canadian Unconventional Resources Conference. Society of Petroleum Engineers.

Wadadar, S. S., & Islam, M. R. (1994). *Numerical simulation of electromagnetic heating of Alaskan tar sands using horizontal wells.* Journal of Canadian Petroleum Technology, 33(07).

Wang, J., Bryan, J. L., & Kantzas, A. (2008, January). *Comparative Investigation of thermal processes for marginal bitumen resources.* In International Petroleum Technology Conference. International Petroleum Technology Conference.

Wise, S., & Patterson, C. (2016, June). *Reducing supply cost with Eseieh™ pronounced easy*, In SPE Canada Heavy Oil Technical Conference.

Wittwer, D. C., & Ziolkowski, R. W. (1996). *How to design the imperfect Berenger PML*. Electromagnetics, 16(4), 465-485.

Yaich, M. I., Kanjaa, M., El Adraoui, S., Mounirh, K., & Khalladi, M. (2018, May). *An Unsplit Formulation of the 3D-PML Absorbing Boundary Conditions for TLM-Method in Time Domain.* In 2018 6th International Conference on Multimedia Computing and Systems (ICMCS) (pp. 1-5). IEEE.

Yee, K. (1966). *Numerical solution of initial boundary value problems involving Maxwell's equations in isotropic media.* IEEE Transactions on antennas and propagation, 14(3), 302-307.

Zhong, L., Yu, D., Yang, H., Sun, Y., Wang, G., & Zheng, J. (2011, January). *Feasibility Study on Produce Heavy Oil by Gas and Electrical Heating Assisted Gravity Drainage*. In Offshore Technology Conference. Offshore Technology Conference.

Zhong, L., Yu, D., Zhang, C., Dong, Z., Ma, S., Wang, C., ... & Guo, L. (2015, June). *Investigation on Combined CO 2 Sequestration and Electrical Heating Assisted Gravity Draingage to Enhance Heavy Oil Production.* In SPE Canada Heavy Oil Technical Conference. Society of Petroleum Engineers.

Zhu, Z., Zeng, F., Zhao, G., & Laforge, P. (2013). *Evaluation of the hybrid process of electrical resistive heating and solvent injection through numerical simulations*. Fuel, 105, 119-127.